MANUFACTURING STRAIN SENSOR VIA PRINTED ELECTRONICS ONTO 3D PRINTED SUBSTRATES

BABAK BADRIAN

A THESIS SUBMITTED TO

THE FACULTY OF GRADUATE STUDIES

IN PARTIAL FULFILLMENT OF THE REQUIREMENTS

FOR THE DEGREE OF

MASTER OF APPLIED SCIENCE

GRADUATE PROGRAM IN ELECTRICAL ENGINEERING AND COMPUTER SCIENCE

YORK UNIVERSITY

TORONTO, ONTARIO

May 2021

Abstract

Inkjet printing is a promising technology in the field of printed electronics. It enables fabrication of electronics with complex geometries and high customizability along with reduced manufacturing time and cost. The key features of inkjet printing include digital customization, reduced cost and time of fabrication, and non-contact printing. While in the conventional silicon electronic industry, electronics are fabricated onto rigid and expensive silicon wafers, the aforementioned advantages enable inkjet printing to fabricate on novel, diverse substrates such as 3D printed substrates. 3D printing technology builds 3D structures with benefits such as freedom of design, mass customization, desktop availability, low cost, simplicity of use, and ability to fabricate complex geometries.

In this research, we use various additive manufacturing techniques including 3D fused filament fabrication (FFF) printing, extrusion printing, and inkjet printing. We deposit a low viscosity UV curable epoxy, as the intermediate material to make the 3D printed surface smooth and protect the 3D printed surface against the aggressive inks, via an extrusion printer. Next, the UV exposure takes place where the UV time considerably determines the quality of line patterns and conductivity. Having the substrate ready, we start the inkjet printing process with silver nanoparticle ink and find the suitable drop spacing for our specific substrate. We optimize the drying condition including temperature and exposure time to dry the ink solvent. Finally, samples go under intense pulsed light that affects the conductivity and length shrinkage of the printed lines. Next, according to the conditions obtained, we print a strain gauge sensor with optimized inkjet patterning and test it electrically and mechanically.

In the last part, we fabricate a similar device and application but with another technology. We pick 3D printing electronics to directly fabricate functional samples via a 3D FFF printer. We create a semi-conducting filament out of thermoplastic polyurethane/carbon nanotubes nanocomposite, then we 3D print the desired strain sensor. At last, we carry out the electrical/mechanical test for this different sensor.

Acknowledgments

I would like to sincerely thank my supervisor, Dr. Gerd Grau. I was extremely lucky that I had this great chance to pursue my master's under his guidance and generous support. I am deeply thankful for this amazing opportunity that allowed me to work on exciting, pioneering projects. I am also grateful for all the environment, laboratories, facilities, and materials that enabled me to work on my research.

I would like to express my gratitude to Dr. Garrett Melenka and Dr. Sunny Leung for their helpful, gentle guidance throughout my study as well as for their presence in my defense and giving me valuable feedback as my supervisor committee and defense committee.

I would also like to acknowledge my colleagues and friends who helped me and made my study memorable particularly MD Saifur Rahman, Fahmida Pervin, Milad Ghalamboran, Paria Naderi, and James Qiu.

I thank the lab technologists who made my job possible and easier including Md Amin Haque Talukder and Giancarlo Ayala-Charca from EECS Department, David Marcinkiewicz from Mechanical Engineering Department, and Shane Guo in the SPARC cleanroom.

I was fortunate to work in M3 Lab in Mechanical Engineering Department. I would like to thank the graduate students of M3 Lab especially Mohammadmehdi Aghelinejad and Hossein Abdoli.

Finally, I deeply grateful to my family, in particular my mother, for their constant encouragement and endless support.

My special thank goes to my beloved wife, Anna, for her infinite patience and support throughout my study.

Table of Contents

List of Tables

List of Figures

Chapter 1: Introduction

1.1 Overview and Research Objectives

In this thesis, we focus on the integration of inkjet printing with 3D printing technology with the aim of fabricating electronic devices. We divide this research project into three chapters: 1) printing a conductive line on 3D printed surfaces and optimize it to obtain the maximum conductivity, 2) fabricating an electronic device, a strain gauge sensor, and perform the related electrical/mechanical test, 3) performing a similar application with 3D printing electronic technology in order to compare both technologies. Once the primary integration is achieved, which is successfully inkjet printing a simple conductive line on the 3D printed substrate, we optimize the simple line to increase the conductivity as much as possible. Having a stable and optimized printing methodology, we start the process of fabricating the electronic device on a 3D printed object as the application. Subsequently, in order to evaluate the fabricated device, we performed several characterization methods including electrical and mechanical. Additionally, we studied another technology to 3D print strain sensors using a conductive filament.

As inkjet printing is a non-contact printing technology in which the printer has no contact with the substrate, one advantage is the ability to fabricate devices on different substrates. Inkjet printing is well-established and can print on many common substrates such as glass. However, printing on novel substrates is still an immature process. One possible issue might be that the ink spreads on the substrate and cannot form well-patterned lines. Moreover, inkjet printing directly onto 3D printed substrates is challenging; because fused filament fabrication (FFF) 3D printing has a lower resolution and much wider and thicker lines compared to inkjet printing, the final surface of the 3D printed substrate is not smooth enough for electronic fabrication. Hence, there is a need for an intermediate material between the 3D printed substrate and inkjet printed patterns. Such intermediate material provides a smooth surface for the electronic patterns. However, another challenge that appears is the main challenge in this research. When the inkjet printer ink is deposited onto the polymeric substrate, in some cases, there are some non-idealities that degrade the electrical conductivity. While, for applicable electronic devices, conductive materials with high conductivity are required. In order to increase the conductivity, we do an optimization including different pre-processing and post-processing steps to finally obtain a highly conductive and well-

patterned line. The optimization includes ultraviolet (UV) time exposure, drop spacing, heating conditions, intense pulsed light parameters, and length shrinkage.

After successfully having an inkjet-printed line on the 3D printed substrate with a good morphology and high conductivity, we start fabricating an electronic device in order to prove this integration properly works and is reliable. We decided to fabricate a strain gauge sensor as an electronic device. We use the optimized conditions obtained in the previous section. We printed the strain gauge on the 3D printed substrate, however, some improvements are required. Although we performed the material and interaction optimization in the previous chapter, since the strain gauge is much larger with more complex geometry, some improvements for patterning are required. Finally, once the desired strain gauge is achieved, we carry out the evaluation step which includes mechanical test and electrical measurement.

In the last section, we fabricate a similar device with a different technology. In this chapter, we chose 3D printing electronics to create a strain gauge sensor. First, we make a functional semi-conducting filament for the 3D printer. We make a thermoplastic polyurethane (TPU)/ carbon nanotubes (CNTs) nanocomposite, and form it into a 3D printing filament. Having the functional filament, we build the desired piezoresistive strain sensor and perform the related mechanical test and electrical measurement.

1.2 Background and Literature Review

1.2.1 Additive Manufacturing

There has been an increasing interest in additive manufacturing (AM) in recent years. AM is commonly used for rapid prototyping with the aim of automatically manufacturing complex products. In traditional technologies, subtractive methodologies, several unwanted layers are deposited and then the extra parts are removed and wasted resulting in material waste and lower fabrication throughput. While in AM, only the required material is deposited for the final product, and hence no material will be removed or wasted. Therefore, complexity, extra steps, reduced material consumption, and in some cases manufacturing costs and time are considerably reduced in AM. Figure 1-1 compares the fabrication process between traditional silicon technology and AM technology. The two principal types of AM include printed electronics (PE) and 3D printing.

1.2.1.1 Printed Electronics

PE is a rapidly growing technology in the field of electronics manufacturing. PE, as the name suggests, is a technology based on printing techniques to fabricate electronic devices and systems. The goal of PE is to fabricate electronic systems by printing techniques instead of more expensive and complex traditional silicon-based technology.

In fact, the traditional silicon microelectronics includes a significantly complicated process. Many different steps are required in order to create a silicon integrated circuits (IC), including preparation of crystal silicon wafers, fabricating transistors, and interconnecting the transistors to form systems; such steps are made of depositing thin films, lithography, and etching. For instance, UV photolithography systems might cost tens of millions of dollars [1]. In general, whereas the traditional silicon electronics enjoys the advantage of super high-performance computation at low power, fabricating large-area and flexible electronics or on any other type of substrates by silicon technology is a challenge.

On the other hand, printed electronics is an easier and shorter process than traditional manufacturing, it only directly deposits a functional material as patterns onto a substrate. Afterwards, only an annealing/sintering step will be needed. In other words, PE is the manufacturing of flexible and large-area electronic devices made of functional inks in a patterned way. PE enables the manufacturing of electronics that are flexible, thin, lightweight, wearable, environmentally friendly, and cost-effective [2].

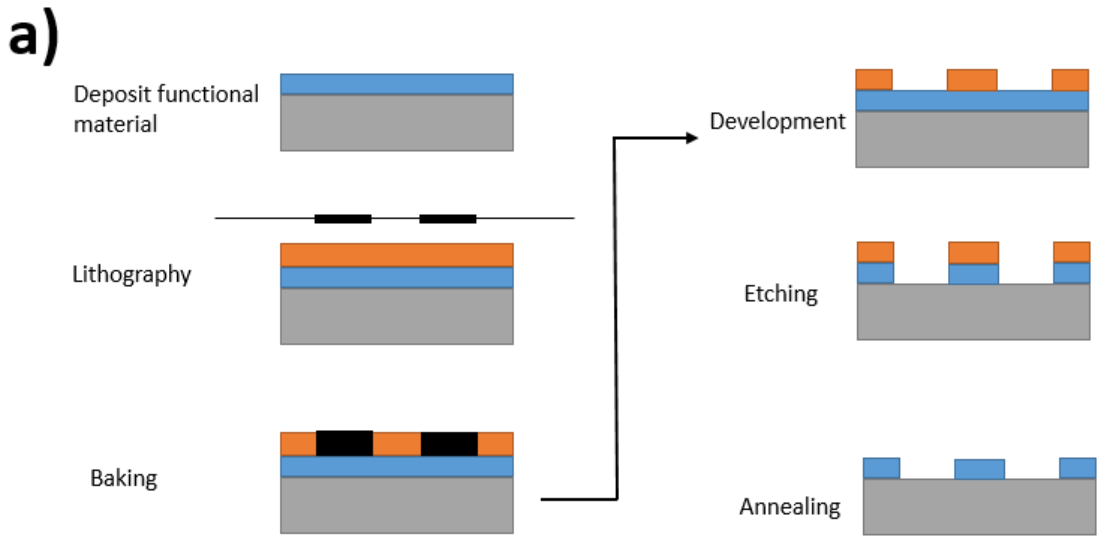

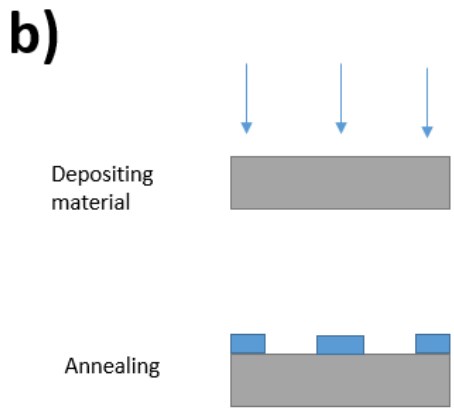

Figure 1-1: Difference between conventional silicon technology and additive manufacturing. (a) Conventional silicon technology and (b) additive manufacturing

The key advantage or PE over traditional silicon electronics are twofold: (1) PE reduces the fabrication costs compared to conventional silicon technology, and (2) PE is able to fabricate applications that silicon industry cannot. The enabling reason of this ability is the processing temperature; in fact, conventional silicon microelectronics requires very high temperatures beyond 1000°C, while PE products can be fabricated by processes under 150°C. Such a low processing temperature allows PE to use novel and cheaper substrates that are not possible by traditional complementary metal–oxide–semiconductor (CMOS) technology. Very cost effective and flexible substrates such as plastic foils can be used in PE method, instead of silicon wafers that are very expensive and rigid. Moreover, the need for high temperature processing imposes extra costs for both materials and equipment, while PE does not need them [3].

Another factor that reduces the manufacturing cost in PE is that the high-cost processes in silicon technology such as photolithography and etching steps are eliminated in PE industry; besides, a significant amount of material is wasted in CMOS technology, while there is almost no material waste in PE as the material is added only where needed [4]. As an example, fabricating a transistor by inkjet printing costs nearly 0.0001 $\$/cm^2$; while in silicon technology, it costs 0.03 $\$/cm^2$ and 3.0 $\$/cm^2$ for a-Si TFT and MOS Si transistors, respectively [4]. Therefore, PE is more a cost-effective technology for large-area electronics.

Printed electronics along with organic electronics are based on novel materials, cost-efficient, large-area manufacturing processes that bring up various new fields of applications. Flexibility, thinness, lightweight, and environmental friendly are the main advantages of printed and organic electronics. As the applications and their specifications cover a large range, parameters like the electrical conductivity of materials and accuracy of patterning are of the greatest importance [5]. Applications have been fabricated using printed electronics include radio-frequency identification (RFID) [6], RF capacitors [7], RF inductors [7], thin-film transistors [8][9], OLED displays [5][10], OLED lighting [5][11], organic solar cell [12], and integrated smart systems [13][14].

As mentioned above, one of the key advantages that PE brings is that it allows fabricating electronics onto different substrates, which were not possible by traditional silicon technology. Substrates under PE technology could be flexible, transparent, thin and lightweight, and cost effective. Polyethylene terephthalate (PET) is the most commonly used and popular plastic film due to its high transparency and low cost. Polyethylene naphthalate (PEN) is another popular and low-cost substrate but with better heat resistance. Some novel substrates for PE are flexible glass [15][16], ultra-thin plastic [17], paper [18][19], and 3D printed substrates [20].

1.2.1.2 3D Printing Technology

3D printing, also known as digital fabrication or additive manufacturing, is a fast-emerging technology that creates three-dimensional physical objects from a digital 3D model or a CAD file. As it is an additive technology, it builds objects layer by layer; compared to traditional subtractive manufacturing technologies like computer numerical control (CNC) machines. 3D printers mostly use plastics as the material, however, some use liquids or powder grains. Thanks to its capabilities, nowadays, 3D printing is widely used in various fields of application including mass customization, automotive industry, healthcare, biomedical, sports industry, agriculture, buildings, protective structures, and locomotive and aerospace industries [21]–[23]. Due to recent developments and low cost, 3D printers can be found in almost any location including laboratories, offices, schools, libraries, and homes.

3D printing has significant advantages that have made it increasingly popular [21]–[23]. The main advantages include:

(1) Freedom of design: as it is a digital technology and is designed in CAD, one can design any customized geometry for any specific application.

(2) Ability to fabricate complex geometries: again as it is designed in CAD, it is able to build complex geometries along with high resolutions, such as lattice structures.

(3) Minimum waste: since this is an additive methodology, it only uses the material for the final desired product, which minimizes the material waste.

(4) Simplicity of use: One is only needed to design the geometry in a user-friendly CAD; no more tools or skills is required.

(5) Mass customization: fabrication of a collection of customized products with minor differences is possible with the lowest cost, as there is no need for mold making or any extra tools.

(6) Easy editing: making changes to previous products is very straightforward with the minimum cost.

(7) Easy availability: as 3D printers are small with no special equipment, they can be moved to any location, such as home, office, schools, and etc.

There are several types of 3D printing, each with its advantages and disadvantages. (1) The most popular methodology of 3D printing is FFF which is a desktop printer and mostly uses thermoplastic polymer filaments. At the nozzle of the printer, the filament is heated to become a semi-liquid state, afterwards, it extrudes on the plate or on the previously printed layers. The main parameters in this method are layer thickness, width, and orientation of the printed lines that affect the mechanical characteristics of the final product. The main advantages of this method are low cost, simplicity of function, and high speed [22]. (2) Selective laser sintering (SLS) is an industrial common method that goes in powder bed fusion category. SLS is able to be used for various polymers, alloy powders, and metals. In SLS, the laser sintering does not completely melt the powders, instead, the high temperature of the grains turns into the fusion of powders [22][24][25]. (3) Stereolithography (SLA) is another popular method. SLA uses an electron beam or UV light to perform a reaction on the layer of the monomer solution. The monomers, after activation, immediately turn into polymer chains. After the polymerization step, inside the resin layer, a pattern is solidified with the aim of holding the next layers. The non-reacted resin is removed and

a post-processing step might be used in order to obtain the desired mechanical properties [22][26][27].

Table 1-1: Comparison of different techniques of 3D printing

Technique	Working principle	Material state	Advantages
FFF	Extrusion and deposition	Filament	Ease of use, low cost, ability of various materials,
SLS	Heat fusion of powders by a laser	Powder	Good strength, excellent mechanical properties, easy removal of support powders
SLA	Selective curing of photopolymer via UV laser	Thermoset liquid	Highest resolution and accuracy, having the smoothest surface,
Binder Jetting	A binder is selectively applied over the powder bed to join them.	Powder	High resolution and accuracy, no need for supports

Various materials could be used to fabricate the structures by 3D printing technologies. Materials such as metals and alloys, ceramics, concrete, and composites; however, the most common materials in 3D printing technology are polymers thanks to their ease of use and diversity [22]. Thermoplastic polymers including polylactic acid (PLA) [28]–[30], acrylonitrile-butadiene-styrene (ABS) [31][29][30], and poly-carbonate (PC) [32][33] are the most popular materials as they have the right rheological and thermal characteristics to be readily processable by 3D printing technology [34]. Besides, 3D printers, particularly FFF printers, are able to use printable polymer composites as well in order to overcome the limited functionalities and mechanical properties of pure polymers [35].

1.2.2 Comparison of Printed Electronics Technologies

In PE, there are various technologies with different properties. The main difference is that whether the method requires a mask/template or is digital. However, there are other key differences between PE methods including ink properties, resolution, and speed.

Different printing technologies are able to work with different ink properties. For instance, the viscosity of some ink might be very low (approximately 5 cp); it is not easy to increase the viscosity and keep the electrical properties constant. More importantly, different methods only work with a limited range of ink viscosity. For the 5cp ink example, it is difficult to print by screen printing while it is suitable for inkjet printing or gravure printing. On the other hand, some inks having inorganic materials in the form of micro particles or nanoparticles usually have a higher viscosity, which makes the ink a paste suitable only for screen printing [1]. Figure 1-2 illustrate some applications fabricated by PE technologies.

Other important factors in PE methodology are printing resolution and speed. Digital methods able to print small-sized devices with less material usage. The resolution of most printing techniques lies between 50-100 µm, although 20 µm or even 1 µm resolutions are also possible with new techniques and optimizations. On the other hand, roll-to-roll printing methods that print on flexible substrates can be considerably fast and enjoy a high throughput [1].

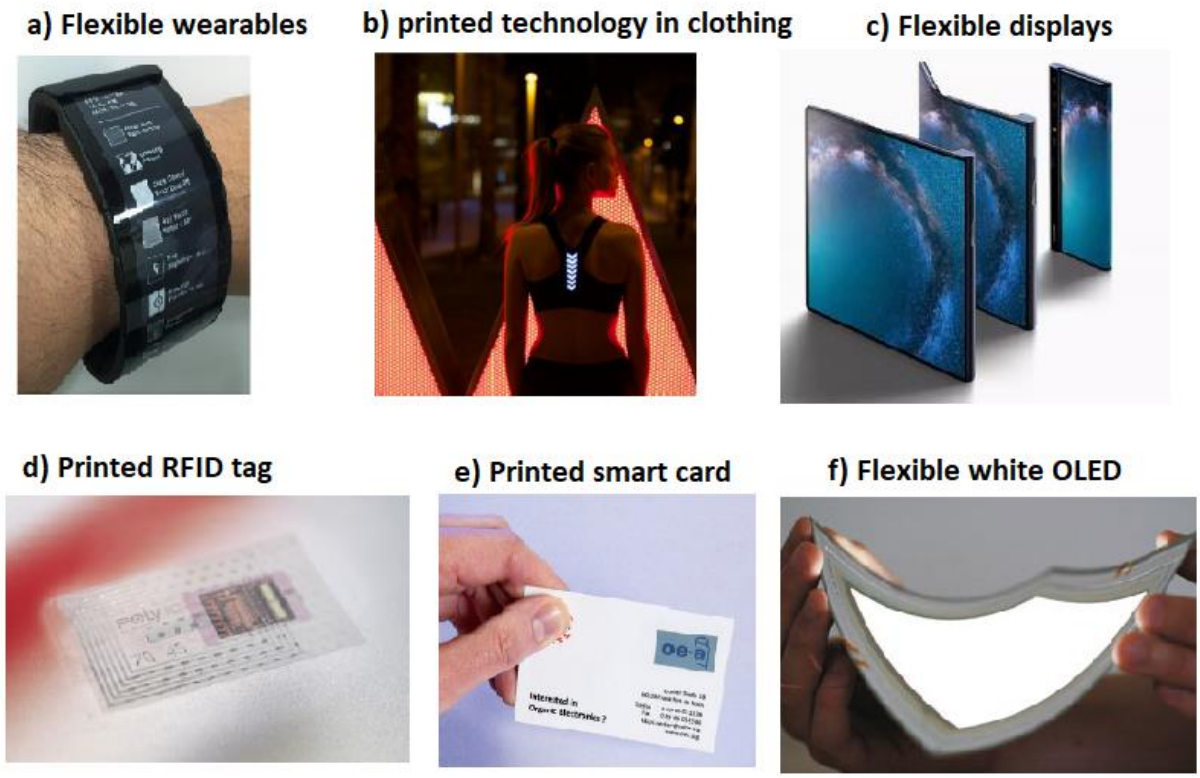

Figure 1-2: Some applications fabricated by printed and organic electronics. (a) Flexible wearables and displays, electronic bracelets (www.polyera.com). (b) Printed active light incorporated in clothing (http://www.eurecat.org/). (c) Foldable AMOLED display (www.huawei.com). (d) Printed RFID tag (www.polyic.com/). (e) Printed smart card involving thin-film battery (www.oe-a.org/). (f) Flexible white OLED (www.holstcentre.com/NewsPress).

1.2.2.1 Screen Printing

Screen printing the most commonly used method in the PE industry. It is a contact method and uses a mesh (screen mask). The ink needs to have a high viscosity and a low volatility, making it suitable for thick films [36].

The advantages of this method include: (1) there are various types of commercial pastes such as metal, carbon, and polymers. (2) It is able to print on flat and curved substrates. (3) It can create thick films (beyond 10 µm) easily. (4) The overall cost is lower than other printing technologies in terms of both equipment and materials.

However, the disadvantages of screen printing are two-fold. (1) Considering the ink must have high viscosity, in order to increase the viscosity some additive needs to be formulated into the ink, which usually degrades the electrical properties of the ink. (2) Another disadvantage is the low resolution, which cannot be used for fine applications.

1.2.2.2 Gravure Printing

Gravure printing is the preferred technology among roll-to-roll PE technologies since it has a high resolution between them. In this method, the pattern is engraved onto the gravure roller consisting of cells. Firstly, the cells of gravure roll are filled with ink as the gravure roll rotates. Next, the doctor blade removes the excess ink of the cells and ink left on the unwanted land areas between cells. After this wiping step, the ink present in the cells transfer onto the substrate. Finally, the printed ink needs to spread on the substrate so that join the individual cells pattern [37]. Substrate used for this technique could be rigid or flexible. In this method, the size and depth of cells determine the amount of ink transferred onto the substrate; therefore, gravure printing is able to accurately control the morphology and pattern thickness. Gravure printing is a preferred option for large-area and high throughput applications.

The advantages of gravure printing technology are: (1) It works with low viscous inks, which means inks without additives can be used. (2) As it is a roll-to-roll method, it enjoys a high throughput. (3) The amount of ink is precisely controllable, hence different thicknesses are possible.

On the other hand, the main disadvantage of this method is the high cost of creating the gravure plate, which is not a good option for prototyping or small batch production.

1.2.2.3 Flexographic Printing

Flexographic printing technology is another R2R technology suitable for high-speed applications. Firstly, a gravure roll, aka anilox cylinder, is coated with the ink, and the excess ink is removed by a doctor blade. Next, the ink inside the image cells is transferred to a secondary roll, flexographic printing plate, and subsequently is deposited onto the substrate [36].

The advantages of this method include: (1) The ink viscosity lies between 20-200 cp, making the ink formulation easier. (2) The flexographic plate is cost-effective and resilient. (3) Flexographic printing is a better choice to print thin films.

However, (1) flexographic plate has a service life shorter than gravure plate. (2) Since the printing plate is elastic, under printing pressure some distortion might happen. (3) In general, flexographic printing is more complicated compared to gravure or screen printing, hence, more physical and chemical interactions are required to be considered.

1.2.2.4 Dispenser Printing

Dispenser printing, also known as extrusion printing, is another digital printing technology in PE. Dispenser printing divides into three categories: (1) positive displacement, (2) time-pressure dispensing, and (3) screw extrusion. In the positive displacement system, the ink inside a cartridge is pressurized by a piston connected to a motor and hence extrudes through the nozzle onto the substrate; therefore, the rate of the motor's displacement determines the rate of ink extrusion. In the time-pressure dispensing, the air is pressurized into the ink cartridge; the pressure difference between the pressurized air and the ambient air determines the extrusion rate of the ink. In the screw extrusion system, the ink is extruded through the rotary screw and the nozzle; the speed of motor controls the degree of rotation and hence the ink extrusion [38][39].

This technology prints high viscosity materials (usually more than 1,000 cP), which makes the printing process easier as the printed ink would be less affected by the surface condition of the substrate. In this technology, the width of the printed lines depends on various parameters including volumetric flow rate of ink, wetting property of the substrate, printing speed, and the nozzle diameter [38]. However, the disadvantage of this technology is its low resolution (> 100 µm). Moreover, the printing speed is slow in this technology because the pressure losses while the ink flows through the nozzle.

1.2.2.5 Inkjet Printing

Inkjet printing is a drop-on-demand (DOD), digital, non-contact, maskless technology. DOD means the printer ejects droplets of ink when required as determined by the digital signal. Inkjet printing creates individual droplets of ink and precisely controls them by a computer in order to make jetting out of the ink nozzle and form the desired digital pattern by ink droplets.

The first challenge in this method is (1) the ink formulation is difficult in terms of viscosity and surface tension. (2) The nozzles of inkjet printers might clog easily as ink particles are large. (3) The ink movement which is unavoidable sometimes causes undesirable phenomena such as the coffee ring effect.

The key advantage that differentiates inkjet printing from other printing technologies is the non-contact patterning method; this property enables this technology to deposit functional ink onto almost any surface including non-planar surfaces, rigid or flexible substrates, or smooth or rough surfaces. Another key advantages is that it is a digital method, hence, does not need any mask or template; therefore, it is able to print a limitless number of droplets/patterns onto the substrate only controlling a computer. The other advantages of this method are reduced material consumption, compatibility to large-area electronics, and affordability [40].

In terms of operation mode, inkjet printers divide into two categories, namely continuous inkjet (CIJ) and drop on demand (DOD) inkjet [41][42]. (1) In CIJ printers, the droplets are ejected from the nozzle continuously and with a constant frequency. Ink droplets are charged before printing and are controlled by a present electrostatic field. The wanted droplets that form the pattern, deposit onto the substrate. While the unwanted droplets are deflected from the substrate and then collected by an ink collector and go back to the reservoir to be used again. (2) In DOD printers, the droplets eject only when is needed to form the pattern. According to the pattern and data file in the computer, a series of pulses is generated; once a pulse is applied to the nozzle, one single droplet is ejected and deposits onto the substrate and form the pattern. Their schematic operation of CIJ and DOD inkjet printers is shown in Figure 1-3.

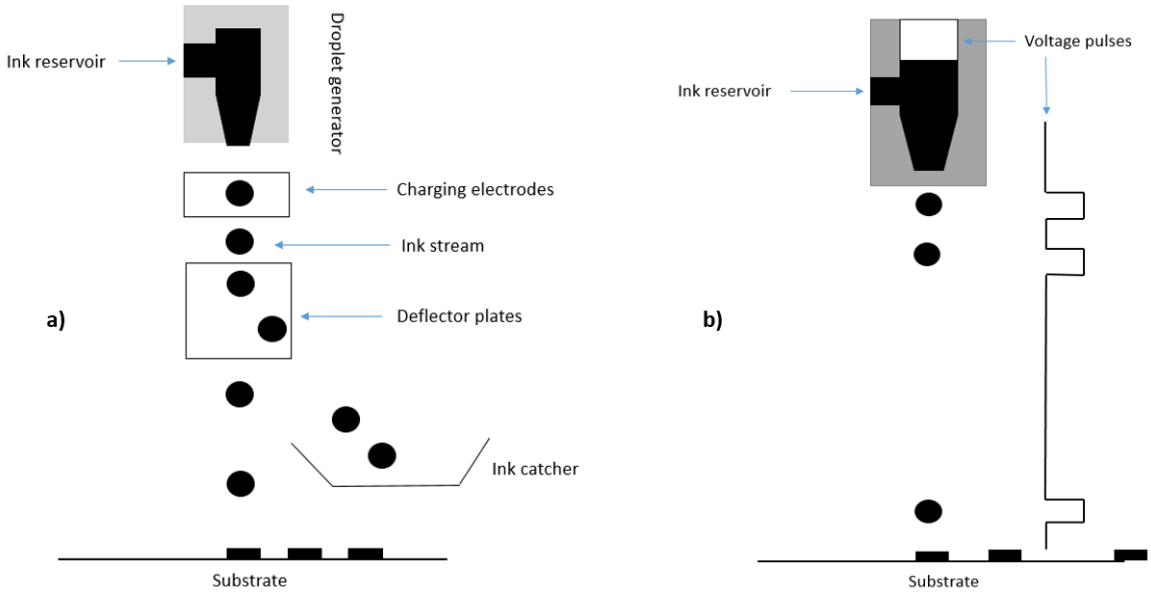

Figure 1-3: General operation modes in inkjet printers. (a) Continuous inkjet (CIJ). (b) Drop on demand (DOD) inkjet.

Besides, in terms of the technique of propelling ink droplets, inkjet printers divide into two main groups including thermal bubble (TIJ) and piezoelectric (PIJ) [41][43]. (1) In TIJ printers, an electrical current passes through a heater and creates a bubble in the chamber; this formed bubble increases the pressure inside the nozzle which causes the droplet to eject from the nozzle and deposit onto the substrate. In PIJ printers, a voltage pulse is applied to the piezoelectric pressure transducer which causes the ink inside the nozzle to bend, and consequently one droplet would eject from the nozzle. Figure 1-4 displays the schematic diagram of a piezoelectric DOD inkjet printer.

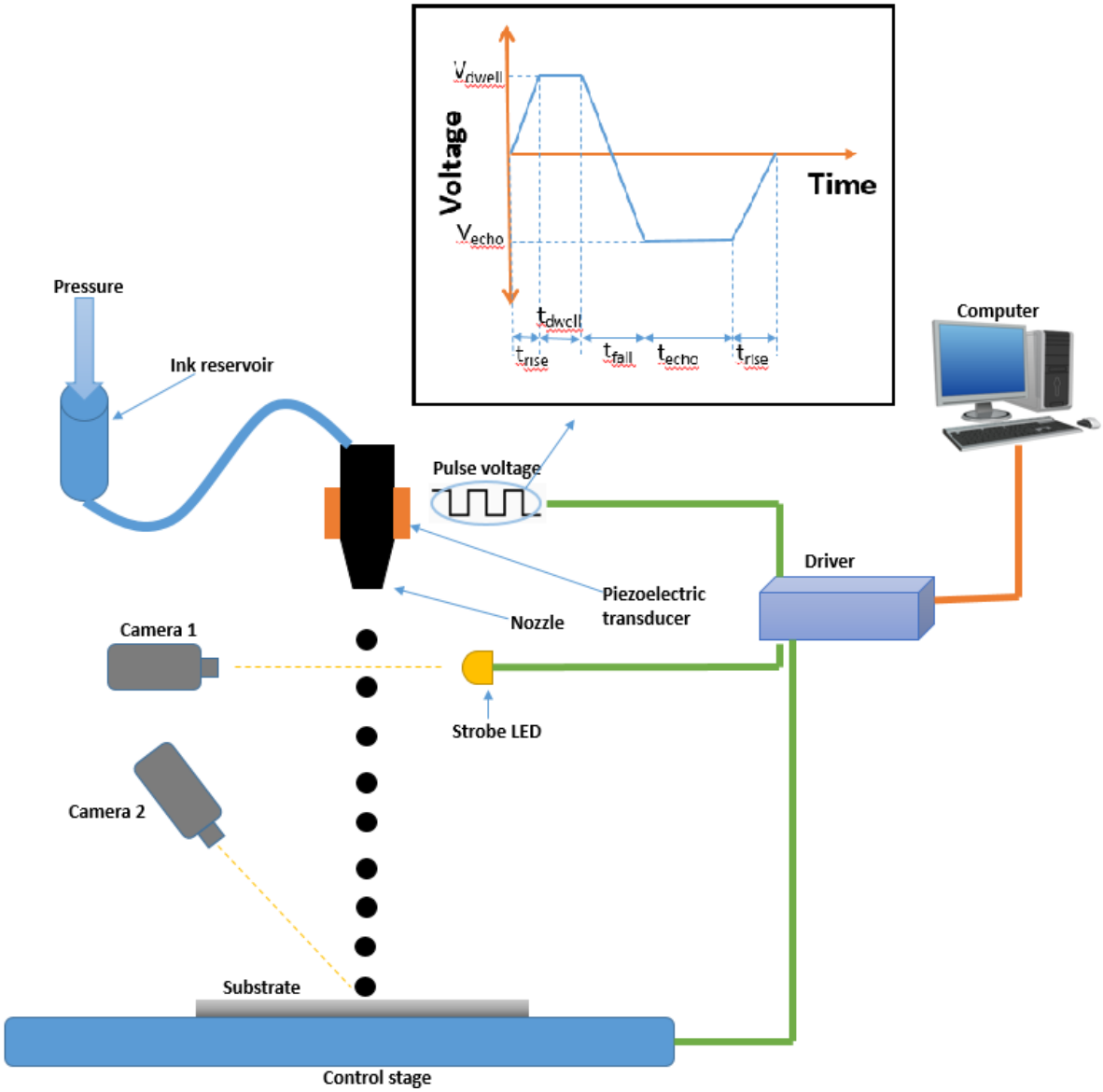

Figure 1-4: Schematic diagram of the inkjet printing system.

Thanks to the digital property of inkjet printing, unlike most PE technologies, it does not require a master plate or template to form a pattern. The desired pattern is created in data file stored in a computer which can be easily edited or recreated to change the desired printing pattern. According to the data file containing parameters such as drop spacing, XY directions, and the desired pattern, a series of pulses is generated going forward to the printer.

Inkjet printing technology is an adaptable technology able to use many different materials and inks. It can print various types of materials such as organic/inorganic materials, polymers, and carbon variants that can have any type of electrical properties including conductors, semiconductors, and insulators. However, there are some limitations on inks to be used by inkjet printers; the inks must have low viscosity (approximately 4-30 cP), low volatility, small size of particles, and high surface tension to readily generate a stream of droplets [36].

The most common and reliable commercial inks for inkjet printing are metallic inks. One of the most commonly used conductive inks is silver thanks to its high conductivity and chemical stability. Because conductive inks usually require post-printing processes to obtain the desired performance (including solvent evaporation, curing, and sintering), some additives can be added in order to optimize the specifications of the ink including viscosity, surface tension, and physical properties of particles. Adding such decomposable and evaporative additives to the ink makes the final ink more proper for inkjet printing. In particular, this idea is true for silver inks, as it is a chemically stable material it readily can be formulated for specific applications.

Polymeric inks are another common category of inks in PE, which can be used for almost all electrical properties such as conductor, semiconductor, insulator, and optoelectronic materials. Some widely used inks are conductive polymer PEDOT:PSS, semiconductor polymers including P3HT and MEH-PPV, and insulating polymer PMMA. Since polymers could be modified and synthesized by various methods, one can obtain more diverse polymeric inks.

Since inkjet printing technology is the most versatile printing technique due to its merits of digital and non-contact printing, it is able to fabricate almost all electronic devices and applications. Some inkjet printed applications include field effect transistors [44]–[49], resistors [50], capacitors [7][51][52], inductor [7][53], sensors [6][54]–[57], antennas [58]–[63], solar cells [64]–[67], memories [68]–[70], and light emitting and displays [71]–[76].

However, there are some challenges in using inkjet printing. (1) The ink formulation for inkjet printing is difficult and complicated in order to have a successful jetting and printing. More specifically, all physical properties including viscosity, surface tension, and volatility need to simultaneously be within a limited window [43]. (2) As inkjet printers are non-contact printers and have nozzles, clogging nozzle is a serious challenge to be considered. Nozzles clog because of different reasons; the size of ink particles might be too large, or ink solvents might evaporate

quickly, or the ink itself has poor stability [43]. (3) The property of being non-contact also brings some challenges including ink movement onto the substrate after printing as it has a low viscosity and the substrate surface has different conditions [77]–[79]. Ink movement means once the droplets are deposited onto the substrate they move from the original place. Ink movement has both positive and negative effects. The main effect is coffee ring effect which is a common phenomenon in inkjet printing. The coffee ring effect happens because the evaporation rate is faster on edges of the droplet/line and while the contact line is pinned to the substrate there is a convective flow from the center towards the edges. This phenomenon usually is undesirable because it avoids a uniform deposition and causes defects when there are multiple layers. However, the coffee ring effect might be useful in some cases, for instance, to obtain high aspect ratio features [80][81]. In order to avoid such undesired effects, some pre-printing and/or post-printing actions are required [82].

The ink and its rheological characteristics considerably determines the quality of inkjet printing. An ink with unsuitable properties might cause satellite droplets (secondary unwanted droplets that eject in addition to the main wanted droplets) which degrade the printing pattern. Besides, the ink material is able to cause nozzle clogging; for instance if the ink solvent is too volatile and evaporate very quickly, it causes nozzle clogging. Therefore, parameters including suppression of satellite drops and solvent evaporation at nozzle orifice should be taken into account. Moreover, the interaction between ink droplets and the substrate and droplet's contact angle determines the pattern morphology [77][83]. However, as [77] displayed, the patterns quality can be controlled by drop spacing, temperature, and drop frequency.

In order to achieve a high-quality printing process, first the printer needs to generate stable, satellite-free droplets. To do so, various studies have defined the jetting window. Such optimized windows are defined by dimensionless numbers and the data are related to viscosity and surface tension of the ink.

1.2.3 3D Printing Polymer Composites and Foamed Piezoresistive Sensing

3D FFF printers mostly uses common single polymer materials such as PLA, ABS, and TPU; each of such materials has its own characteristics suitable for specific applications. However, such commercial single materials typically have a limited range that are compatible with commercial printers and they are limited in physical and chemical properties. This issue can be solved by using

multi-material printing and composite printing which could be blended or layered composite materials [84][85].

Polymer nanocomposites are different from conventional polymers in which fillers are incorporated inside their polymeric matrices. Introduction of a particular filler enhances some properties like electrical conductivity; however, in the meantime, it might cause the loss of some other characteristics. According to their properties, polymer nanocomposites are a good option for areas such as flexible and wearable electronics.

Among various polymers, TPU is widely used thanks to its great physical properties including mechanical flexibility. TPU is a linear segmented block copolymer made of alternating sequences of soft and hard segments. The hard segments could be categorized as either aromatic or aliphatic, according to the type of isocyanate. While soft segments could be either polyether or polyester. By manipulating the ratio of hard segments to soft segments, one is able to tailor the hardness of TPU. We also can tailor TPU properties by introducing different types of filler into its matrix [86][87].

CNTs are powerful fillers in order to improve the multifunctional properties of polymer nanocomposites. CNTs enjoy great advantages including high electrical conductivity (σ) as well as large aspect ratio, which make CNT an ideal option as filler for electrically conductive polymer composites. Such nanocomposites are common in various applications such as temperature/strain sensing, flexible electronics, EMI shielding, and thin film transistors [88][89].

Despite the advantages of incorporating fillers, loading of a high amount of filler may negatively affect weight, cost, and processability of polymer composites. Considering the decreasing cost could be achieved by decreasing the material density, foaming seems very promising in order to decreased the cost and enhance some properties of polymers. Hence, introducing both functional fillers and foaming process could be a novel method to fabricate lightweight polymer composites by 3D printing [90].

1.3 Integrating Electronics with 3D Structures

As mentioned in previous sections, additive electronics and 3D printing each has its own significant advantages; moreover, integrating the two technologies opens up even new possibilities that are not possible by other technologies. This integration brings on-demand creation of highly-

customized electronics on customized and conformal surfaces. Integration of 3D printing and electronic fabrication enables low-cost fabrication of electronics as well as freedom of design as electronic devices and circuits are directly fabricated on customized 3D substrates. By doing this integration, we will no longer need to fabricate electronic circuits only on integrated circuits (IC) and printed circuit boards (PCB), which are expensive and time-consuming.

Such integration provides major advantages which are not easily possible by other technologies. The key advantages include:

1) Complex geometries: As the end-use product is designed by a CAD file with a high resolution, this integration is able to achieve complex geometries[91][92].

2) Customizability: Since this was is only based on a data file, customizing or altering the product is simply possible depending on the specific application[91][93].

3) Freedom of design: Design freedom is not limited to shape complexity, this integration is also able to fabricate different materials and functional structures as desired[94].

4) Functionalizing substrates: This integration allows functionalizing of substrates unlike traditional planar circuit boards.

5) Reduced time: As both techniques are digital and AM, there is no need for designing masks/models and extra steps to be removed.

6) Reduced cost: Cost is reduced from multiple perspectives. 3D printed materials are very cheap compared to other common substrates in the electronic industry. Both techniques are AM so there is no need for extra equipment and materials.

7) Reduced footprint: As 3D technology is customizable and able to build complex geometries, the footprint of the circuit could be as minimized as the circuit footprint.

Integration of 3D printing technology with electronics could be used in different fields of application as it is able to create complex geometries with multiple functionalities. Such integration is revolutionary in flexible electronics, embedded electronics, stretchable electronics, conformal electronics, 3D structural electronics, solid-state displays, efficient batteries, and etc. [94][95]. Integrated electronics with 3D printing is able to be used in various fields including robotics, biomedical, pharmaceutical, automotive, defense, aerospace, and consumer industries

[96]. Functional elements including electronic devices and circuits, sensors, and embedded components are being integrated with 3D printed structures which provides new opportunities. In order to have a viable technology, it needs to be able to fabricate both active and passive devices that could be made of conductors, semiconductors, insulators, polymers, etc. with any possible form of inks, solids, pastes, and etc. [95]. Each application requires different and specific characteristics, which this flexible technology suits the best. As an example, applications in aerospace engineering need to be lightweight and high performance, hence, integrated electro-mechanical systems could be found very helpful [97]. While next generation electronics will be focused on mobile devices but in thinner and smaller dimensions. In order to achieve all mentioned applications along with many others, integrating electronics with 3D structures is a viable method by which increased performance in the meantime decreased footprint can happen.

Integration of electronics with 3D structures could be achieved through different approaches:

1) Integration of electronics with 3D structures using common 2D electronic technologies, and then, projecting it onto the desired 3D structure.

2) Current injection molding, also known as molded interconnect devices (MIDs).

3) Inserting electronic components into cavities inside the 3D structures.

4) Depositing functional inks onto 3D substrates by PE technologies.

1.3.1 2D Fabrication and Transferring to 3D

The most basic way to integrate electronics with 3D structures is to use the traditional 2D electronics and then transfer it to the desired 3D structures. For instance, one can fabricate the electronic circuit on a 2D flexible sheet and subsequently mold it around the purpose 3D object. However, this basic method can only be realized for 3D structures with simple geometries like cylinders, it cannot be used for 3D structures with complicated geometries. Some previous work done by this approach are [98]–[100].

3D printing technology is able to be used to print electronics on flexible and stretchable bio-compatible skins involving integrated circuits able to conform to non-smooth surfaces. Muth et al. [100] used a novel embedded 3D printing method to fabricate stretchable sensors. They made the sensors out of carbon-based inks within an elastomeric matrix. They successfully fabricated complex and scalable sensors by controlling the rheological properties of the ink, reservoir, and

filler fluid. In this technique, a viscoelastic ink is extruded via a deposition nozzle into an elastomeric reservoir. The ink serves as a resistive sensing material, whereas the reservoir is used as a matrix material. While the nozzle translates through the reservoir, accordingly void space is created. Subsequently, A capping, filler fluid, layer is used in order to fill the void space. After the printing process is finished, both the filler fluid and reservoir are co-cured to create a monolithic structure, at the same time, it keeps the embedded conductive ink as fluid. To ensure that the fabricated devices work properly, they performed various tests including failure test and the response of fabricated sensors to step strain inputs. Figure 1-5(a) illustrates the schematic diagram of this embedded technique, and Figures 1-5(b-c) illustrate two fabricated applications via this technique.

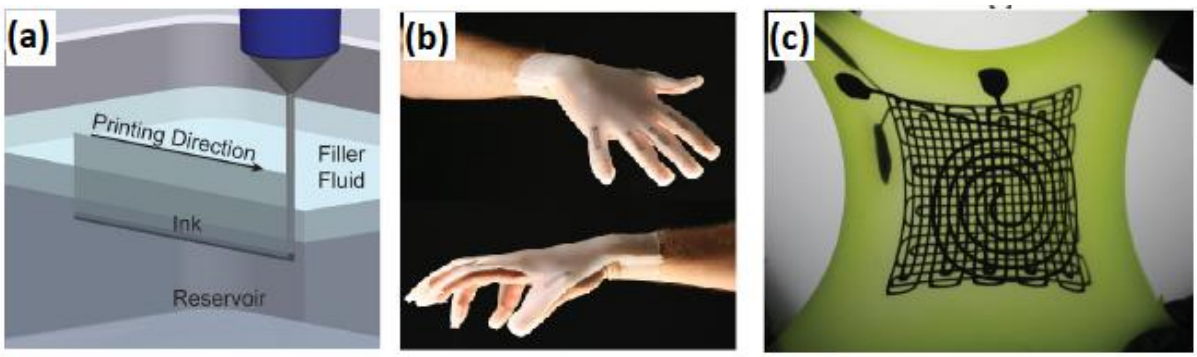

Figure 1-5: Embedded 3D printing process and 3D printed highly stretchable electronics. (a) Schematic diagram of the embedded 3D printing process. (b) Gloves with embedded strain sensors by embedded 3D printing. (c) A 3-layer strain and pressure sensor in the stretched state. Used with permission from [100]. Copyright (2014) Wiley.

1.3.2 Molded Interconnect Devices (MIDs)

A more common way to integrate electronics and 3D structures is the fabrication of Molded Interconnect Devices (MID). In this method, an injection molded thermoplastic involving conductive materials can provide electrical and mechanical properties. This approach can be realized by two different methods, including two-shot injection molding and Laser Direct Structuring (LDS).

In two-shot molding, two polymers are combined and molded together and result in a single object. Usually the one that is shot into mold is not platable. However, the strength of polymer to polymer bond and the interface quality are challenges in this method.

In the LDS method, at first, a single shot molding fabricates the physical part. Then, the laser projects the desired pattern onto the physical object, this pattern will be used for the conductive traces. Thereafter, in the metallization step, the plastic part will be plated with copper. However, limited diversity of usable materials, the requirement for advanced tools, the necessity for chemical plating, and multi-step processing are the main challenges[101][32].

1.3.3 Embedding Electronics into 3D Structure Cavities

This strategy usually is a hybrid manufacturing system that uses two or more technologies. Initially, there is a monolithic 3D structure with cavities created during the fabrication, usually 3D printing techniques. Then, the physical electronic components are embedded into the cavities or onto the surface; the components usually are discrete and surface mount technology (SMT) components. Finally, the interconnections and conductive tracks are deposited by another technology in order to connect the discrete SMT devices. In fact, the 3D structure acts as a package or housing for the electronic components.

However, as can be seen, this approach still uses traditional silicon fabrication as it requires conventional electronic components. Therefore, almost every limitation of traditional electronics is valid in this methodology. The disadvantages of this technique include lack of flexibility, extra steps, high price, and limited design[20][102]–[106].

Espalin et al. [20] used an automated manufacturing platform, namely multi^{3D} system. This platform uses two different FDM technologies to fabricate products, a computer numerical control router and a precision dispenser. It fabricates 3D multifunctional structures in five steps: (1) In the first step, the base 3D structure is built using the FDM technology; (2) The CNC machine micromachines and etches the pattern including channels and cavities; (3) the dispensing system then fills the channels with conductive inks; (4) subsequently, the physical electronic components are placed into their related location and the conductive traces join the components, forming the circuit; (5) In the final step, the deposited conductive ink undergoes thermal curing. This platform aimed to fabricate conformal applications in aerospace engineering. The fabricated products can have different functionalities including electronic, mechanical, electromagnetic, and thermal.

Figure 1-6(a) shows the process flow of fabrication by multi^{3D} system. Figure 1-6(b) shows a final fabricated product by multi^{3D} system.

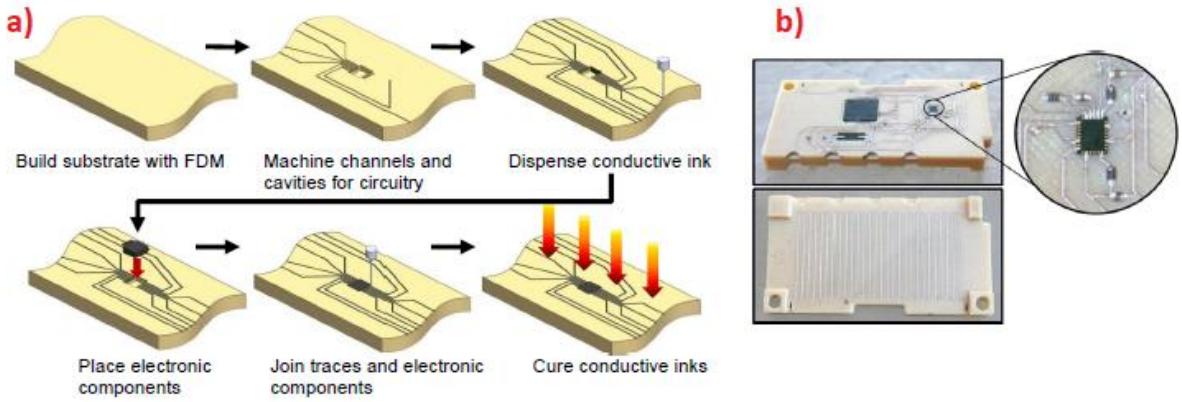

Figure 1-6: Fabrication of 3D structures with electronics by multi^{3D} system. (a) Process flow for fabrication of 3D printing electronics using FFF and conductive inks by multi^{3D} system. (b) The fabricated part. Reprinted by permission from [20]. Copyright 2014, Springer Nature.

Wu et al. [106] used AM techniques to fabricate 3D multifunctional devices including resistors, capacitors, inductors, circuits, and passive wireless sensors, as shown in Figure 1-7(b-c-d). This manufacturing method uses a fused deposition modeling technology along with a multiple-nozzle system. The manufacturing systems fabricates the 3D structures consisting of supporting and sacrificial structures. In the next step, the sacrificial materials are removed. Thereafter, silver particles are injected through the cavities formed and solidify to create the conductive elements and traces, as shown in Figure 1-7(a). This method fabricated various devices including an inductor-capacitor-resonant tank with a resonance frequency of 0.53 GHz. Moreover, they also fabricated a 3D smart cap that installs on top of liquid food packages in order to monitor the quality of the liquid food wirelessly, shown in Figure 1-7 (e).

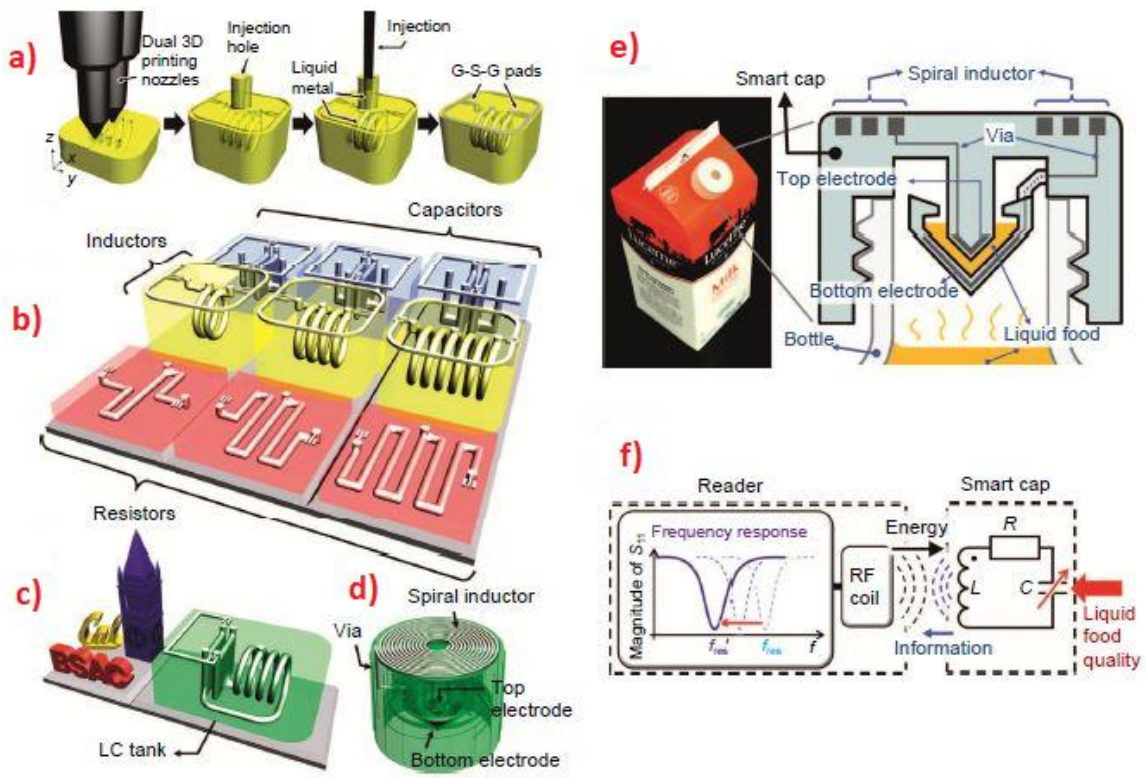

Figure 1-7: 3D fabrication process by the means of filling of liquid metal paste for manufacturing basic electronic devices. (a) 3D manufacturing process with embedded and conductive structures. (b) Fabricated 3D electronic devices including capacitors, inductors, and resistors. (c) A 3D inductor-capacitor tank. (d) Demonstration of a "smart cap", wireless passive sensor involving a 3D printed LC resonant circuit. (e) Practical application of a smart cap on a milk package, and the schematic diagram of cross-section. (f) The sensing principle and the equivalent circuit diagram. Reprinted with open access from [106]. Copyright 2015, Springer Nature.

Lopes et al. [103] used a hybrid manufacturing method integrating SLA with direct print (DP) dispensing system. The aim of this hybrid method was to fabricate 3D embedded electronic structures. Generally, the SLA system fabricates the 3D structure while the DP systems creates the conductive traces and interconnects. As the electronic devices are inside the 3D structure, the SL systems needs to work with multiple starts and stops in several repeats. In each repeat, various processes take place: (1) the uncured resins are removed using a vacuum systems; (2) the electronic components are inserted into the receptacles and vias; (3) the SL continue to embed the electronic

components and form channels; (4) SL stops to clean the channels and top surface; (5) DP starts to fabricate the interconnects; (6) the ink traces are cured via SL laser. This six steps repeat until the product is complete. At the end, this hybrid system succeeded to fabricate functional 2D and 3D 555 timer circuits packaged inside 3D SL substrates, as shown in Figure 1-8 (a-b-c).

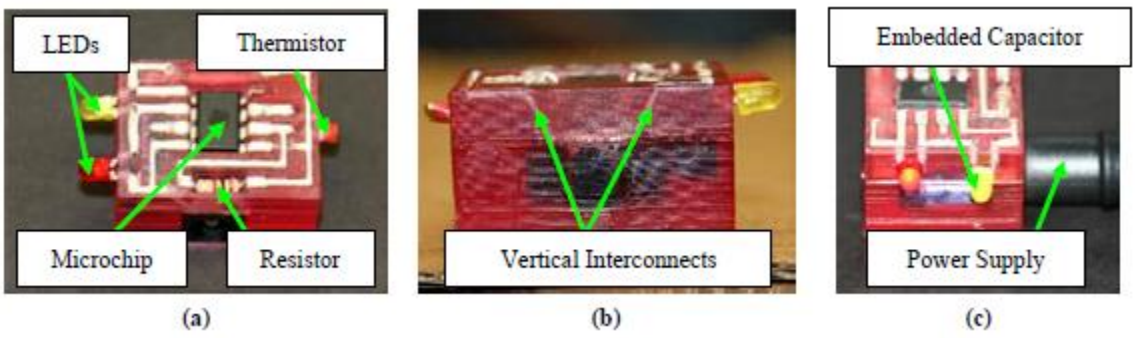

Figure 1-8: Fabrication of 3D structural 555 timer circuit packaged inside SL substrates. (a) 3D 555 timer circuit. (b) Cross-sectional vertical interconnects. (c) Working 3D 555 timer circuit. Reprinted with permission from [103]. © Emerald Publishing Limited all rights reserved.

1.3.4 Depositing Functional Inks by Printed Electronics Technologies

The most innovative method to integrate 3D structures with electronics is to use PE technologies, in order to deposit functional inks onto 3D substrates. Non-contact and maskless technologies including extrusion printing, aerosol jet printing, and inkjet printing are able to deposit ink on almost any substrate material or geometry. Thanks to this combination, the limitations mentioned in previous sections can be removed. Although this technology achieves virtually all advantages of additive manufacturing methods, each of the PE methods has different characteristics such as resolution and material types.

Paulsen et al. [107] used aerosol jet printing technology to fabricate electronics onto 3D substrates. Aerosol jet printing is a novel, non-contact, maskless technique with the aim of printing onto conformal substrates. Firstly, this method converts the ink in the atomizer into a dense aerosol of tiny droplets. Next, the aerosol of ink is focused by aerodynamics in the nozzle, and finally, it will spray onto the substrate. In this work, they printed silver nanoparticle ink onto non-planar surface

and orthogonal surface. The fabricated various devices onto 3D structures including a phase-array antenna, capacitive sensors, and a 3D sensor structure. Some fabricated conformal applications in this work are illustrated in Figure 1-9.

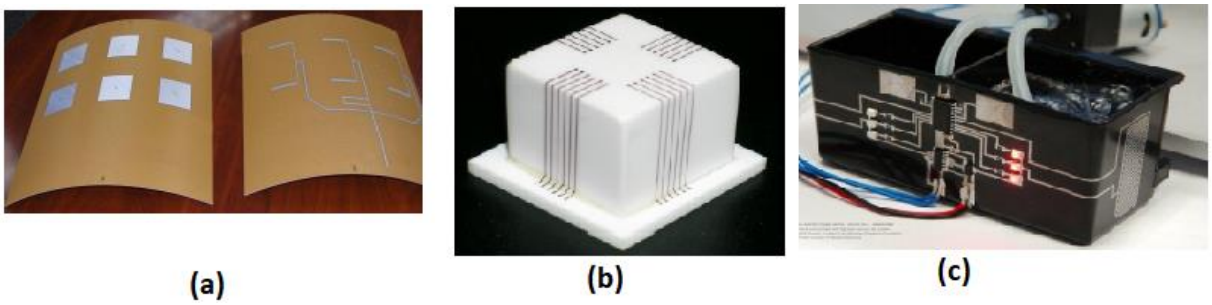

Figure 1-9: Printing conformal electronics onto 3D surfaces by aerosol jet technology. (a) Phase-array antenna embedded onto a rigid and cylindrical surface. (b) Conductive lines printed on orthogonal surfaces of a ceramic cube. (c) Printed fluid level sensors on a 3D structure. Reprinted with open access from [107] © 2012 IEEE.

1.3.4.1 Integration of Inkjet Printing with 3D Printing Technology

As mentioned in Section 1.2.2.5, inkjet printing as a non-contact and digital technology is gaining interest in low-cost, large-area fabrication of high-performance electronic components and systems with improvement in cost and functionality. Combination of inkjet printing technology with FFF 3D printing opens up new possibilities for conformal electronics embedded in complex 3D structures. We review some of the previous work on the integration of inkjet PE technology with 3D manufacturing.

1.3.4.1.1 Inkjet Printing and Fused Filament Fabrication

Roach et al. [108] proposed an innovative technique to integrate inkjet printing with 3D FFF technology. In this work, they could not directly print conductive silver ink onto the 3D printed polyetherimide (PEI) substrate due to significant surface roughness of the 3D substrate. As a consequence, they performed a surface modification process in which they inkjet printed an intermediate layer, polyimide (PI), between the 3D PEI substrate and the conductive silver ink. They also deposited another layer of Polyethylene (glycol) Diacrylate (PEGDA) as the protection between PI and PEI layers. Having carried out the surface modification, they obtained a highly

smooth surface followed by direct ink-write (DIW) printing of silver ink. Finally, they fabricated RF devices only by AM technologies. Figure 1-10 displays the process flow of this proposed technique including (a) PEI substrate fabrication, (b) inkjet printing of PEGDA, (c) inkjet printing of PI layer, and (d) DIW printing of silver ink.

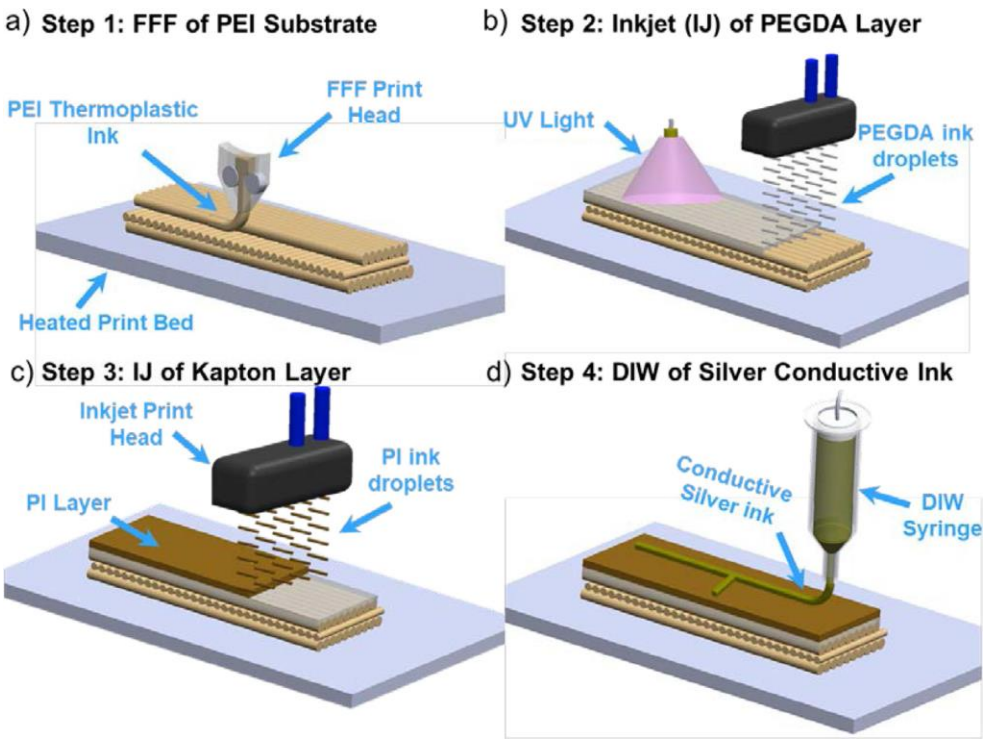

Figure 1-10: Process flow for fabricating printed RF devices onto FFF printed substrate. (a) FFF 3D printing of PEI substrate. (b) Inkjet printing of PEGDA layer over the PEI substrate. (c) Inkjet printing of PI (Kapton) layer onto the PEGDA layer. (d) DIW printing of silver NP ink to fabricate the final device. Reprinted from [108]. Copyright 2020, with permission from Elsevier.

At first, a standard PEI filament is used for the FFF 3D printer to fabricate the substrate. For comparison purposes, they directly printed the AgNP ink onto the PEI substrate by DIW 3D printing. The resulting silver traces were with low conductivity due to present voids and had poor geometries. Therefore, a surface modification is required to make a smooth enough surface for AgNP traces.

In order to make the PEI 3D surface smooth, they printed three layers of PEGDA by the inkjet printer and cured over the untreated PEI printed substrate. The profilometer showed a surface roughness of 5 µm which is a very smooth surface.

Thereafter, they inkjet printed PI, also known as Kapton which is a common material in the electronics industry as an isolator layer and as a protective coating due to its robust properties. They used polyamic acid (PAA) which is a common pre-cursor to PI for the PI printability by inkjet printing. They inkjet printed two layers of PAA ink onto the PEGDA surface. The sample then was baked under 130°C to transform PAA into PI material.

Once the drying and curing are done, AgNP can be printed onto the PI surface. Measurements showed that silver traces on the PI surface have a good trace geometry. Besides PI surface has gained a good adhesion to the PEI substrate. AgNP ink is printed by a high-resolution DIW printer. The results showed the silver ink achieved the minimum resolution of 100 µm. They also studied the extrusion pressure required for different line widths and the nozzle sizes, as shown in Figure 1-11(a).

Finally, to test the methodology, they fabricated RF microstrip lines, as shown in Figure 1-11(b). They fabricated the RF microstrips on both unmodified PEI substrate and PI-modified PEI substrate for comparison purpose, as shown in Figure 1-11(c-d). Moreover, they measured the RF power of devices across 1-6 GHz in order to estimate the dissipative loss of devices, as shown in Figure 1-11(e).

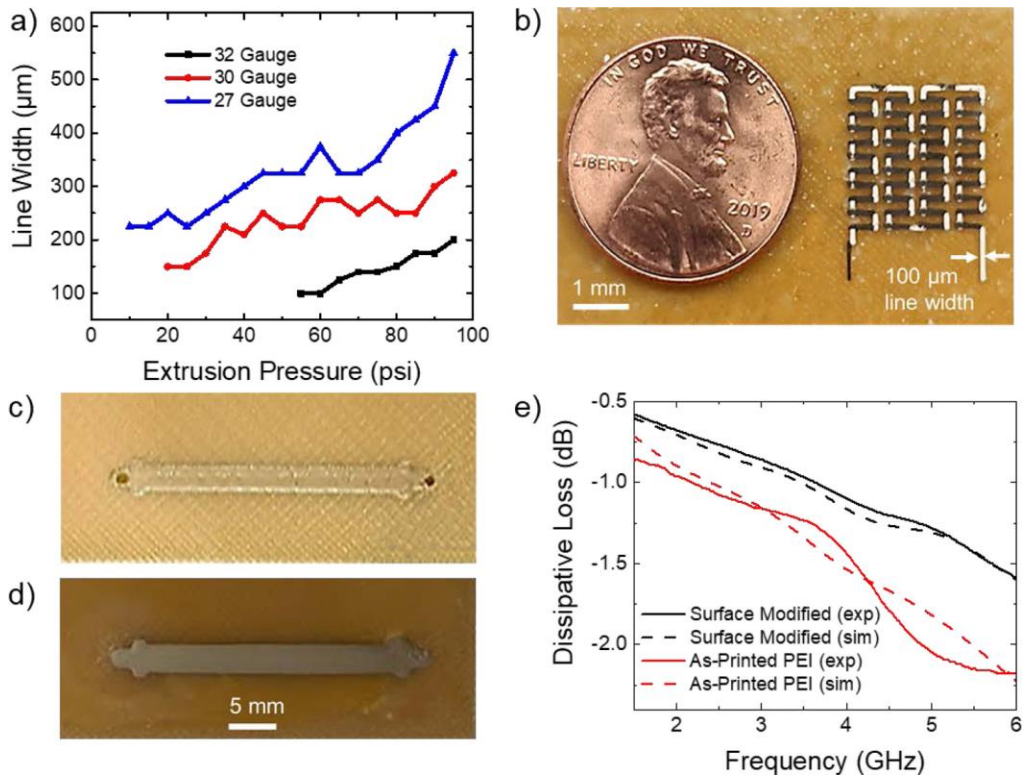

Figure 1-11: Fabricating RF microstrips on FFF 3D printed PEI substrate. (a) Effect of DIW extrusion pressure and the nozzle size on the width of DIW printed silver lines. (b) A fabricated high-definition thermocouple with 100-µm-width lines. (c) Printed RF microstrip onto unmodified PEI substrate. (d) Printed RF microstrip onto modified PEI substrate. (e) Experimental and simulated RF measurements including transmission loss for RF traces printed onto modified PEI substrate. Reprinted from [108]. Copyright 2020, with permission from Elsevier.

Although this study integrated printed electronics with 3D FFF technology, it has some drawbacks compared to our proposed method as follows:

(1) They used two intermediate layers, PEGDA and PI layers, while we use only one intermediate layer. Therefore, our method uses less materials usage and has fewer steps.

(2) Not only the intermediate materials is more in this method, but also it imposes more curing steps to cure each layer as well, which results in increased manufacturing time and complexity. In this method, the PI layer needs 60 minutes of curing and the PEGDA layer needs a small amount of time for UV curing, while in our method the UV curable adhesive only needs 120 seconds of

curing. In this method, the PEGDA layer needs to be UV cured, and the PAA layer requires two different baking steps (at 80℃ for 20 minutes and at 130℃ for 40 minutes) to be converted to PI. Therefore, this method increases both the manufacturing time and complexity.

(3) Besides, as they deposit the two intermediate layers by inkjet printing which is a low throughput technology, it takes more time. While we use extrusion printing to deposit the intermediate layer, which makes the process faster.

(4) As they used a DIW technology to print the silver ink, they achieved a low resolution, 100 µm. While our proposed method is able to obtain the minimum feature size of 60 µm, the nozzle orifice diameter.

In summary, our novel method requires less materials and hence complexity. The manufacturing time of our method is also considerably reduced as it needs fewer curing steps and uses extrusion printing technology. Finally, our technology fabricates electronics with higher resolution.

1.3.4.1.2 Inkjet Printing and 3D stereolithography

Jeong et al. [109] used a hybrid methodology to integrate SLA with inkjet printing technology. In this work, they 3D printed a 3D flexible structure as the base substrate. Next, in order to decrease the surface roughness of the 3D substrate, they inkjet printed an intermediate layer, SU-8, onto the 3D substrate followed by UV curing. Finally, they successfully inkjet printed conductive silver traces onto the substrate. As the application, they printed a square ring as the metamaterial absorber (MMA) unit cell and fabricated an electromagnetic (EM) pressure sensor. Figure 1-12 displays the general process flow of this novel technique, and Figure 1-13 shows the device design and geometry.

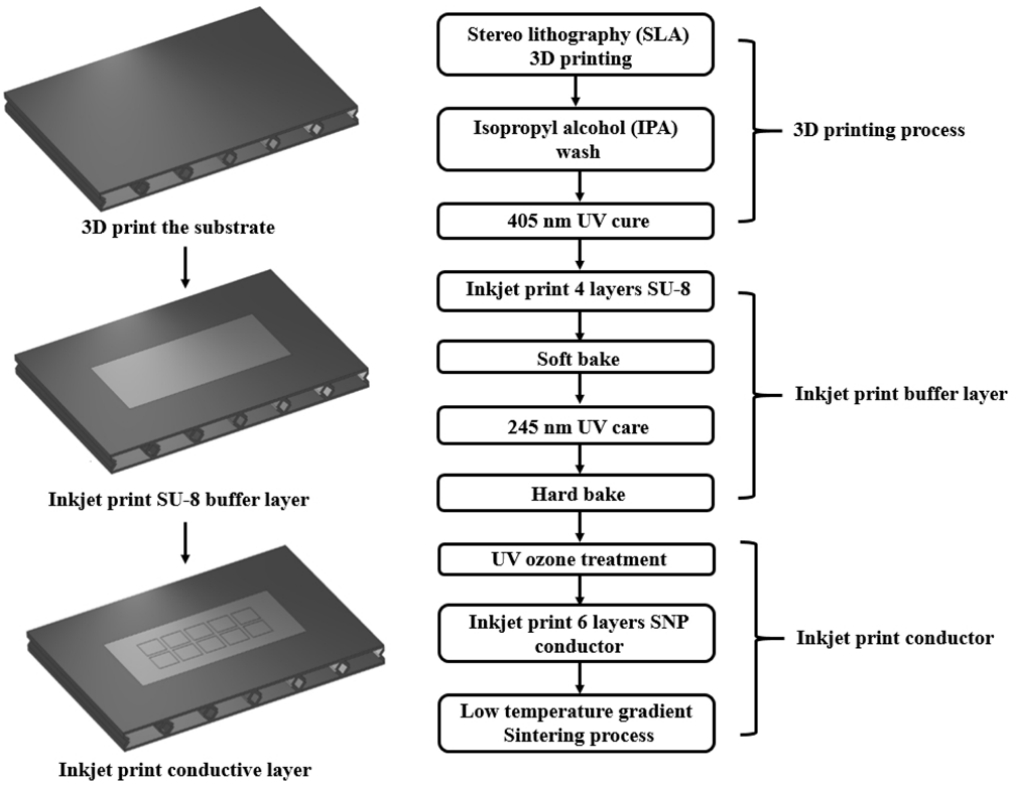

Figure 1-12: Process flow for the fabricated hybrid (3D and inkjet) printed EM sensor. Reprinted from [109]. Copyright 2020, with permission from Elsevier.

Initially, Jeong et al. fabricated the substrate by the SLA 3D printing system using flexible photopolymer resin, which is a rubber like elastomer. The 3D substrate goes under the usual wash process and cure post-processing, as such processes considerably improve the printed substrate accuracy, structural strength, and consistency, and reduce the EM losses resulted from improved polymer cross-linking.

Although the surface of the obtained 3D substrate was relatively smooth (nearly RMS= 42 µm), it was not smooth enough for the inkjet printed silver nanoparticle (AgNP) ink with 0.8 µm thickness. Therefore, an intermediate material is required between the 3D surface and the conductive tracks. They deposited SU-8 layers onto the 3D surface and measured the surface roughness by a stylus profilometer. The inkjet printed four layers of SU-8 and achieved a smooth enough surface (RMS < 1.6 µm). Thereafter, the SU-8 is cured in two baking steps, soft and hard baking, under 95°C for 5min and 10min, respectively.

They performed ultraviolet ozone treatment in order to improve the AgNP ink wettability and adhesion without degrading the resolution. However, this process reduced the AgNP contact angle on the SU-8 surface from 46° to 29°.

Subsequently, they inkjet printed AgNP layers via a Dimatix 2800 inkjet printer with 20 µm drop spacing.

For sintering the conductive patterns, AgNP inks usually need a high temperature around 180°C to achieve the best conductivity and adhesion. However, such high temperature is able to reduce the elasticity significantly, causing the structure to break under compression, also causing the substrate shrinkage and therefore crack AgNP traces. Hence, they cured the samples under 90°C for a longer time to avoid the mentioned consequences.

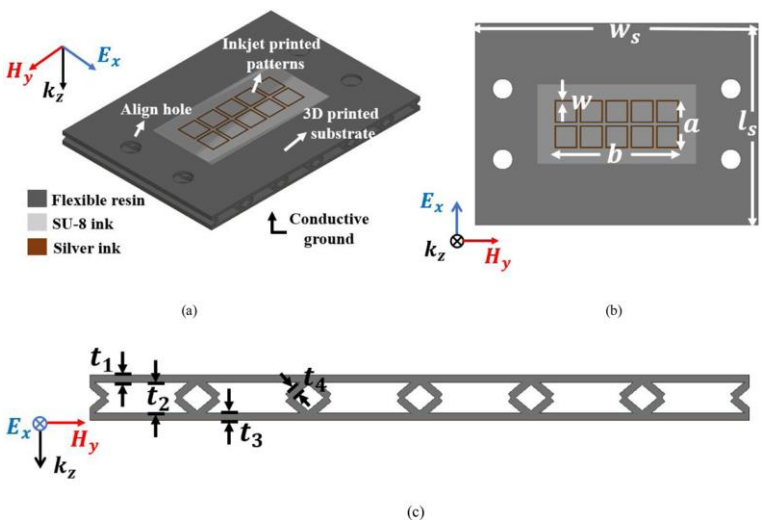

Figure 1-13: The EM pressure sensor geometry. (a) Perspective. (b) Top view. (c) Side view. Reprinted from [109]. Copyright 2020, with permission from Elsevier.

The final product, shown in Figure 1-14, was an EM pressure sensor that achieved $7.75*10^8$ Hz/mm sensitivity and the results were consistent for beyond 100 cycles because of the resilience resulted from the elastic force of the 3D printed material. In conclusion, the fabricated device had sufficient sensory value and successfully passed the experimental validations.

(a) (b)

Figure 1-14: The final fabricated EM pressure sensor. (a) Top view. (b) Side view. Reprinted from [109]. Copyright 2020, with permission from Elsevier.

While in this work, Jeong et al. integrated printed electronics with 3D printing technology, it has some disadvantages compared to our method:

(1) They used SLA 3D printing technology, while we used FFF technology. SLA printed products require post processing steps including rinsing in IPA and 405 nm UV curing, whereas FFF technology does not need any post printing step.

(2) They used SU-8 as the intermediate layer, while we used UV curable adhesive to reduce the surface roughness. In our method, we simply UV cured the adhesive, while SU-8 used in their method required multiple complex steps: soft baking at 95℃ for 5 minutes, UV curing under 254 nm, and hard baking at 95℃ for 10 minutes. Besides they also performed a UV ozone treatment to improve the substrate wettability and adhesion. But in our method, we just UV cure the intermediate layer for 120 seconds.

(3) Besides, this technique imposes the limitations of the SLA technology. SLA technology has higher price of equipment and materials, and the materials range and colors are more limited compared to FFF technology.

In general, this method requires more steps and material. It also increases the manufacturing time and complexity compared to our proposed method.

1.3.4.1.3 Inkjet Printing and 3D FDM Printing

Mangoma et al. [110] used a hybrid AM method to integrate inkjet printing with 3D FDM printing. In this work, they fabricated organic electrochemical transistors (OECTs) using this hybrid technique. The FDM printer prints the dielectric and conductor layers while the inkjet printer prints the semiconductor layer. The aim was to obtain low-cost and low-power computational devices with the help of flexible and digital manufacturing techniques. Figure 1-15 displays (a) the schematic design of OCET, (b) fabricated OCET, and (c) flexibility of fabricated OCET.

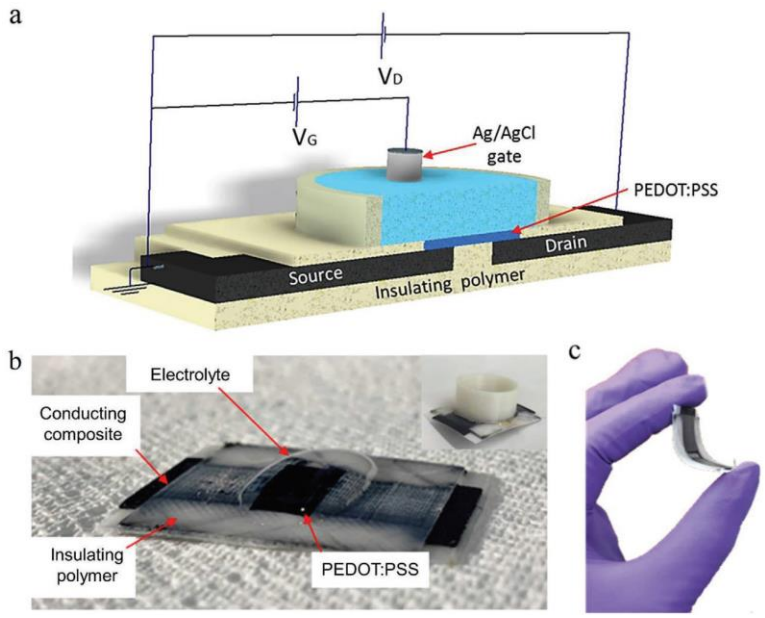

Figure 1-15: The fabricated printed OCET device. (a) Schematic of the designed OCET. (2) The fabricated device by 3D printing and inkjet printing. (3) Displaying the final device flexibility. Reprinted with open access from [110]. Copyright 2020, John Wiley and Sons.

At first, the FDM printer printed the bottom layer of insulating thermoplastic co-polyester (TPC), as the insulating polymer substrate. The FDM printer then prints a conducting layer, carbon-filled polylactide resin composite (c-PLA), as the source and drain on top of the insulating layer.

Before the inkjet printing process, in order to enable the formation of semiconducting thin film across the channel, a corona treatment was used with 21 kV under ambient air. Hence, the c-PLA areas were covered with masking tape in order to prevent any damage from the plasma process.

In the next step, a FUJIFILM DMP-2850 inkjet printer prints a commercially available semiconducting ink, PEDOT: PSS, to function as the active layer which connects the c-PLA previously printed source and drain. During the printing, multiple nozzles were used with a drop spacing of 15 µm.

In the last step, insulating TPC again is FDM printed on top of layers in order to insulate source and drain electrodes, and to create a well for the electrolyte (phosphate-buffered saline (PBS)). Lastly, an Ag/AgCl pellet is used for the gate electrode. The fabricated sample finally is baked under 130°C.

For the measurement process, a semiconductor device analyzer carried out the device characterization. The testing was repeated 10 times over a one-month period to ensure the device stability. The characteristics results of the transistor are shown in Figure 1-16 including (a) current response to a single pulse, (b) output characteristics, and (c) transfer characteristics.

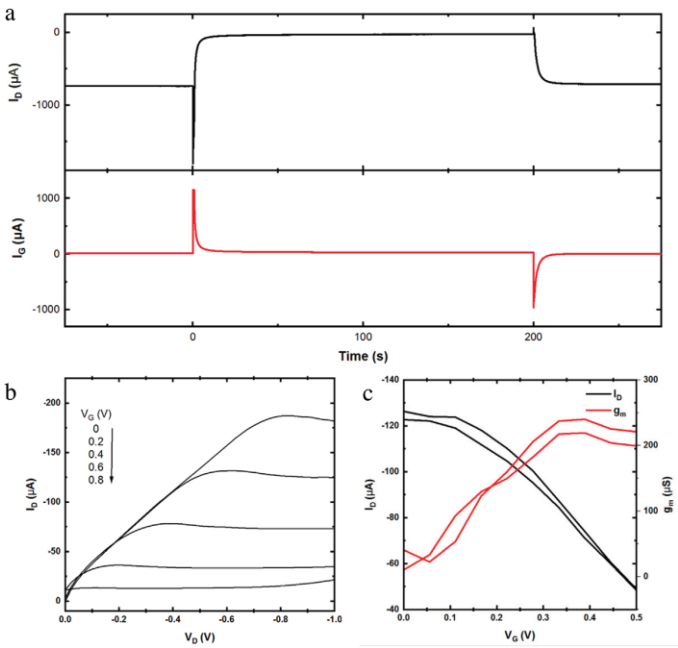

Figure 1-16: The device characteristics. (a) Response to a single gate pulse. The amplification in I_d is obvious. Also to indicate the neuromorphic behavior of the device, a spike and recovery trend is visible around T=0. (b) Output characteristics. (c) Transfer characteristics. Reprinted with open access from [110]. Copyright 2020, John Wiley and Sons.

In this work, while Mangoma et al. integrated printed electronics with FFF 3D printing technology, it has some drawbacks compared to our proposed method. In this method, Mangoma et al. deposited c-PLA by a FDM printer as the conductive material, while we used AgNP ink by an inkjet printer.

(1) As they used c-PLA, they obtained a high resistivity, 0.18 Ω.m; while we achieved a resistivity of 0.44 μΩ.m for our conductor, AgNP ink, in our proposed method.

(2) Since they deposited the conductor by the FDM printer, the resolution was limited, nozzle diameter of 0.4 mm, while the resolution in our method was much higher with the nozzle diameter of 60 μm.

In summary, our novel method provides a much lower resistance for the conductive material, which is the key element in PE. Moreover, our approach has a considerably higher resolution to deposit the conductive layer.

1.4 Thesis Organization

This work attempts to fabricate electronic devices via different methods of additive manufacturing including 3D FFF printing, extrusion printing, and inkjet printing, focused on the integration of 3D FFF printing and inkjet printing. This novel technology opens up new possibilities and provides advantages including fabricating 3D electronics with complex geometries, customizability, freedom of design, reduced fabrication time, reduce cost, and reduced footprint.

This thesis consists of five chapters:

Chapter 1 includes thesis introduction, research motivation, background and literature review, and research objectives.

Chapter 2 presents successfully inkjet printing simple lines onto a 3D FFF printed substrate.

In order to achieve well-patterned lines with high conductivity, various materials under different conditions are studied to achieve this goal. Materials include direct 3D printed PLA, 2-component epoxy, heat curable epoxy, and UV curable epoxy under different curing conditions. After obtaining a conductive line on a 3D printed substrate, in this chapter optimization steps are described to achieve the highest conductivity and a good line morphology. The optimization step generally includes different pre-processing and post-processing steps to obtain a high conductive and well-patterned line. More specifically, it includes UV time exposure, drop spacing, heating conditions, intense pulsed light parameters, and length shrinkage.

Chapter 3 describes the fabrication process and the related measurements of a strain gauge on a 3D printed substrate. It takes advantage of conditions obtained in the previous chapter to fabricate the desired electronic device in order to display this integration work properly and is reliable. To improve the strain gauge, some improvements for patterning are required. At the end, after the fabrication is properly done, the test measurement takes place. The measurement step includes mechanical test and electrical measurement to ensure the device functions well.

Chapter 4 studies another 3D printing electronic technology to compare with the proposed method in previous chapters. In this chapter, a strain gauge sensor is fabricated by 3D printing electronics only. At first, a functional semi-conducting filament is created for 3D FFF printer. The functional filament is made out of TPU/CNT nanocomposite. After manufacturing the 3D printed piezoresistive strain sensor, it undergoes mechanical test and electrical measurements.

Chapter 5 summarizes the key results of this thesis and introduces directions for future work.

Chapter 2: Inkjet Printing a Conductive Line onto a 3D Printed Substrate

2.1 Introduction

Inkjet printing onto a 3D fused filament fabrication (FFF) printed substrate provides various advantages and possibilities including customizability, freedom of design, reduced cost, easy manufacturing process, reduced manufacturing time and material, and producing electronics with complex geometries.

Inkjet printers are able to deposit inks with different electrical properties including conductors, semiconductors, and insulators or dielectrics as well as optoelectronic materials. Each electronic device is composed of one or multiple functional layers of materials. For instance, transistors need all three types of electrical properties including conductor, semiconductor, and insulator, as the structure is shown in Figure 2-1. As another example, RF inductors and capacitors require two materials including insulator and conductor [7]. While most sensors can be fabricated by only one material of conductors or semiconductors.

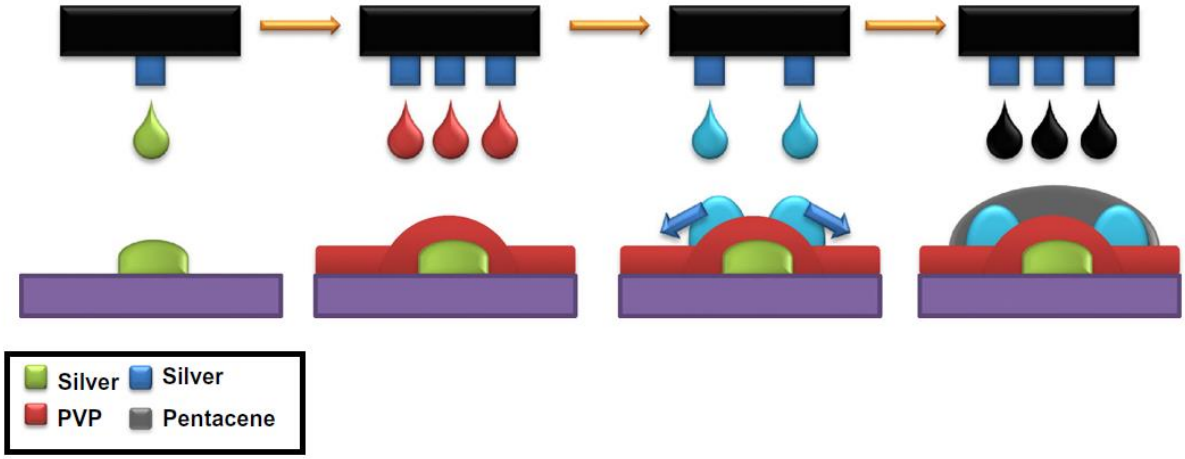

Figure 2-1: Fabrication process of an inkjet printed transistor. Silver nanoparticles, PVP (Polyvinylpyrrolidone), and Pentacene are used as the conductor, dielectric, and p-type semiconductor, respectively. Silver is used for electrodes of gate, source, and drain. PVP layer insulates the electrodes. Finally, Pentacene forms the p-type channel. Reprinted from [9]. Copyright 2011, with permission from Elsevier.

In various techniques of PE, inks are the most important element because they significantly affect printing conditions and the printed device quality. Therefore, choosing the right ink with suitable characteristics, including viscosity and surface tension as well as electrical properties, is of great importance. For each purpose, a different property is required such as high conductivity for conductors, high mobility in semiconductors, and low leakage in dielectrics.

In addition, making a material printable by PE techniques is another challenge. To make the materials printable, every ink has a specific formulation with a complex mixture of additives and ingredients such as additives and solvents, resins, and oils. For instance, solvents are key to control the rheological properties of the ink.

Inks also could be organic or inorganic for each electrical property. For inorganic conductors, there are metal nanoparticles, metal flake, and metal nanowires; while organic conductors include polymers. For semiconductors, small molecules and polymers or in more advanced case polymer-small molecule blends are available.

Conducting materials are of special importance in PE as they are used in almost every device as well as wiring. Conducting materials in PE include metallic nanoparticles such as Ag, Cu, and Au, conductive polymers such as PEDOT/PSS (poly(3,4-ethylenedioxythiophene) polystyrene sulfonate), metal oxides, and carbon materials.

The most important feature in conductive materials is conductivity. Metallic nanoparticle (NP)-based inks are the most common conducting inks in PE as they have the highest conductivity compared to other available materials. Table 2-1 compared common conducting inks in terms of electrical conductivity.

Table 2-1: Comparison of electrical conductivity in various available inks in PE. Numbers for metal NPs are for bulk conductivity. Reprinted/adapted by permission from Springer Nature Customer Service Centre GmbH: Springer Nature, Conducting Materials for Printed Electronics by Katsuaki Suganuma [COPYRIGHT] 2014 [2].

Type	Material	Electrical conductivity (Siemens/cm)
Metal NP	Silver (Ag)	$6.30 * 10^5$
Metal NP	Copper (Cu)	$5.98 * 10^5$
Metal NP	Gold (Au)	$4.52 * 10^5$
Metal NP	Aluminum (Al)	$3.50 * 10^5$
Metal NP	Platinum (Pt)	$1.00 * 10^5$
Organic	PEDOT/PSS	$1\text{-}10^3$
Ceramics	ITO	$10^3\text{-}10^4$

Ag inks are the most common ink in PE as they have the highest electrical conductivity, shown in Table 2-1, and they have a lower cost than Au inks. Besides, AgNP inks have better air stability and easier sintering process compared to Cu inks.

After the printing process, NP inks need post-printing processes to be annealed. Annealing is required to evaporate the solvent, dissociate and evaporate ligands, and sinter the film. Although for the drying process a lower temperature, as low as 60 °C, for a limited time is required, for the sintering step usually a higher temperature in some cases up to 200 °C is needed to obtain the highest conductivity, as shown in Figure 2-2.

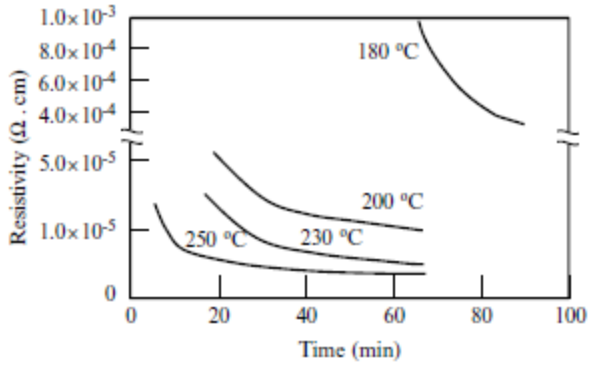

Figure 2-2: Sintering trend for a typical AgNP ink as a function of heating time. Reprinted by permission from [2]. Copyright 2014, Springer Nature.

However, the sintering process can be carried out by photonic sintering instead of traditional thermal sintering with a temperature of nearly 200 °C. In fact, thermal sintering has two main disadvantages; it takes a long time and might damage the substrate. However, photonic sintering, also known as Intense Pulsed Light (IPL), uses high-intensity light pulses and is able to solve the problems of high temperature harmful for substrates as well as the long time required.

On the other hand, one challenge of NP inks, including AgNP ink, is that they use different solvents as mentioned previously. Some of the solvents might be aggressive and, consequently, attack the substrate.

Therefore, it is necessary that the substrate used for AgNP inks to be chemically resistant. Chemical resistance is the ability of a material to not be chemically attacked, dissolved, or react with the solvent. A polymer with low chemical resistance, when exposed to specific solvents and materials, might start swelling which causes absorbing the solvent and changing the original mechanical properties and shape. In the PE area, the worst part is that such swelling and reaction also negatively affects the solvent and ink and might degrade the functionality. Hence, it is important to use chemically resistant substrates to avoid both substrate swelling and ink degrading.

To sum up, printing conductive inks onto 3D printed substrates is challenging due to two reasons: (1) Most nanoparticle inks, including AgNP ink, are highly aggressive and consequently can attack and dissolve the surface of the 3D plastic material, here polylactic acid (PLA); therefore, the

conductive ink deposited onto the 3D substrate loses its functionality and cannot conduct. (2) The surface of a 3D printed object is usually rough and is not suitable for fine patterns of electronics particularly for inkjet-printed patterns. In practice, we performed this experiment, printing AgNP ink directly onto a 3D printed substrate, and observed both problems happening in Section 2.3.1.

Therefore, an intermediate layer is required to be chemically resistant and have a smooth surface. In this chapter, we used such intermediate layer to overcome the aforementioned problems and consequently print conductive lines onto 3D printed substrates.

2.2 Methodology

In this chapter, the aim is to successfully inkjet print AgNP ink onto a commercial PLA 3D FFF printed substrate by AgNP ink; more specifically, we aim to achieve conductive lines with good morphology and high conductivity onto a 3D substrate.

In order to achieve this goal, there are various challenges including unwanted chemical reaction of the conductive ink with the substrate, low conductivity of printed lines, and poor morphology of lines. To overcome the challenges, we will need to perform different processing steps explained with details and reasons in their related sections. After finding the solutions and optimal methods, we found the final workflow as displayed in Figure 2-3.

The first step is to 3D print the desired substrate with a customized design by a 3D FFF printer. Thereafter, an intermediate layer, to overcome the problems of the 3D printed substrate surface, is deposited onto the previously 3D printed substrate by the Voltera extrusion printer. The printed intermediate layer, which is an ultraviolet (UV) curable epoxy, then is cured by UV light. Having the substrate prepared, now we inkjet print the AgNP ink onto the substrate and create the desired pattern. Subsequently, we dry the printed silver ink by thermal annealing using an oven in order to evaporate the solvent from the ink materials. Thereafter, to sinter the printed films which results in increased conductivity, we perform IPL process via the Xenon flash lamp. Finally, we electrically measure the fabricated samples to compare and optimize the electrical conductivity.

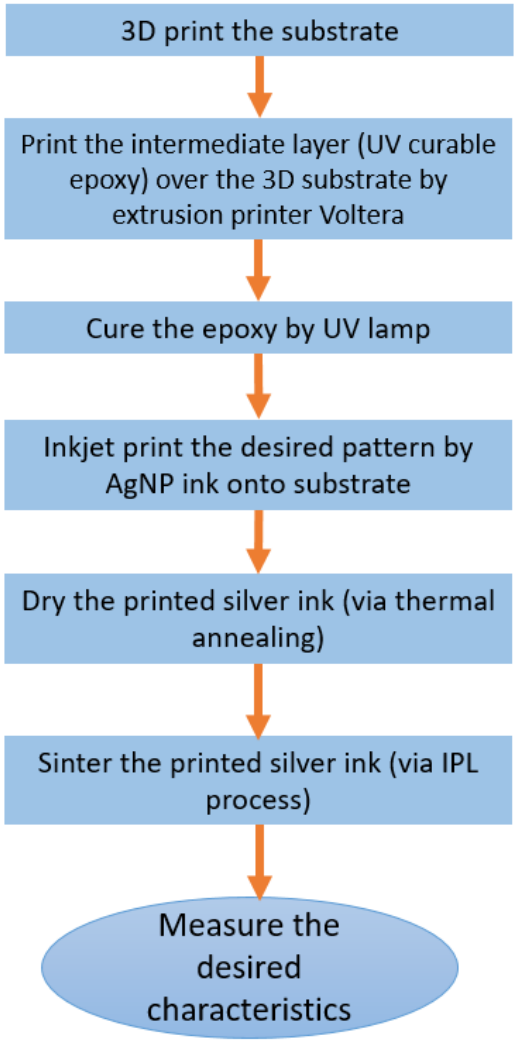

Figure 2-3: The workflow of steps required to successfully inkjet print AgNP ink onto a 3D printed substrate.

2.2.1 3D Printing

In this thesis, all 3D printed parts are fabricated by FFF method, which builds the objects layer by layer from bottom to top. Parts are created by UltiMaker 3 (Ultimaker, Utrecht, Netherlands) with print core AA 0.4.

Initially, the model of the desired part is designed in a computer-aided design (CAD) software, such as SolidWorks, which outputs an STL format file.

The CAD file is imported to the software Cura in which the material and other settings are chosen. The output would be a gcode format file.

Finally, the gcode file is imported to the 3D printer. Then, the 3D printer starts the printing process with the settings determined in the software.

2.2.2 Inkjet Printing AgNP Ink onto 3D Substrates

In order to inkjet print AgNP ink onto a 3D PLA substrate, there are two challenges: (1) The surface of the 3D printed substrate is not smooth enough for PE application. (2) The AgNP ink including its solvents might attack the PLA substrate.

Due to the properties of 3D FFF printing technology, the surface of fabricated parts is rough. In general, it is not an important issue, but for our application of fabricating microelectronic devices, it is vitally important.

As the second challenge, the AgNP ink (ANP DGP 40LT-15C) attacks the PLA surface. The AgNP ink is inkjet printed via a customized inkjet printer with a 60µm-diameter nozzle (MJ-ATP-01-60-8MX, MicroFab Technologies, Inc., Plano, TX) onto a 3D printed PLA substrate. The AgNP ink (ANP DGP 40LT-15C) containing organic solvents such as triethylene glycol monomethyl ether (TGME) attacks the PLA substrate.

2.2.3 Chemically Resistant and Smooth Intermediate Material

In order to solve both problems, the idea is to use an intermediate material between the 3D substrate and the functional inkjet printed films. More specifically, a low viscosity, chemically resistant dielectric material needs to be deposited onto the 3D substrate. The chemical resistance property of the intermediate material avoids any degrading of the conductivity of the AgNP ink. Besides, the low viscosity property helps that the intermediate material not follow the surface roughness of the 3D substrate, but instead form a smooth layer. By realizing this idea, we will overcome both issues and will be able to successfully inkjet print AgNP ink onto a 3D printed PLA substrate.

Of course, there are limitations on selecting the intermediate material. (1) It should not need thermal treatment for temperatures beyond 80-90°C, depending on the 3D object thickness, as this damages and deforms the PLA object. (2) It must be highly chemically resistant so that it keeps the quality of the AgNP ink and avoids any conductivity degrading. (3) The material should not be aggressive so that it does not damage the PLA surface. The material or its treatment method

should not remove the advantages of our novel integration. (4) The materials should be adhesive so that it remains constantly on the PLA surface. (5) For instance, a material requiring spin coating cannot be used, since complex geometries, which are one of the key motivation for our method, no longer can be used in the spin coating process. (6) Moreover, the material should not have shrinkage or any deformation after the deposition or treatment, as it will distort patterns.

The most suitable option to meet the aforementioned criteria is resin. It is easy to deposit, it does not need a very high heating process, some types are very chemically resistant, and it does not show considerable shrinkage.

2.2.4 Resin Materials

Resins can be divided into three main categories including epoxy resin, polyester resin, and polyurethane resin. Most resins consist of two components, the base resin and the hardener (catalyst), and after combining the two parts, a chemical reaction takes place and the material becomes hard. Moreover, in terms of curing method, resins can be cured typically in two ways, thermal curing and UV curing. Thermally curable resins are usually two-component, while UV curable resins are one component and the UV light exposure begins the chemical reaction

2.2.4.1 UV Curable Resins

UV resin, commonly known as UV curable epoxy, is another promising material as the intermediate, protective material. UV curable resins are materials that cure (polymerize or harden) when they are exposed to UV light. The key advantage is that UV resins are one component, and there is no need for mixing. The time needed for a chemical reaction is much less than that of epoxy resin. UV resins do not require any heating process as it cures by UV light, hence it is preferred for PLA substrates. However, UV resins are less chemically resistant.

There are two main types of UV curing resins in terms of curing mechanism: free radical and cationic. Free radical resins cure very quickly; and when a radical photoinitiator is exposed to UV light, immediately free radicals are formed and the reaction starts; and when the UV is stopped, the polymerization stops. While cationic resins are mainly made of cycloaliphatic epoxies. There is no oxygen inhibition and hence dark cure. When UV light is radiated to cationic photoinitiator, an acid is released which catalyzes the reaction; hence, even when the light is stopped, the polymerization still continues.

It is noteworthy that the UV time required is not the same for every condition. The needed UV time depends on the UV epoxy type, UV light source, the thickness of deposited material, distance from the light source, and UV transmission of substrates of the UV equipment.

The majority of UV curable resins are of free radical type with acrylic compounds. However, sometimes oxygen inhibition, the air stops the polymerization of the top layers (surface) and leave them tacky, happens in radical acrylic types. However, oxygen inhibition happens in radical free products (or acrylate based UV curable products), not in epoxy based UV curable products. The three main types of oligomers in free radical UV resins are acrylated polyester, epoxy acrylate, and urethane acrylate. Urethane acrylate is the most popular one thanks to its great chemical resistance and mechanical properties.

The resin materials that we studied in this thesis are listed in Table 2-2.

Table 2-2: List of resin materials studied in this research.

Name	**Chemical Class**	**Curing Condition**	**Viscosity**
System 2000 Epoxy Resin (Fibre Glast Developments Corp)	Two-component epoxy	12 hours at 60°C	Resin 1,650 cP Hardener 150 cP
UV Cure Epoxy 60-7170 (Epoxies, Etc)	UV curable epoxy	UV light: 2-5 seconds	4,500 cP
UV Cure 60-7114 (Epoxies, Etc)	Acrylated Urethane Adhesive	UV light: 2 seconds	3,000 cP
Multi-Cure®6-630 (Dymax Corporation)	Acrylated Urethane Adhesive	UV light: 3 seconds ; or At 150°C : 15 minutes	500 cP
Multi-Cure®6-621 (Dymax Corporation)	Acrylated Urethane Adhesive	UV light: 2 seconds ; or At 150°C : 15 minutes	800 cP

2.2.5 Extrusion Printer Voltera V-One

In order to deposit various epoxies, we used extrusion printing using V-One printer (Voltera, ON, Canada). Generally, this extrusion printer is for printing onto PCBs and prints its specific commercial inks. However, we are using customized inks for this printer, which will be

challenging. The main issue was the physical properties difference. For instance, V-One printer is designed for high viscosity inks, more viscous than 45,000cP, while the viscosity of epoxies is usually nearly 4,000cP. So the printing settings of V-One needed some changes.

The default settings in V-One software are provided in Table 2-3.

Table 2-3: The default settings in V-One extrusion printer.

Pass spacing	0.15 mm		Anti-stringing distance	0.1 mm
Dispense height	0.08 mm		Kick	0.40 mm
Feedrate	500 mm/min		Soft start ratio	0.10
Trim length	50 mm		Soft stop ratio	0.25
Trace penetration	0.15 mm		Rheological setpoint	0.18

However, the most important parameters to have a consistent and high-quality printing are "*Kick*" and "*Rheological setpoint*", which function as follows:

Kick: This parameter controls the stroke length of the piston of the dispenser, which is the amount of applied pressure to the ink. More compressible and viscous inks need a large kick to be able to initiate flow and force the ink through the nozzle, while low viscosity inks need a smaller kick.

Rheological setpoint: It controls how the printer compensates for the flow rate over time. For high viscosity inks, this parameter needs to be increased if the flow rate reduces over time.

2.2.6 UV Curing Method

In the electromagnetic spectrum, UV light lies in the wavelength range from 100 to 400 nm. Generally, the UV spectrum is divided into three categories: UVC (100-280 nm), UVB (280-315 nm), and UVA (315-400 nm).

In order to UV cure the UV curable resins, we use a UV source machine. As the UV source, Dymax PC-2 (Dymax Corporation, CT, USA) is used, which produces UVA light (315-395 nm).

2.2.7 Flash Sintering

In flash sintering, the IPL is used. In fact, instead of thermal curing via a high temperature (nearly 200°C) for a long time, we use this method. Using traditional thermal curing has two drawbacks: (1) the high temperature might damage the substrate depending on the substrate material; (2) it is time consuming. Flash sintering solves both problems; as our substrate was PLA and could not endure high temperatures, we used flash sintering; it also reduced the processing time considerably.

Flash sintering applies intense pulses of visible light. There are several parameters involved in this process that affect the total energy produced and transferred to the sample. Such parameters determine the quality of printed films, they include pulse voltage, pulse on-time, pulse off-time, period, and pulse number.

Voltage: pulse voltage determines the intensity of pulses applied.

Pulse on-time: The duration of each pulse.

Pulse off-time: if several pulses (not applicable for the single pulse mode) are used, this is the time length between two consecutive pulses.

Pulse number: How many pulses to be applied. In the single mode pulse, this parameter is equal to one.

The IPL experiments in this thesis are performed by a XENON X-1100 machine (XENON Corporation, USA).

2.2.8 Four-Point Probe Measurement

The simplest method to measure resistance is 2-point probe measurement. In this method, the two probes inject a current into the conductor and measure the voltage and then the resistance is calculated using Ohm's Law (R=E/I).

Where R, E, and I are the resistance, voltage, and current, respectively.

This method might be well suited for high resistances, but it is not a good option for low resistance elements. The main issue of this method is that it adds the contact and wire resistances to the desired resistance. Because the injected current by probes causes an extra voltage drop on the

contacts, and hence results in considerable error. Therefore, two-point probe measurement is not an accurate method for low resistance applications.

To overcome this problem, four-point probe measurement is used. This method is able to measure the resistance while removing the contact and wire resistances. In fact, as the two outer probes are responsible for current injection, the current flows through the samples. Besides, as voltmeters have a very high input impedance, almost no current can enter the voltmeter probes. Therefore, only the voltage between the two inner probes is measured (ΔV), which means it removes contact and wire resistances. Figure 2-4 shows how we measure and calculate sheet resistance of the printed lines using the four-point probe method.

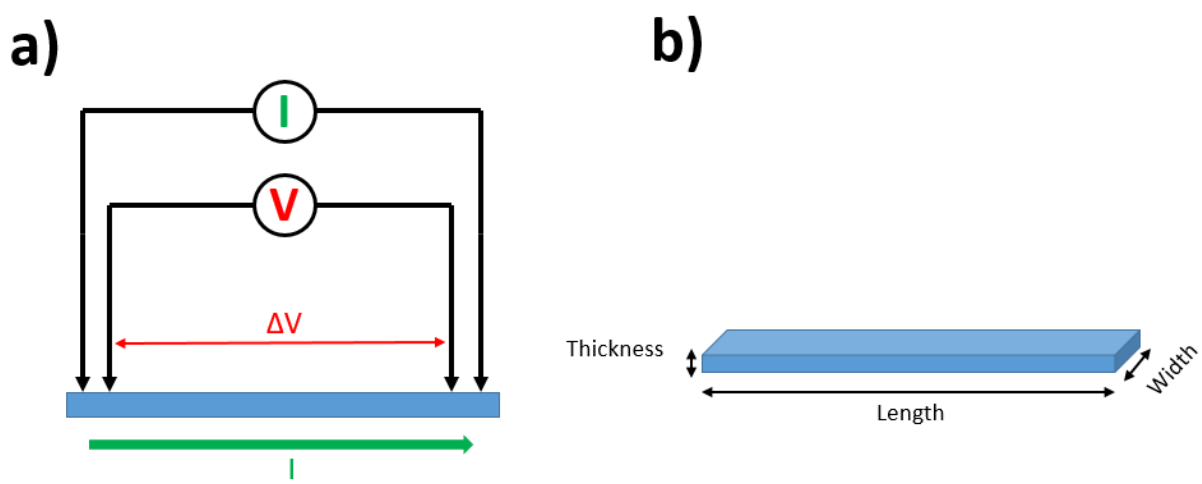

Figure 2-4: How four point probe measurement works. (a) The configuration of probes. (b) 3-dimensional perspective of a line film with dimensions displayed.

Having ΔV, I, and the film dimensions, we are able to calculate sheet resistance given by Equation (2-1):

$$R_S = \frac{\Delta V}{I} \cdot \frac{W}{L} \tag{2-1}$$

ΔV is the voltage measured by the two inner probes, I is the current injected by two outer probes, W is the film width, and L is the spacing between voltage electrodes. Equation (2-1) is valid if

films are thinner than 40% of the spacing, and if t and W are very small compared with L so that the current is restricted to the region between the current probes. The resistance is measured by Keithley 4200A-SCS Parameter Analyzer (Keithley Instruments, Ohio, USA), and length and width are obtained via an optical microscope.

2.2.9 Stylus Profilometer

In order to measure surface profiles, a profilometer is used. Using a profilometer, the surface roughness and film thickness can be measured. While there are a variety of profilometers, the stylus profilometer is a common type. It is a contact technology in which the stylus is moved across the desired surface while it is in contact with that sample. We use Alpha-Step D-600 Stylus profilometer in this thesis.

2.3 Results and Discussion

2.3.1 Inkjet Printing AgNP Ink Directly onto a 3D PLA Substrate

As mentioned in Section 2.2.1., inkjet printing AgNP ink directly onto a 3D PLA substrate would face two challenges: (1) the surface of the 3D printed substrate is not smooth enough, (2) The AgNP ink might spread over the PLA uncontrollably and fail to create a good morphology.

Due to the properties of 3D FFF printing technology, the surface of fabricated parts is rough. The surface roughness is measured by a profilometer. Figure 2-5 shows the surface roughness of a typical 3D printed PLA surface by a stylus profilometer. As can be seen from Figure 2-5, the surface is not smooth enough for inkjet printed lines. The root mean square (RMS) roughness of the PLA surface is 4.27 µm and the peak-to-peak roughness is nearly 20 µm, while the thickness of inkjet printed silver lines is 6.4 µm. Therefore, the surface roughness needs to be reduced.

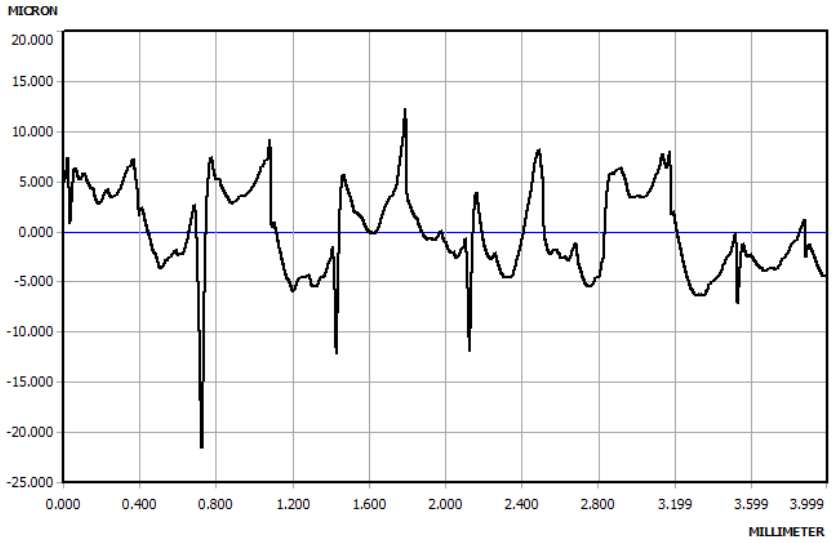

Figure 2-5: Surface roughness profile of a 3D printed substrate.

Next, we inkjet printed AgNP ink to print four simple lines onto the 3D substrate, and the sample was dried at 80°C for 60 minutes in the oven. As can be seen from Figure 2-6, the printed lines have a poor morphology. The surface roughness of the PLA has affected the ink; moreover, even on the smoother areas of the substrate, the ink is spread over the substrate and could not form lines with acceptable patterns.

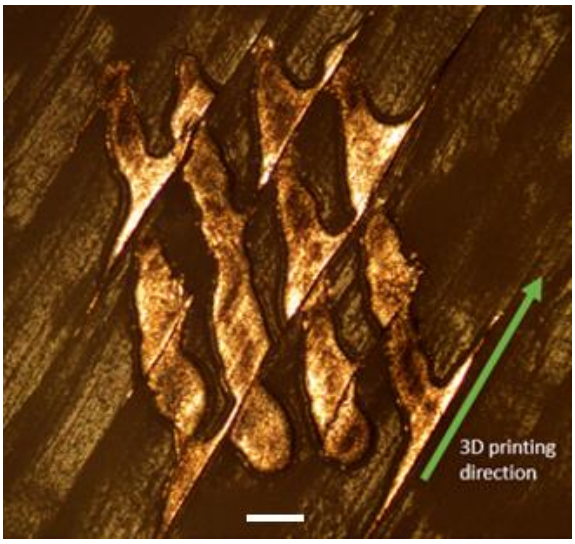

Figure 2-6: Four lines of inkjet printed AgNP ink onto a 3D printed PLA substrate. The scale bar represents 250 µm.

Figure 2-6 clearly shows that both aforementioned challenges exist. Firstly, the four lines suffer very poor patterns especially at the edges of 3D printed lines, and at some points the lines are even separated due to surface roughness. Secondly, even in locations that AgNP films are continuous, they displayed no electrical conduction as the ink solvent has dissolved the PLA substrate.

2.3.2 Selecting the Intermediate Layer and Related Defects

While studying different materials to select the intermediate layer, some materials showed defects and non-idealities in the subsequently printed metal lines. We categorized such defects in the intermediate layers.

2.3.2.1 Air Bubbles

Two-component epoxy resins are amongst favorable available resins that could be used in a variety of applications. They are very chemically resistant and adhesive, and do not require high temperature to cure.

For this test, System 2000 Epoxy Resin as the base resin and 2020 Epoxy Hardener (Fibre Glast Developments Corp., OH, USA) are used. We used this combination as it is a popular material, chemically resistant, and it does not require a high temperature to be cured. The pot life of this epoxy/hardener was 20 minutes. According to the product instruction, we mixed the two components with the ratio of 4:1 for base resin : hardener and deposited onto a glass substrate. We cured the material in an oven for 12 hours at 60°C. Thereafter, we inkjet printed AgNP ink as simple line patterns onto the solid epoxy. Samples were cured in the oven for 1 hour at 80°C. The electrical measurement was carried out by two point probe method.

The results are displayed in Figure 2-7. As can be seen, the substrate, epoxy resin, is full of air bubbles, which are created during the curing of the epoxy. The air bubbles significantly affect the quality of silver lines. In Figure 2-7(a-b), the lines are mostly not on the bubbles and they have relatively good electrical conductivity; the sheet resistance was 707 Ω/sq and 607 Ω/sq, respectively. While in Figure 2-7(c), the silver line is partially on an air bubble and its sheet resistance is 225 kΩ/sq. However, the lines in Figure 2-7(d-e) are completely on the air bubbles, they do not conduct at all and the resistance is infinite.

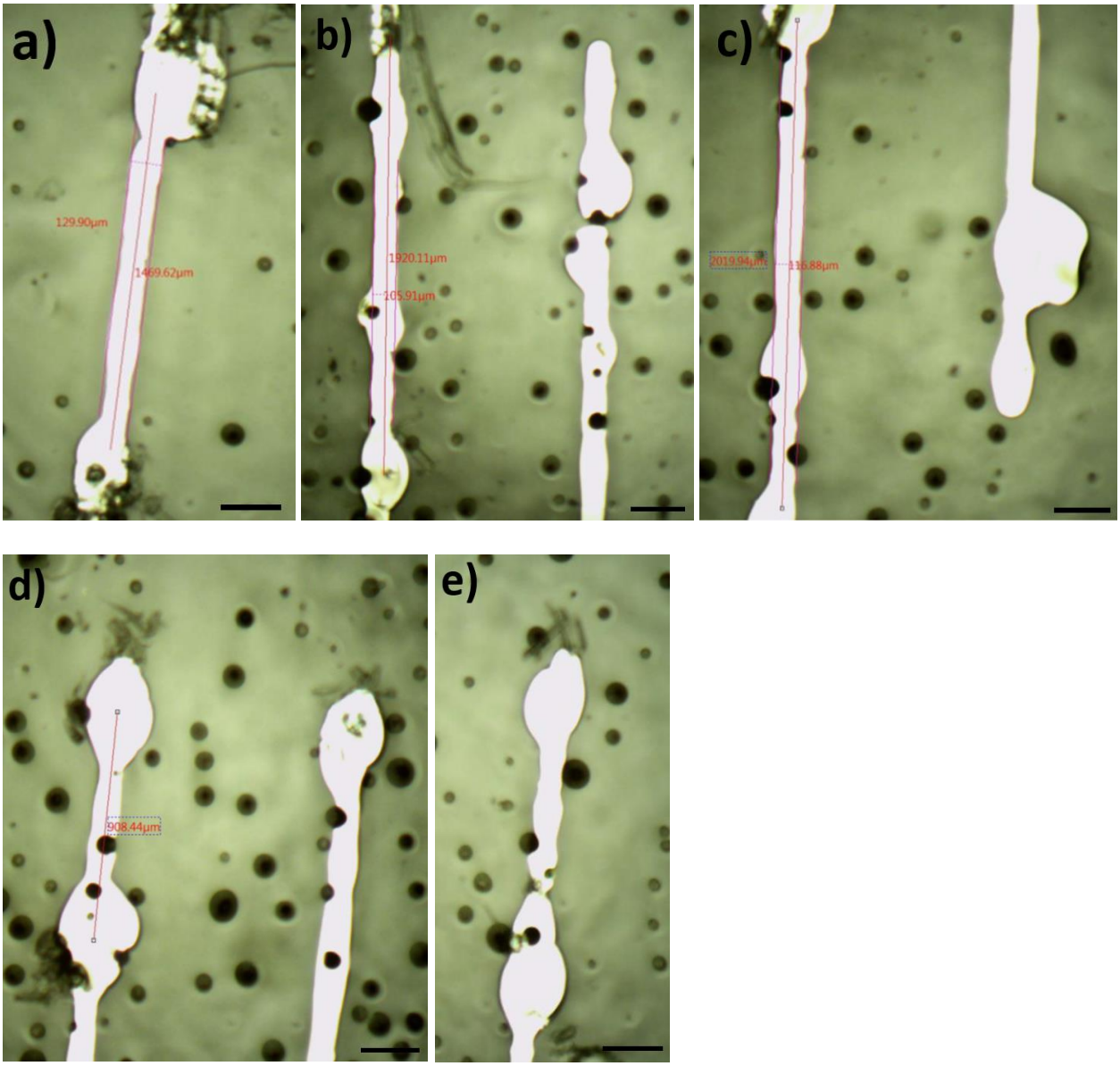

Figure 2-7: Optical micrographs of AgNP ink printed onto 2-component epoxy resin. (a-b) Air bubbles are not on the silver lines. (c) Air bubble partially is on the silver line. (d-e) air bubbles are completely on the silver lines. The scale bars represent 250 µm.

In order to solve the problem of air bubbles, various pre-deposition and post-deposition actions were tested to either avoid or remove the air bubbles.

Pre-deposition actions include various methods. As the first step, two different methods of depositing were tested. We deposited the previously mixed resin/hardener manually by a syringe

and by a spin coater. The results were the same and the resin was still full of air bubbles. So it was not a matter of deposition method. We also tried the addition of isopropyl alcohol and 70% alcohol before curing, as it might pop the air bubbles, due to lowered surface tension, and decrease the viscosity. Again, they did not make any change and the resulting epoxy was full of air bubbles. In terms of method of mixing, we also mixed manually and by sonicator. Again, samples fabricated with both methods contained air bubbles.

We also used post-depositing actions. As the main solution, we put the sample immediately after mixing it into the vacuum in order to bring the trapped air bubbles to the surface and release them. The success of this approach depends on the material viscosity and surface tension. Surprisingly, even vacuuming for up to 4 hours did not remove the air bubbles. In fact, the present bubbles are gas formed during the curing process due to the chemical reaction. Right after the mixing of two components, they are small bubbles, and as time goes on, they become larger. Because they are formed during the curing reaction as the viscosity of the epoxy resin increases, bubbles cannot be removed even by applying vacuum. Since this 2-component epoxy resin had the problem of micro-air bubbling we considered another type of resin.

2.3.2.2 Low Chemical Resistance

We used an UV curable epoxy, namely UV Cure Epoxy 60-7170 (Epoxies, Etc, USA). In order to print the epoxy by Voltera printer, we used values of 0.40 and 0.25 for Kick and Rheological setpoint, respectively.

We printed the epoxy on a glass substrate and then UV cured it. Thereafter, we inkjet printed AgNP lines onto the UV cured epoxy by different drop spacing including 90, 220, and 360 µm, shown in Figure 2-8(a-c). From Figure 2-8, it is obvious that the ink has attacked the epoxy layer and deformed it. Figure 2-8 (d) is a zoomed in line, it clearly shows that the margins of the AgNP ink is corroded and the epoxy has deformed and is dissolved by the ink. Electrical measurement also showed that the printed lines do not conduct as they are dissolved with the epoxy and lost the functionality.

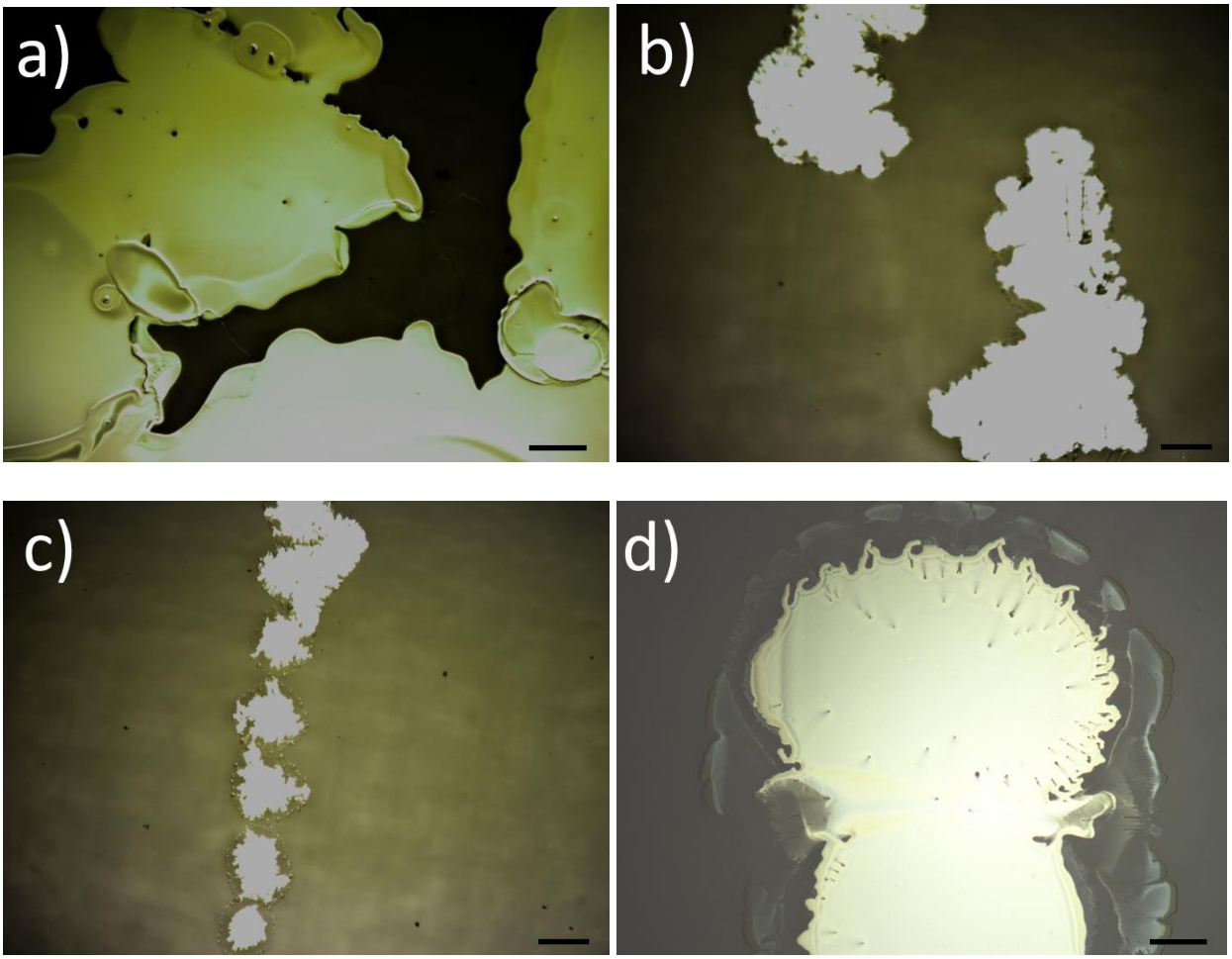

Figure 2-8: Inkjet printed AgNP ink onto UV curable epoxy. (a) A printed line with drop spacing of 90 µm. The scale bar represents 50 µm. (b) A printed line with drop spacing of 220 µm. The scale bar represents 250 µm. (c) A printed line with drop spacing of 360 µm. The scale bar represents 250 µm. (d) A zoomed in printed line with obvious corrosions of the epoxy around the printed ink. The scale bar represents 50 µm.

2.3.2.3 Oxygen Inhibition

Oxygen inhibition, which sometimes happens in radical acrylic resins, means the air can stop the polymerization of the top layers (surface) and leave them tacky and even wet. Certain resins are more likely to be affected by oxygen inhibition due to their formulation. Hence, one way to avoid oxygen inhibition is to change the product. However, oxygen inhibition happens in radical free products (or acrylate based UV curable products), not in epoxy based UV curable products.

We used two different adhesives namely UV Cure 60-7114 (Epoxies, Etc, USA) as well as Multi-Cure 6-630 (Dymax Corporation, CT, USA) which is in the acrylated urethane class. We printed the adhesives by Voltera extrusion printer onto a glass substrate with values of 0.40 and 0.25 for Kick and Rheological setpoint, respectively. Subsequently, we UV cured two different samples for 2 minutes and 10 minutes for each type. After inkjet printing AgNP ink onto the samples, we cured the ink over a hot plate at 120°C for 60 minutes.

Unfortunately, the microscopic images showed that the adhesive was exposed to oxygen inhibition resulting in a non-smooth and not fully cured surface. Figure 2-9 (a-b) and Figure 2-10 (a-b) show the results for UV Cure 60-7114 and Multi-Cure 6-630, respectively.

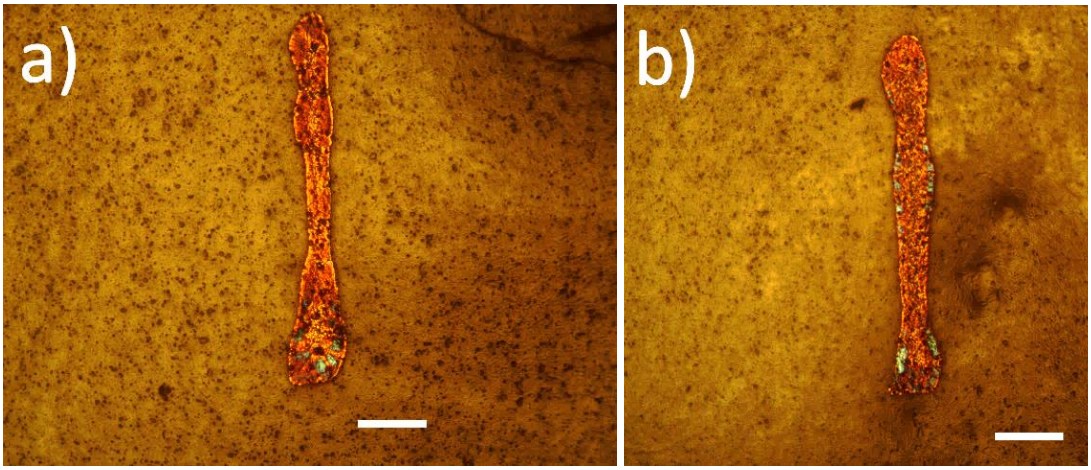

Figure 2-9: Optical micrographs of inkjet printed AgNP lines onto UV Cure 60-7114. (a) Adhesive UV cured for 2 minutes. (b) Adhesive UV cured for 10 minutes. The scale bars represent 250 µm.

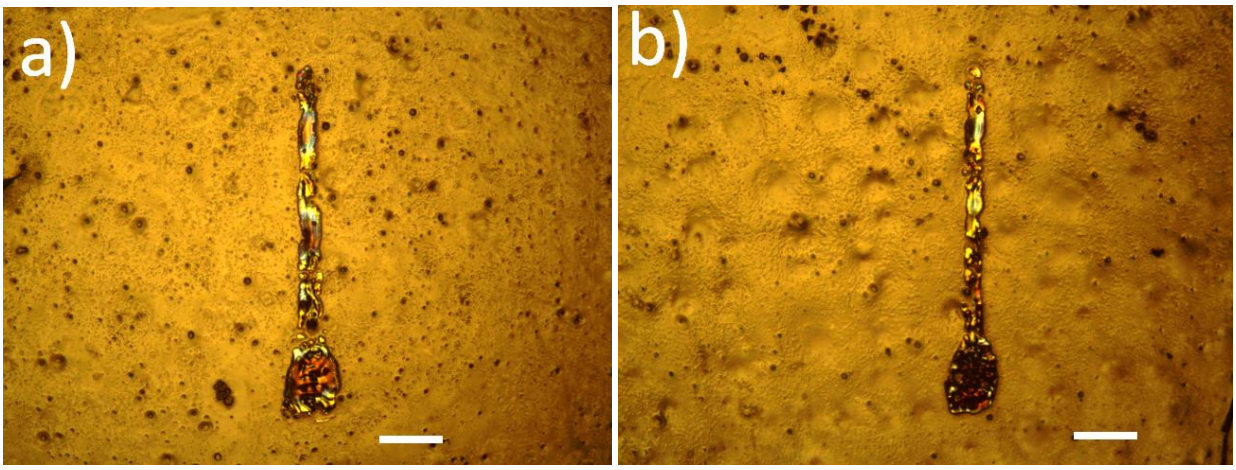

Figure 2-10: Inkjet printed AgNP lines onto Multi-Cure 6-630. (a) Adhesive UV cured for 2min. (b) Adhesive UV cured for 10min. The scale bars represent 250 µm.

2.3.2.4 Defect-Free Intermediate Layer

As another option with a different formulation to overcome the oxygen inhibition, now we used Multi-Cure 6-621 (Dymax Corporation, CT, USA). This product had a much lower viscosity than every adhesive used so far, which was 800cP. In fact, Voltera prints a pattern line by line and at the beginning of each part it re-pressurizes the cartridge. At the first half of each line, the adhesive is extruded sufficiently, but in the second half it stops extruding as the pressurization was not enough. Hence, we needed to manipulate the extrusion printer parameters for printing consistency.

We used the values of 0.40 and 0.40 for Kick and Rheological setpoint, respectively. Thereafter, we UV cured different samples for 2 minutes and 10 minutes. After inkjet printing of AgNP ink onto the samples, we cured the ink on a hot plate at 120°C for 60 minutes.

This time, the microscopic images show a very smooth surface of adhesive, shown in Figure 2-11, as well as well-patterned lines, as shown in Figure 2-12(a-b). Besides, unlike previous samples, the electrical measurement shows conductivity.

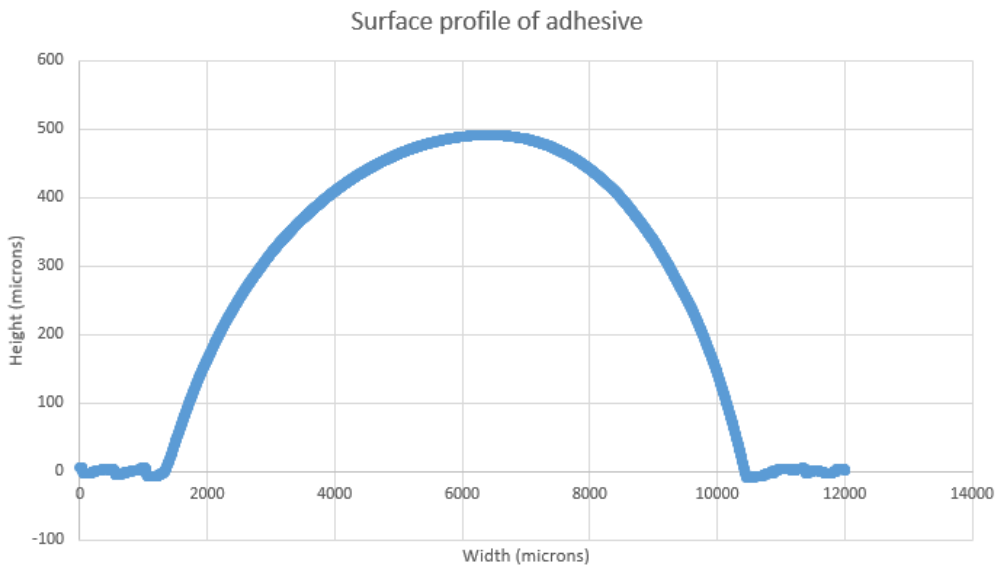

Figure 2-11: Surface profile of the adhesive measured by stylus profilometer.

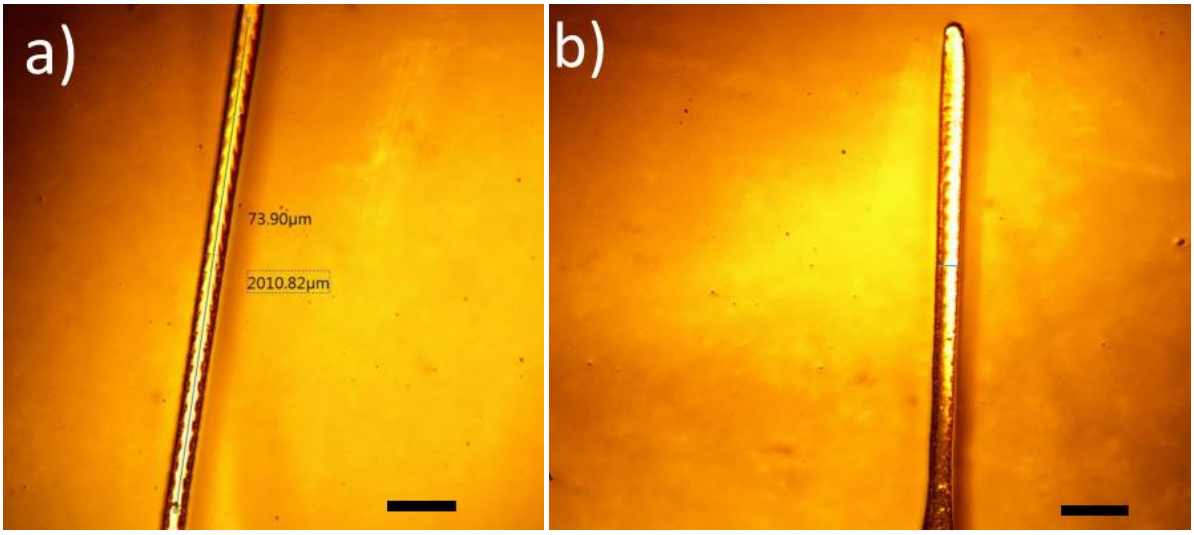

Figure 2-12: Inkjet printed AgNP lines onto Multi-Cure 6-621. (a) Adhesive UV cured for 2 minutes. (b) Adhesive UV cured for 10 minutes. The scale bars represent 250 µm.

We concluded that this formulation of acrylated urethane adhesive suits our purposes due to two reasons: (1) it is chemically resistant against the silver ink as the ink did not attack the adhesive

and it maintained the pattern of an ideal line. (2) Oxygen inhibition did not happen for this product as the surface of adhesive is very smooth and fully cured.

Hence, we choose this UV curable product as our substrate for the rest of this research.

2.3.3 Inkjet Printing Drop Spacing Optimization

In inkjet printing technology, patterns consist of a matrix of droplets. Drop spacing (DS) plays a key role to obtain high-quality patterns. Drop spacing is defined as the center-to-center distance of droplets. In order to have an ideal printed pattern, DS must be determined according to the droplet volume and ink spreading over the substrate surface. If DS is too small, the printed pattern will be a bulging pattern. While, if the DS is too large, the printed pattern will be scalloped, or even individual droplets for further smaller DS instead of continuous lines. Hence, an intermediate DS value must be chosen. The main factor affecting the ink movement is the property of substrate surface; as a consequence, for a similar ink and condition but a different substrate, the optimal DS would be different and needs to be found.

We studied drop spacing values of 50, 60, 70, 80, 90, 100, and 110 µm. The adhesive Dymax 6-621 was printed onto a glass substrate by Voltera extrusion printer, and then was UV cured for 2 minutes. We inkjet printed AgNP ink for two lines each consisting of 16 droplets for each drop spacing.

We noticed that DS of 50 µm and 60 µm create bulged lines, as shown in Figure 2-13(a-b). DS of 70 µm, 80 µm, and 90 µm look like an acceptable morphology, as shown in Figure 2-13(c-e). While DS of 100 µm resulted in scalloped lines, as shown in Figure 2-13(f). Finally, DS of 110 µm created individual droplets, as shown in Figure 2-13(g).

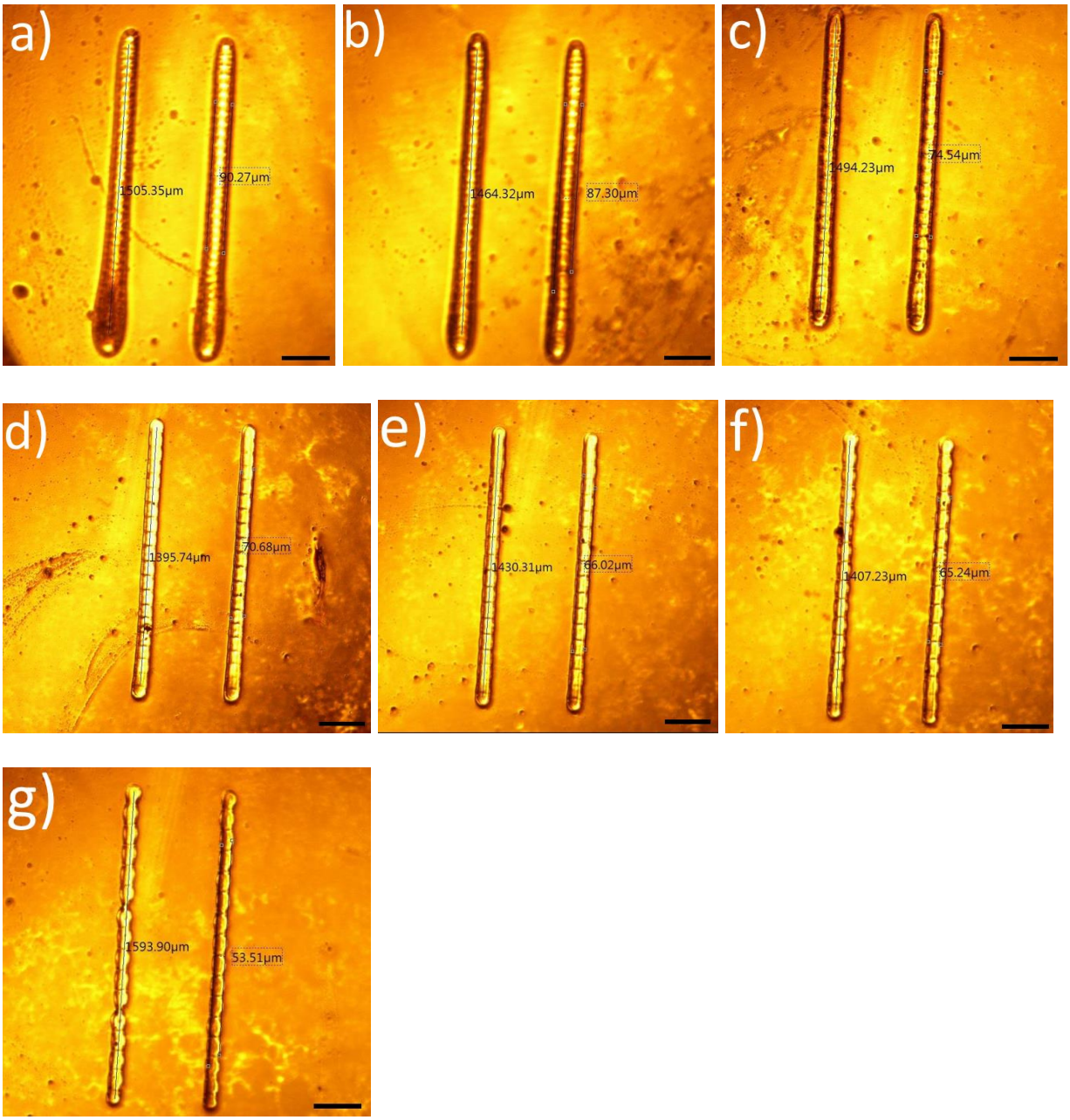

Figure 2-13: Inkjet printed AgNP lines on UV cured adhesive for different drop spacing. (a) DS= 50 µm. (b) DS= 60 µm. (c) DS= 70 µm. (d) DS= 80 µm. (e) DS= 90 µm. (f) DS= 100 µm. (g) DS= 110 µm. The scale bars represent 250 µm.

Although DS of 70, 80, and 90 µm provide perfect line morphologies, we picked up 80 µm DS which is in the middle and the safest option. From now on, we use the 80 µm DS for inkjet printing AgNP onto adhesive substrates.

2.3.4 Drying Ink and Thermal Conditions

Once nanoparticle inks are deposited, they need to be annealed to evaporate the solvents and sinter particles in order to make the printed film conductive.

Usually, to fully anneal NP inks, a temperature beyond 150℃ is needed. However, such a high temperature is not possible for our application as the substrate is PLA and cannot endure temperatures beyond 80-90℃. Accordingly, we need to divide the annealing process into two steps: (1) Drying the film to evaporate the solvent; this process normally needs temperatures around 60℃. (2) Sintering the film by the IPL sintering method; as it uses high-intensity light for a very short time and hence does not damage the PLA substrate.

In order to dry the printed ink solvents, normally a hot plate is used. However, as the substrate in our application was 3D structures, putting it over the hot plate does not work as the heat does not reach the top layer and adhesive. Therefore, we used an oven as the thermal source which uses convective heat transfer.

The aim of this experiment is to find the best conditions, including temperature and exposure time, for the drying process. For each sample, six lines were printed at different locations of the adhesive in order to have more reliable results. We performed the test for four different temperatures including 50℃, 60℃, 75℃, and 90℃. For each temperature, we also carried out the test for four different timing values including 30, 60, 90, and 120 minutes. We also used a sample only dried at room temperature, not in oven, for 30 minutes for comparison purposes, indicated as RT. Hence, we processed 17 samples ((4 temperatures * 4 timing = 16) + 1 sample dried at room temperature = 17). We also report standard deviation as error bars which are according to six lines for each sample.

In the flash sintering process, we applied one single pulse of 1400 V with 2000 µs on-time. To measure the sheet resistance we used 4-point probe measurement as described in Section 2.2.5.

The surface profile of lines shows a thickness of 6.4 µm, as shown in Figure 2-14. The final results are displayed in Figure 2-15 for resistivity.

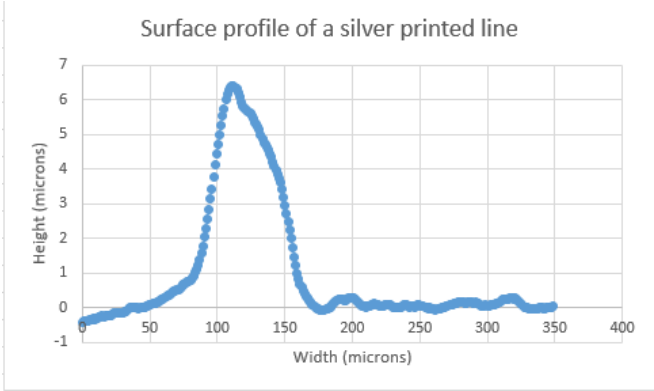

Figure 2-14: Surface profile of an AgNP printed line measured by stylus profilometer.

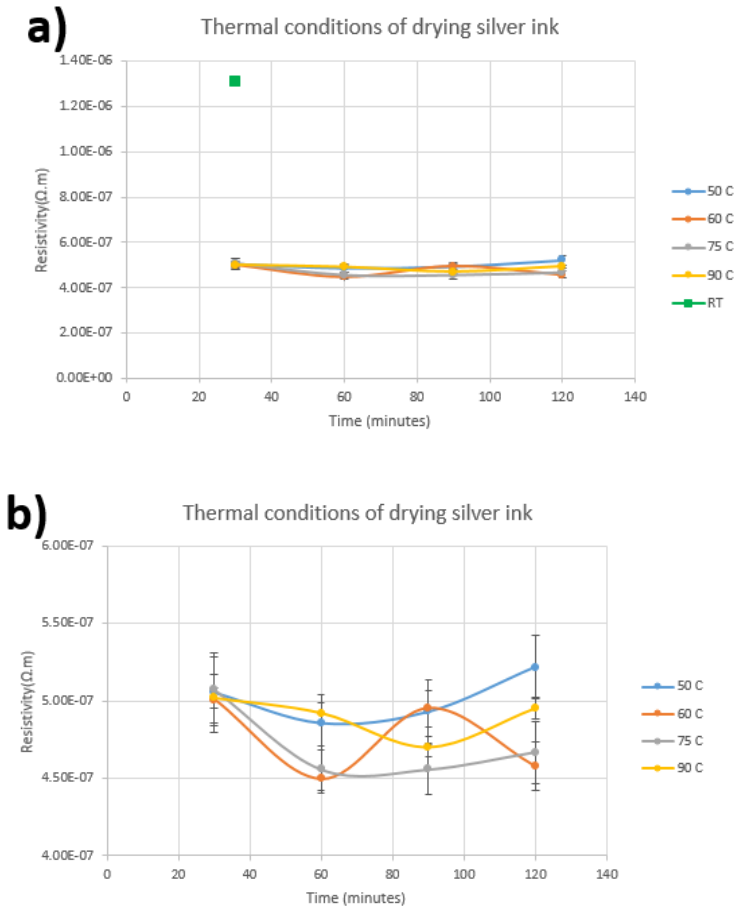

Figure 2-15: Different thermal conditions for drying off the silver ink solvents. (a) Room temperature value included (b) Room temperature value not included.

* RT: sample was dried at room temperature for 30 minutes.

Initially, the 0-time sample is displayed which was the sample that skipped the thermal process in the oven and only experienced the flash sintering. As expected, the silver lines were not fully dried and still sticky. Its sheet resistance is shown as the green data point, showing sheet resistance of 0.285 Ω/sq which is almost four times higher than the dried samples.

The other 16 samples that experienced both drying and sintering processes show quite close values. The standard deviation of the average sheet resistance for each condition was $3.3*10^{-3}$, $2.0*10^{-3}$, $2.9*10^{-3}$, and $2.9*10^{-3}$ Ω/sq for 50°C, 60°C, 75°C, and 90°C, respectively. The lowest resistivity happens at 60°C and 75°C for 60 minutes. However, we prefer 60°C for the safety of PLA substrates in order to avoid any damages due to the high temperature. In conclusion, from now on, we dry the samples at 60°C for 60 minutes.

2.3.5 UV Curing Time

After printing the UV curable adhesive onto the 3D substrate, the adhesive needs UV curing to be polymerized and converted from the liquid state to the solid state.

The time length of UV curing is very important because it not only makes the adhesive hard and chemically resistant, it determines the surface properties such as surface energy and hence the contact angle and wettability of the silver ink on the adhesive surface.

In this experiment, we studied different UV curing time durations to find the optimal time. We printed the UV curable adhesive using Voltera extrusion printer onto 3D printed substrates. The printed adhesive patterns were simple 7.5 mm * 7.5 mm squares.

We UV cured the samples for 15 seconds, 30 seconds, 1 minute, 2 minutes, 3 minutes, 5 minutes, and 10 minutes. Afterwards, we inkjet printed six lines of AgNP ink onto each sample, dried the samples in the oven at 60°C for 60 minutes, and flash sintered by Xenon 1100 lamp with one single pulse of 1400 V and 2000 µs on-time.

Figure 2-16 shows the results as resistivity. As can be seen, samples of 15 s and 30 s have considerably higher sheet resistance compared to more UV cured samples, with 690 and 41 Ω/sq, respectively. 15 s and 30 s samples are not fully cured as they did not show enough chemical resistance and hardness. As can be seen, the 1 minute sample still has considerably higher sheet resistance compared to the rest; it indicates that 1 minute of UV curing is not good enough. While

2 minutes and beyond show very low and similar sheet resistance. However, the optimal UV time seems 2 minutes as it has the lowest value among the six samples.

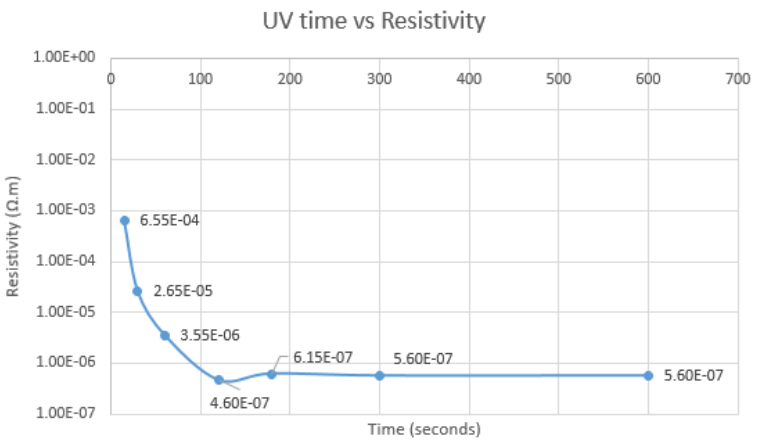

Figure 2-16: The effect of UV time exposure for the adhesive on the resistivity of lines.

Next, we analyzed the morphology of inkjet printed silver lines onto UV curable adhesive for different UV time exposures. The properties of the adhesive surface change with UV time significantly.

The adhesive has a percentage of photoinitiators. In the polymerization process, once the adhesive is exposed to the UV light, the photoinitiators start generating free radicals which attach to acrylates (State 1). This process repeats until all free radicals are attached to acrylates, which cause polymer termination (State 2). Once all photoinitiators are used up by the UV light exposure, the UV light starts baking the surface of adhesive, which degrades the adhesive properties (State 3).

Therefore, the adhesive can have three states. State 1 and State 3 result in undesirable printing including low conductivity and poor morphology, respectively. Therefore, we need the middle state, State 2, which is a narrow length of UV time.

For this test, all conditions are the same, only UV time exposure of the adhesive is varied. We fabricated samples UV cured for 30 seconds, 45sec, 60sec, 75sec, 90sec, 105sec, 120sec, 135sec, 150sec, 165sec, 180sec, and 195sec. We did all the steps the same as the previous tests except for UV curing time. Figure 2-17 displays the resulting samples under the optical microscope once all steps were done.

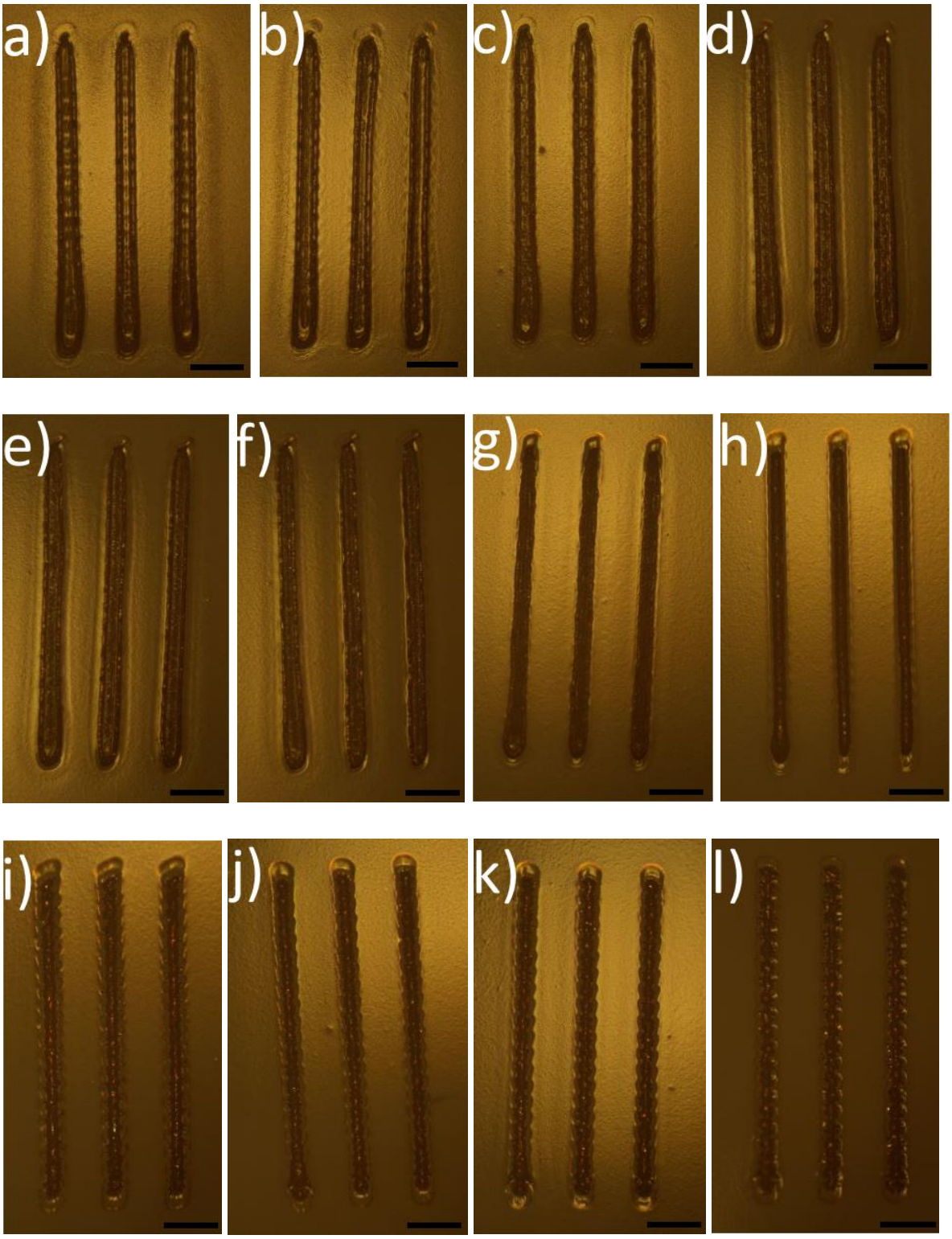

Figure 2-17: Inkjet printed silver lines for various UV curing time. (a) 30sec. (b) 45sec. (c) 60sec. (d) 75sec. (e) 90sec. (f) 105sec. (g) 120sec. (h) 135sec. (i) 150sec. (j) 165sec. (k) 180sec. (l) 195sec. The scale bars represent 250 µm.

In Figure 2-17, we can clearly see all three states of UV curing with their different printed lines. As mentioned previously, we need to be able to differentiate these three states and their UV time, so that we use only the fully cured UV time for the rest of our work.

UV exposure time in the range between 30 seconds and 105 seconds provides low conductivity, Figure 2-17(a-f). We can see that the coffee ring effect had occurred for such samples which is an undesirable phenomenon. In such samples, silver nanoparticles are placed on the edges of lines, and the middle is almost left empty.

In the range between 120 seconds and 150 seconds, we see that the printed lines are straight and have good morphology, Figure 2-17(g-i). The coffee ring effect is removed, and the silver drops have merged to form a continuous line.

In the range of 165 seconds to 195 seconds, we see that printed lines exhibit strong scalloping, and a uniform film is not formed, Figure 2-17(j-l). In fact, the silver droplets during and after inkjet printing could not merge and join completely. However, in this case we still have good conductivity.

As mentioned, the best range of UV exposure time is between 120 and 150 seconds. In this range, we obtain the optimal printing results, which are lines with the highest conductivity and good morphology. Therefore, we choose 135 seconds as the UV exposure time which is at the middle of the range. In conclusion, from now on, we UV cure the samples for 135 seconds.

2.3.6 Photonic Sintering Parameters

The photonic sintering process is a vitally important step in our fabrication process. After we dry the inkjet printed silver lines in the oven, we need to sinter the samples in order to form a continuous film which increases the conductivity.

We applied a single pulse to limit the involved parameters, therefore the variables were voltage and on-time. The on-time values were 500 µs, 1000 µs, 2000 µs, 3000 µs, and 4000 µs, and the voltage were 1400 V, 1500 V, 1600 V, 1700 V, 1800 V, 1900 V, and 2000 V. All other processing steps were the same as previous experiments. The results are displayed in Figure 2-18.

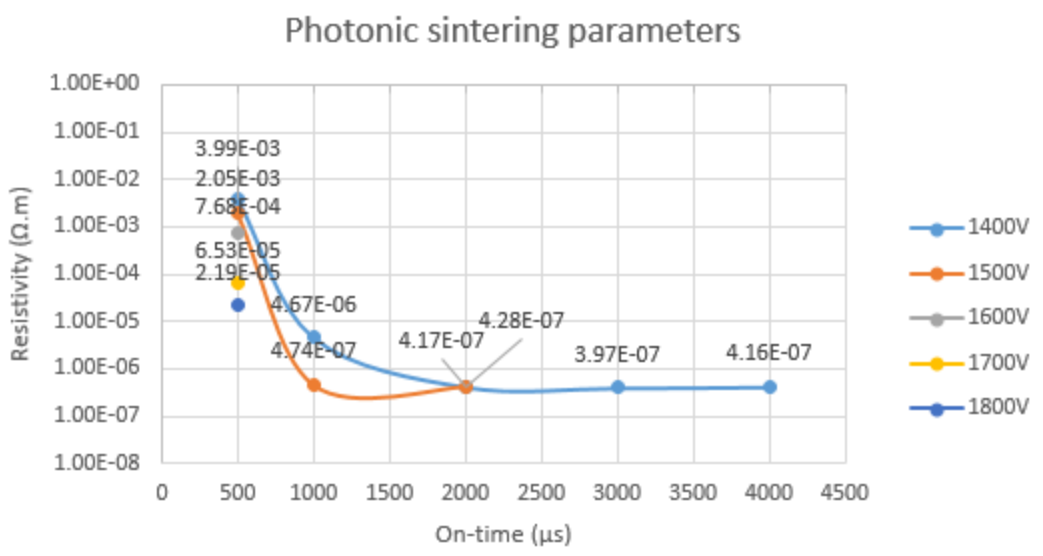

Figure 2-18: The effect of parameters of photonic sintering process, including pulse voltage pulse on-time, on resistivity.

In the experiment, for high voltage and high on-time, the printed silver lines were damaged and removed from the substrate. For 500 µs on time, from 1400 V to 1800 V were present, while samples cured by 1900 V and 2000 V were removed. For 1000 µs and 2000 µs on time, only samples cured by 1400 V and 5000 V were remained, and higher voltages damaged the samples. For 3000 µs and 4000 µs, the 1500 V also was removed and only the 1400 V was present. The results are shown in Figure 2-18.

One problem that happened in this step was length shrinkage. In fact, once the photonic sintering was done, the lines become small. This shrinkage depends on the photonic sintering parameters. We measured the original length of lines before the sintering and compared them to the length after the sintering process. The calculated length shrinkage for the previous test samples are provided in Figure 2-19. The optical micrographs of the four samples are also provided in Figure 2-20 (a-d).

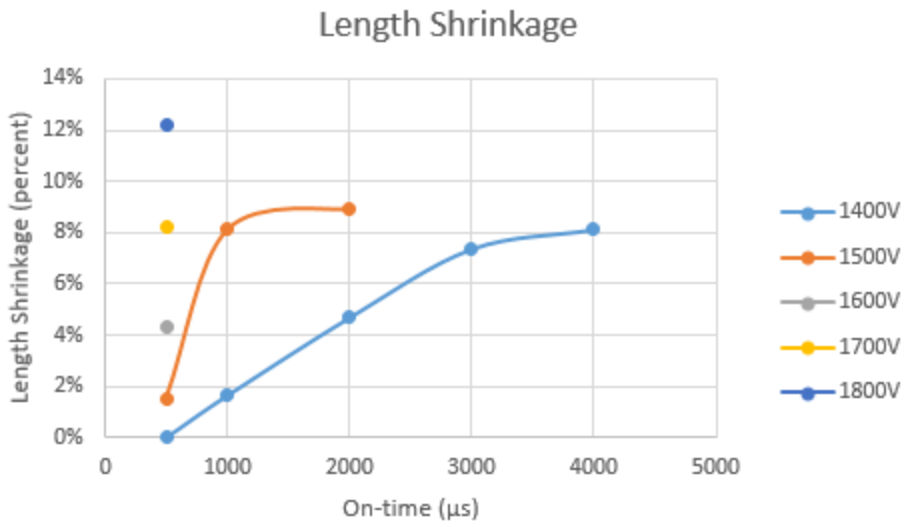

Figure 2-19: The effect of parameters of IPL on the length shrinkage.

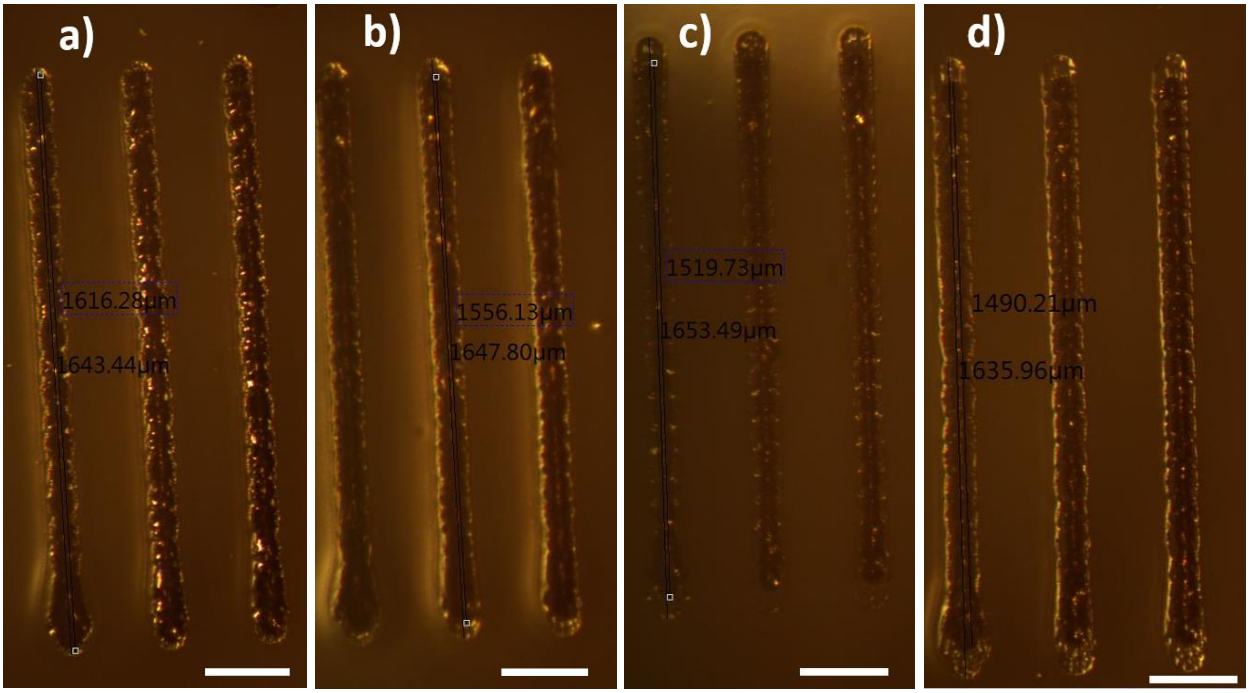

Figure 2-20: Optical micrographs of silver lines with length shrinkage for different IPL parameters. (a) Sample 1400 V / 1000 µs. (b) 1400 V / 2000 µs. (c) 1500 V / 1000 µs. (d) 1500 V / 2000 µs. The scale bars represent 250 µm.

Figure 2-19 indicates that generally lower voltage causes less length shrinkage. The least length shrinkage belonged to 1400 V / 500 µs which didn't shrink, but such parameters provided poor sintering. While samples of 1400 V / 2000 µs, 1400 V / 3000 µs, 1400 V / 4000 µs, 1500 V / 1000 µs, and 1500 V / 2000 µs had low and close resistivity, the least length shrinkage was for 1400 V / 2000 µs. Therefore, this is the optimal condition as it provides good conductivity and low length shrinkage. In conclusion, from now on, we use one single pulse of 1400 V and 2000 µs on-time.

2.3.7 Effect of Color PLA Substrate

In this experiment, we aim to see how the color of 3D PLA substrate affects the inkjet printed silver lines. Because the intermediate layer, UV cured adhesive, is transparent, the color of 3D substrate is the dominant color for the background of silver lines. So far, every test carried out was with white PLA. We 3D printed three different PLA substrates with similar factors but with three different colors including white, transparent, and black.

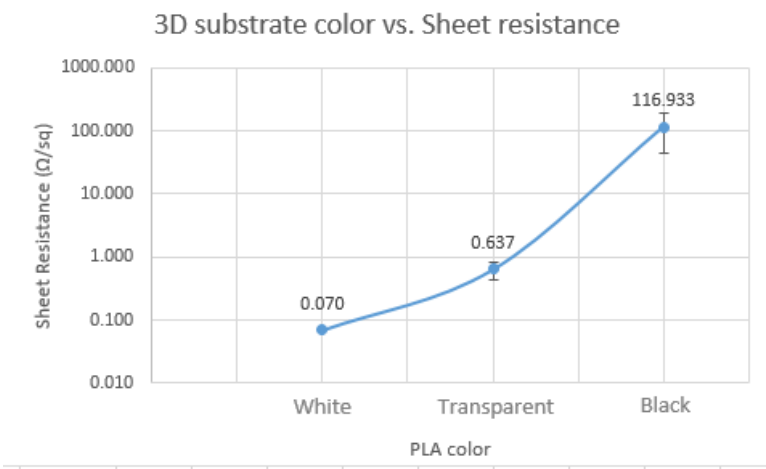

Figure 2-21: The effect of color of 3D PLA substrate on inkjet printed silver lines.

Figure 2-21 indicates that the color of the 3D PLA substrate significantly affects the final conductivity of inkjet printed silver lines. More specifically, the black and transparent substrates had nearly 1600 and 10 times higher sheet resistance than their white counterpart. This huge difference happened during photonic sintering. Objects with white color reflect back all the

wavelengths of light and absorb very little. On the other hand, dark colored objects, including black, reflect back only some of the wavelengths, they absorb the rest. In this experiment, as the white color reflects more wavelengths of light, potentially more energy is transferred to the silver lines and hence enhances the sintering and conductivity. In conclusion, white 3D printed substrate provides the lowest sheet resistance, consequently, the highest conductivity, compared to other colors. Therefore, from now on, we use white 3D PLA substrates as our samples.

2.4 Conclusion

In this chapter, we succeeded to inkjet print silver nanoparticle lines onto a 3D FFF printed substrate and obtain a highly conductive single line. Firstly, we selected the intermediate layer; we noticed that the material must be free of air bubbles, be chemically resistant, and do not show oxygen inhibition. Consequently, we used UV curable acrylated urethane adhesive as the intermediate layer between the 3D substrate and inkjet printed patterns. We deposited this UV curable adhesive by the extrusion printer onto the 3D substrate with some changes in the printing parameters including values of 0.40 and 0.40 for Kick and Rheological setpoint, respectively. Thereafter, we tried to find the best drop spacing of inkjet printing onto this substrate, which was found to be 80 µm. In the next step, we found the optimal UV curing time to have the maximum conductivity and to obtain continuous films; the best UV time is 135 seconds. After inkjet printing the silver lines onto the substrate, we dried the sample in the oven, and the preferable condition was the temperature of 60°C for 30 minutes. Thereafter, we analyzed the parameters of the flash sintering process. We found that the optimal parameters to have the maximum conductivity and the least length shrinkage is one single pulse of 1400 V with 2000 µs on-time. Finally, we compared different colors of the 3D PLA substrate including white, transparent, and black, and we noticed that the substrate color is very important, and the PLA substrate with white color provides the highest conductivity. Using all of the mentioned findings, finally, we fabricated silver lines onto 3D FFF printed substrate with a sheet resistance of 0.07 Ω/sq and a conductivity of $2.23 * 10^6$ (S/m).

Chapter 3: Fabricating a Strain Gauge onto 3D Printed Object

3.1 Introduction

In this chapter, in order to validate the obtained methodology in the previous chapter, we fabricate a strain sensor. More specifically, we aim to inkjet print a strain gauge via silver nanoparticle ink onto a printed polylactic acid (PLA) 3D fused filament fabrication (FFF) substrate. We include the parameters of extrusion printing, inkjet printing, thermal curing of the ink, and photonic sintering of the ink.

Having fabricated the strain gauge onto a 3D printed substrate, we perform a mechanical test. We apply a normal stress on the 3D substrate, consequently, the strain gauge measures the resulting strain.

In order to measure the electrical resistance of the sensor, we use a digital source meter connected to a standard wheatstone bridge to minimize errors. For measuring the applied strain to the 3D structure, we use an optical method and vision camera to record the movement as images, and consequently, calculate the strain. Finally, we will be able to synchronize the electrical and mechanical behavior of the fabricated sensor.

3.2 Characterization Methods

3.2.1 Mechanical Experiment

In order to test a strain gauge sensor, we need to carry out a mechanical experiment. We apply the mechanical force by a manual hydraulic press (10-Ton hydraulic press, MAXIMUM). We apply the mechanical force on top of the fabricated cube on which the strain gauge is printed and attached. The sensor is on the right side of the cube, while we apply the force from the top side and the bottom side is the surface of the press; therefore, the printed strain gauge is not touched or damaged by any physical device. Moreover, the markers required for the optical imaging strain measurement are on the front side of the cube, as displayed in Figure 3-1.

As the compressive force applies from the top and the sensor is horizontally located on the right side of the cube, tensile strain occurs due to the Poisson effect.

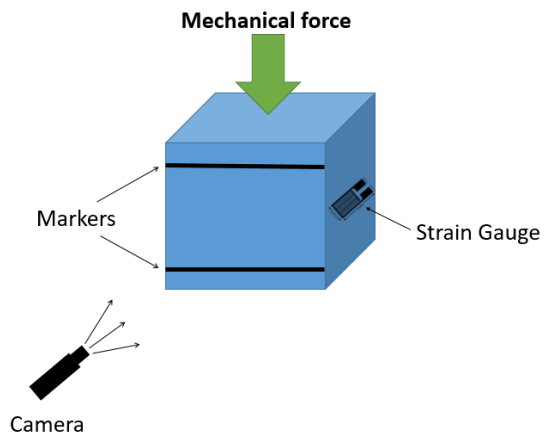

Figure 3-1: The schematic view of the sensor.

3.2.2 Measuring the Strain

Strain is the deformation of material that is created by an applied stress. Normal strain, which can be compressive or tensile, is defined as in Equation (3-1):

$$\varepsilon = \frac{\Delta L}{L} \tag{3-1}$$

Where ε is the strain, which is unitless but usually expressed in percentage, ΔL is the change of length (in m), and L is the original length (in m).

Normal stress is defined as in Equation (3-2):

$$\sigma = \frac{F}{A} \tag{3-2}$$

Where σ is normal stress (in Pa or N/m^2), F is applied force (in N), and A is area (in m^2).

Young's modulus is the relationship between stress and strain and measures the stiffness of a solid material. In the elastic region, the stress-strain relationship is linear and defined by Equation (3-3):

$$E = \frac{\sigma}{\varepsilon} \tag{3-3}$$

Where E is the Young modulus in (Pa), and σ and ε are stress and strain, respectively, as defined above.

The Poisson effect is the deformation of material in a direction perpendicular to a specific direction of applied force. Poisson ratio is the ratio between the transverse strain and the axial strain applied to a material stressed along an orthogonal axis. Poisson's ratio is defined by Equation (3-4):

$$\nu = -\frac{d\varepsilon_{trans}}{d\varepsilon_{axial}} \tag{3-4}$$

Where ν is the Poisson's ratio, and $d\varepsilon_{trans}$ and $d\varepsilon_{axial}$ are the transverse strain (in m/m) and axial or longitudinal strain (in m/m), respectively.

By applying the mechanical force and stress, a strain is created in the 3D cube. In order to measure the resulting strain, we use an optical imaging technique [111]. OSM-Classic is program designed in MATLAB to accurately measure the strain using optical imaging. This approach has advantages over more common methods including using extensometers and linear variable differential transistors. Most importantly, this method does not require any physical contact with the sample. OSM-Classic captures and processes a series of images before and while the sample is under stress; hence, it compares the taken images and accordingly determines the strain. In this part, a vision camera (acA2440-35 μm, Basler) captures the images, which is installed on a tripod. Moreover, two LED lights are installed behind the camera to provide enough light. In this experiment, 1D strain measurement is used. Accordingly, two markers are required to be drawn on a side of the sample to enable the program to follow and calculate the strain.

Figure 3-2: Image showing calculation of strain in OSM-Classic software. (a) Image of software with sample showing the Region of Interest; (b) the sample with marks for tracking, C and E represent the current edges, while C_0 and E_0 are the initial positions of the edges.

3.2.3 Measuring the Electrical Resistance

Piezoresistive effect is the change in electrical resistivity of a metal or semiconductor when a strain is applied. An applied strain changes the inter-atomic spacing inside the material, which affects the bandgap and electrons to be raised into the conduction band. However, in metals, the resistance usually changes because of the change in the dimensions of the metal resulting from an applied stress. The resistance can be calculated using Ohm's Law as in Equation (3-5):

$$R = \rho \frac{l}{A} \tag{3-5}$$

Where R is the resistance (in Ω), ρ is the material resistivity (Ω.m), l is the conductor length (m), and A is the cross-sectional area of the current flow (m^2).

In order to measure the electrical resistance of the sensor, a digital source meter (Keithley 2400) is used. Two copper wires are connected to the contact pads of the sensor using a silver paste.

The sensor is connected to a Wheatstone bridge circuit, as shown in Figure 3-3. The Wheatstone bridge converts the resistance change of the sensor to voltage changes in order to measure accurately and reduce the potential errors such as temperature-related errors. The source meter reads the voltage from V_1 and V_2. The general configuration how the equipment is installed is shown in Figure 3-4.

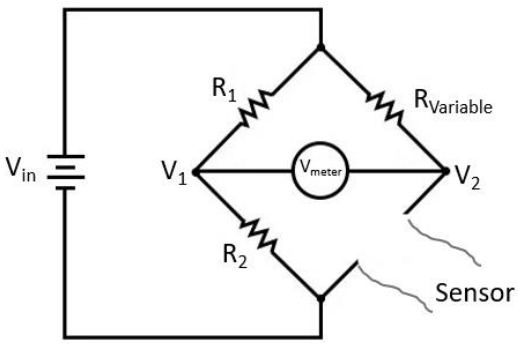

Figure 3-3: A standard Wheatstone bridge. The strain gauge connects to this circuit, and the source meter measures the voltage changes from the points V_1 and V_2.

R1 and R2 are constant resistors with equal values. $R_{variable}$ is a potentiometer. At first, we change the value of $R_{variable}$ until the voltmeter shows 0 V, which is the null point; which means that $V_1 = V_2$. Next, we start the mechanical test and the resistance of the sensor starts changing, consequently, the value of the source meter display starts varying from zero to other values.

The source meter records the input data which is voltage from terminals V_1 and V_2. V_{meter} is V_1 relative to V_2. Next, the sensor resistance can be obtained using Equation (3-6):

$$R_{sensor} = R_{Variable} \frac{R_2 \,.\, V_{in} - (R_1 + R_2) \,.\, V_{meter}}{R_1 \,.\, V_{in} + (R_1 + R_2) \,.\, V_{meter}} \qquad (3\text{-}6)$$

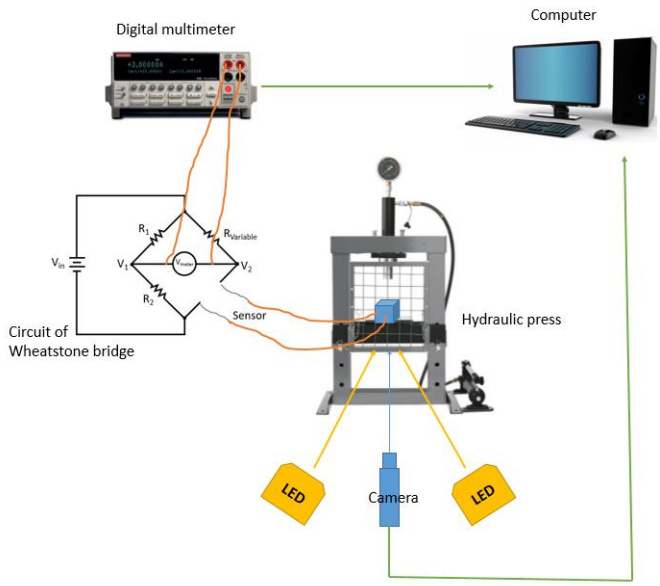

Figure 3-4: Configuration of equipment used in this experiment.

We can calculate the gauge factor using the obtained values in the experiment including ΔR/R0 and the strain. Equation (3-7) indicates the formula to calculate the gauge factor:

$$GF = \frac{\Delta R/R0}{\Delta L/L0} = \frac{\Delta R/R0}{\varepsilon} \quad (3\text{-}7)$$

Where ΔR is the resistance change in the strain gauge, R0 is unstrained resistance of strain gauge, ΔL is the change in length, L0 is the original length, and ε is the strain.

3.3 Fabrication Methods

3.3.1 Fabricating the Substrate

At the first step, we built the 3D structure as the base substrate. We fabricated 10*10*10 mm PLA cubes using the FFF printer. The material color is white to have the maximum electrical conductivity, as mentioned in Chapter 2. We also 3D printed the structures with 70% of infill density with triangle pattern in order to have softer structures and hence to have more strain during the mechanical test.

Once we 3D printed the cubic structure, we start printing the intermediate layer, ultraviolet (UV) curable acrylated urethane adhesive, onto one side of the cube. We printed a 7.5*7.5 mm square

of adhesive onto one side of the cube using the Voltera extrusion printer. To print this adhesive, we used 0.4 mm and 0.4 mm for the Kick and Rheological setpoint, respectively.

Subsequently, we UV cured the adhesive on the cube using the Dymax UV lamp for 135 seconds.

3.3.2 Fabricating the Strain Gauge

Having prepared the substrate, we inkjet printed the desired pattern of the strain gauge onto the 3D cube and adhesive using AgNP ink. Figure 3-5 displays the desired matrix pattern of the strain gauge along with the printing direction shown by yellow arrows; the orange dots form the strain gauge and blue ones form the contact pads for wire connections.

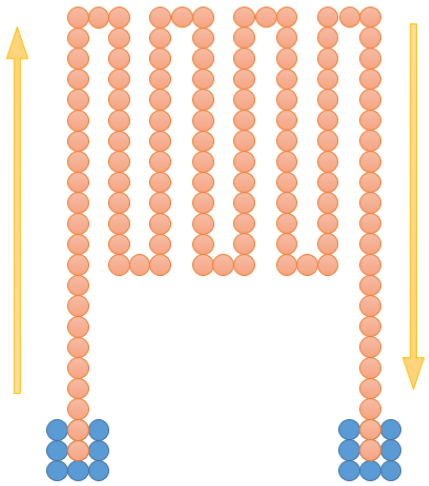

Figure 3-5: The matrix pattern and printing direction of the strain gauge. The orange dots are the strain gauge and blue ones are the contact pads. The sensor dimensions are 2080 µm * 1560 µm.

The drop spacing of printing was 80 µm as it had the optimal result and morphology. The pattern was inkjet printed onto the substrate using the AgNP ink.

Thereafter, for the drying process, the sample was put in the oven for 60 minutes at 60°C.

Once the silver pattern was dried, photonic sintering was carried out. We performed the IPL process by one single pulse of 1400 V with 2000 µs on time.

However, after the fabrication was finished, we noticed that the lines of the strain gauge are separated from the two contact pads, shown in Figure 3-6. The reason is due to the length shrinkage described in Section 2.3.7. that appears during the IPL process.

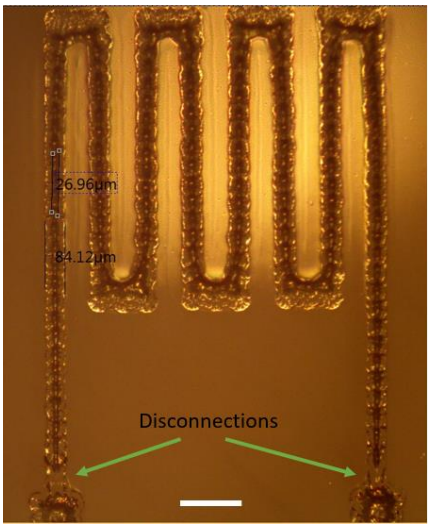

Figure 3-6: An optical micrograph of a fabricated strain gauge onto a 3D printed cube; long lines are separated from the contact pads. The scale bar represents 250 µm.

In order to solve this problem, we printed the long lines as two parallel lines next to each other, instead of one single line. Moreover, as we aimed to manually connect wires to the contact pads using silver paste, contact pads needed to be far away enough from the strain gauge to avoid applying the silver paste over the strain gauge. Therefore, we made the two long lines longer and wider, as shown in Figure 3-7 and Figure 3-8.

After inkjet printing the strain gauge, the printed silver is dried in an oven at 60°C for 60 minutes. Next, we sinter the device using the IPL by one single pulse of 1400 V with 2000 µs on time.

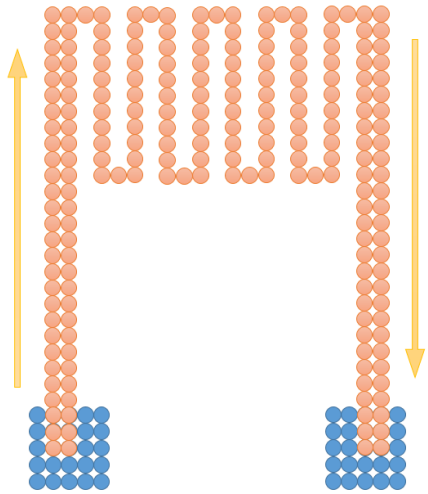

Figure 3-7: A revised pattern of strain gauge with wider and longer lines as well as with two parallel lines instead of one. The sensor dimensions are 4960 µm * 2590 µm.

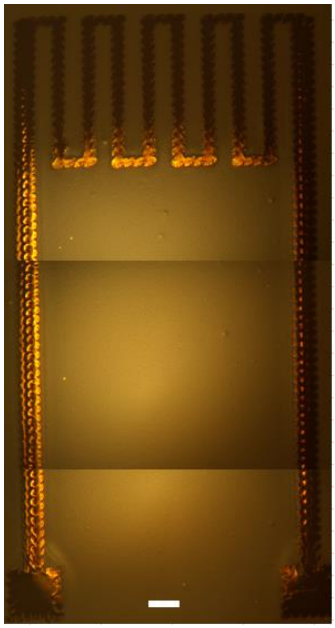

Figure 3-8: Optical micrograph of the revised fabricated strain gauge with wider and longer lines as well as with two parallel lines. The scale bar represent 250 µm.

The total length of the fabricated strain gauge was 21.4 mm. The width of normal lines was 82 µm and the width of the double printed long lines was 150 µm. The resistance of the strain gauge was found to be 32 Ω.

Figure 3-9 displays the final fabricated sample, which is a strain gauge printed onto adhesive and a 3D PLA cube.

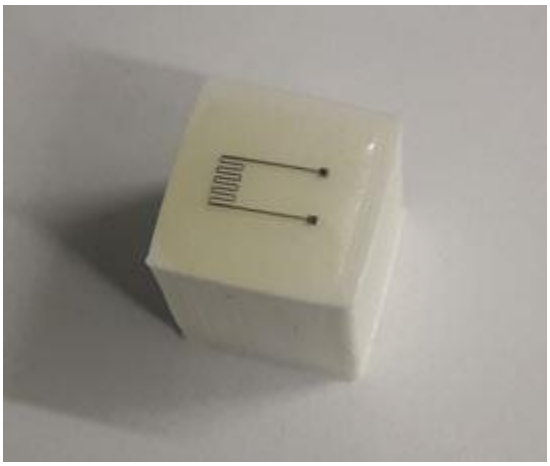

Figure 3-9: The fabricated sample; the strain gauge printed onto the adhesive on one side of the 3D printed 10 mm cube.

3.4 Results and Discussion

Once all fabrication process was completely done and we achieved a sample, the mechanical and electrical test was performed to observe the sensor behavior.

The compressive force from the top side creates tensile strain in the longitudinal direction of the sensor.

We performed the experiment by applying compressive force and measuring the electrical resistance change in the sensor, and the results are displayed in Figure 3-10.

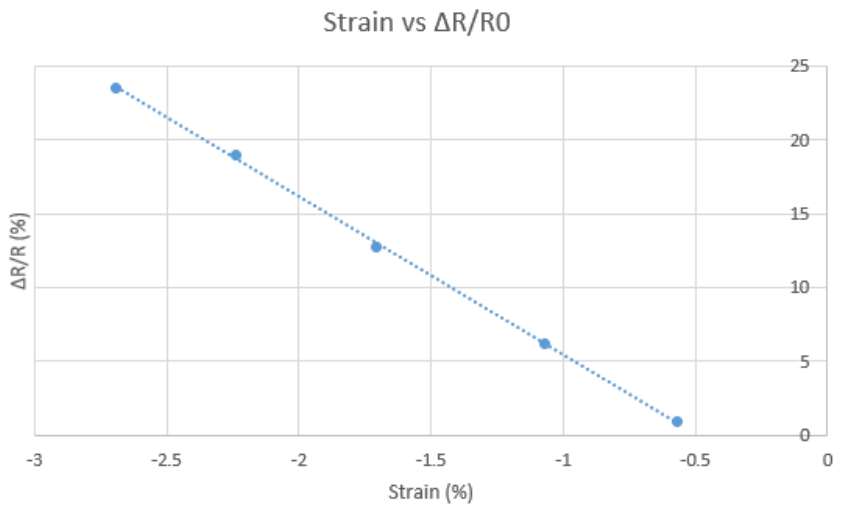

Figure 3-10: Effect of strain applied on the printed strain gauge

As can be seen from the results in Figure 3-10, the ΔR/R0 % linearly increases with the increase of strain. The GF of this sensor was found to be 10.69. As the yield point of PLA is 3.3%, the device is in the area of elastic deformation. We performed this test on five different samples, and the average GF and the related standard deviation were found to be 9.16 and 1.71, respectively. The manufacturing cost of a fabricated sensor is analyzed in Table 3-1.

Table 3-1: Describing the amount of materials used and the related prices.

	UV adhesive	**Silver NP ink**
Material price	2.4 $/mL	$1.59*10^{-8}$ $/pL
Calculation of used amount	7.5mm*7.5mm*0.5mm (L*W*H)= 28.12mm^3	95 pL (drop volume) * 450 (drops count)
Used amount	0.02812 mL	42750 pL
Used price	$ 0.0674	$ 0.00068
Total price of one sample	$ 0.068	

A key factor to compare our novel technology with other present techniques is economics. Table 3-1 shows the amount of materials used and their relevant price. All three materials used are commercially available. The used price is the cost of the amount of material that is consumed in the device. The total cost of the material for one strain gauge that was fabricated is $0.068. However, this price could be reduced by minimizing the dimensions and scaling up production. The cost of material for our strain gauge is $0.068, while a typical commercial strain gauge in the market is nearly $10-20. This includes many other costs such as labor, equipment, assembly and distribution that are difficult to predict. Due to the fact that our method allows manufacturing of the strain gauge directly integrated with 3D printing, many of these costs will be reduced or eliminated making it an affordable approach.

In this chapter, we conclude that we can use the integration of 3D FFF printing technology with inkjet printing to fabricate a strain sensor. Thanks to abilities of inkjet printing technology, we are able to fabricate the sensor with any desired pattern or dimensions as required. The sensor presented in this chapter is only an example of the possibilities of fabricating electronic devices onto 3D structures with this low-cost customized direct writing technique. Similar process can be adopted to fabricate other electronic devices as needed.

The function of this novel technique was experimentally verified in this chapter. The mechanical characterization of the fabricated sensor showed that it could be used within the range of 0-2.69% strain, while providing $\Delta R/R0$ up to 23.5%. The obtained gauge factor was 9.16.

Chapter 4: Fabricating 3D Printed TPU/CNT Composite Strain Sensor

4.1 Introduction

In this chapter, we aim to fabricate a device similar to chapter 3 but with another technology in order to compare both technologies and see the advantages of our proposed novel technology in Chapter 3. More specifically, while in Chapter 3, we used a novel integrating method to fabricate a strain sensor, here we fabricate a similar application using another technology. We select 3D printing electronics which directly fabricates functional samples via a 3D fused filament fabrication (FFF) printer.

Initially, we create a (semi-conducting) nanocomposite filament out of thermoplastic polyurethane (TPU)/carbon nanotubes (CNTs) nanocomposite. It is TPU polymer filled with CNTs that form a flexible and piezoresistive material. A great challenge is to make the composite filament printable as it is not a commercially available filament made by manufacturers. TPU material is a flexible and non-conductive polymer and CNTs are electrically conductive filler. Hence, TPU provides mechanical flexibility and CNT provides electrical conductivity. This flexible, electrically conductive composite is a promising option for a strain sensing application.

Thereafter, we 3D print the filament and fabricate our sensors as desired, the samples undergo the foaming process via batch foaming using supercritical carbon dioxide ($ScCO_2$) in order to provide the samples with thermal insulation.

Finally, we analyze the piezoresistive behavior of the sample under various tensile forces and measure the resistance change simultaneously.

4.2 Methods

4.2.1 Fabricating the Filament

3D printers feed on perfect filaments manufactured and provided by manufacturers. They were of precise diameter and limited materials such as acrylonitrile-butadiene-styrene (ABS), polylactic acid (PLA), and TPU. However, in this work, in order to fabricate our desired nanocomposite and then the filament out of it, we used a micro-conical twin screw compounder (Thermo Haake MiniCTW). In order to make this nanocomposite, two materials were used. Commercially available TPU (Estane® 2103-70A TPU, Lubrizol) as the base polymer material and commercially available Multi-walled carbon nanotubes (MWCNT)/ high-density polyethylene (HDPE)

masterbatch (Nanocyl, Plasticyl HDPE1501) and the CNT/HDPE composite contains 15 wt% of CNT.

Kim et al. [112] also found that CNT/TPU composite with more than 3 wt% CNTs provides much higher conductivity compared to less than 3 wt% CNTs, and in fact, the electrical resistance of the composite with less than 3 wt% CNTs cannot be measured by available tools.

Moreover, CNT/TPU composite with more than 5 wt% of CNTs did not provide enough flexibility as the TPU percentage reduces. Hence, we fabricated three composites with different weight percent of 3%, 4%, and 5% of CNTs.

Kim et al. in [112] found that ideal conditions for compounding of TPU/CNT composite is a temperature of 215 °C for mixing circulation of 5 minutes so that the materials mix together properly and enough.

Therefore, we used the idea and made the composite at 215 °C for 5 minutes of circulation.

The result was extruded, continuous filament made of TPU/HDPE composite which was both flexible and conductive thanks to TPU and HDPE/CNT materials, respectively.

However, this customized filament has two drawbacks compared to commercially available filaments: (1) The diameter of our composite filament was not the same all over the filament length and it was variable to some extent (2.36 mm and 2.98 mm for the lowest and highest diameter, respectively) beyond the acceptable tolerance of our 3D printer. The standard diameter of the 3D printer is 2.85±1 mm. This caused the filament to stick in the feeder or the tube. (2) As this was a customized filament, the stiffness of it was not standard. Because the feeder (on the backside) of the printer was responsible for moving the filament forward, and the stiffness of the filament was not the same as the commercially available filaments, the feeder could not move the customized filament and consequently it stacked in the tube of the 3D printer. The feeder has degree connected to a spring which determines the pressure of the feeder on the filament, even after changing the degree to the lowest pressure, it could not move forward the filament.

4.2.2 3D Printing the Sample

As we used a customized filament, we face two problems to solve, physical issues and printing parameters optimization. Considering the two drawbacks mentioned in Section 4.3.1., the composite filament was stuck in the feeder and the printing did not happen.

Therefore, we needed to use a trick in order to overcome the problem. The trick was that we needed a short part of composite filament and a long commercially available filament. We manually inserted the small composite filament in the tube and on the nozzle side and inserted the long commercially available filament from the feeder. Hence, the feeder fed the long commercially available filament which was a perfect filament and moved forward without any problem and pushed the small composite filament forward to the nozzle side, and thus, the printer printed the composite filament.

However, after printing the samples, they were not acceptable. The printed lines were not uniform, and there were some distance and gap between them, which reduced the electrical conductivity considerably. Hence, we needed to change the default printing settings. We found the optimized settings as in Table 4-1.

Table 4-1: Comparison of default and optimized parameters of 3D printer software for TPU/HDPE filament.

	Default	**Optimized**
Printing temperature	200 ℃	220 ℃
Print speed	70 mm/s	25 mm/s
Infill density	20%	50%
Infill pattern	Lines	Lines
Plate temperature	60℃	60℃

We 3D printed samples with dimensions of 30*3*0.5 mm which are length, width, and thickness, respectively. We chose the length equal to 30 mm because this is the size of the chamber of batch foaming and more than 30 mm length would not fit. We also chose a thickness of 0.5 mm for the time required for the foaming process. Since the foaming time depends on the thickness of the sample, we decided to print as thin as 0.5 mm.

The 3D printer usually prints the lines at 45° angle in which both the X and Y motor work together. However, in order to increase the conductivity, in the printing setting, we set the print angle to 0°

which prints the lines in the vertical direction as shown in Figure 4-1. A fabricated sample after 3D printing process is shown in Figure 4-2 (a-b).

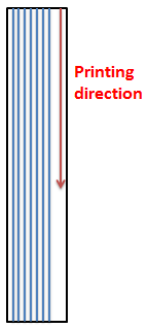

Figure 4-1: Printing direction which is vertical to align the printed filament with the direction of current flow.

4.2.3 Volume Expansion Ratio

In order to determine the volume expansion ratio of $ScCO_2$ samples, we used ASTM D792 standard. At first, we measure the samples' weight in air and in water; then we can obtain the apparent density (ρ_f) and the volume expansion ratio (VER) by equation (4-1) and (4-2), respectively.

$$\rho_f = \frac{m_{air} * \rho_{water@Tw}}{m_{air} - m_{water}} \quad (4\text{-}1)$$

where m_{air} and m_{water} are the weights of sample measured in air and water, respectively. $\rho_{water@TW}$ is density of water.

$$VER = \frac{\rho}{\rho_f} \quad (4\text{-}2)$$

where ρ is density of the bulk HDPE/TPU composite, which is given by:

$$\rho = \frac{M_1 + M_2}{\frac{M_1}{\rho_1} + \frac{M_2}{\rho_2}} \quad (4\text{-}3)$$

Where ρ is the density of bulk composite, M_1 and M_2 are the mass of material 1 and material 2, respectively. ρ_1 and ρ_2 are bulk density of material 1 and material 2 respectively, that are provided in safety data sheet of each material.

4.2.4 Foaming Process

Having the 3D printed samples made out of TPU/HDPE/MWCNT material, we can start the foaming process by $ScCO_2$. To do this, we used multiple batch foaming chambers using a Teledyne ISCO 260D Syringe Pump.

Batch foaming via $ScCO_2$ was a simple process. At first, the 3D printed sample was inserted into the high pressure and high temperature chamber. Next, the chamber and samples were heated to the favorable saturation temperature (T_{sat}). As soon as the chamber temperature reached T_{sat}, previously pressurized CO_2 was injected into the chamber containing the sample. After a certain time was passed, we turned off the heater, and immediately, we suddenly released the $ScCO_2$ in the chamber. This rapid pressure drop resulted in thermodynamic instability in the sample and hence cellular structures inside the composite matrix. Finally, we removed the sample from the chamber and quenched it in an ice bath in order to stabilize the resultant microstructure [113].

In order to achieve ideal foaming, the settings needed to be of the right values. We chose the pressure equal to 2000 psi. For temperature, it is recommended to be 10 ℃ less than the melting point of the material. The melting point of the TPU is 135 ℃. However, we tried 125 ℃ temperature but the foaming did not happen. Hence, we increased the temperature to 130 ℃ which worked and the foam structure formed. In terms of timing, we tried 30 minutes, 60 minutes, and 120 minutes.

4.2.5 Mechanical and Electrical Test

Samples were characterized using tensile force. We apply the force using a Discovery Hybrid Rheometer + Dynamic Mechanical Analyzer (TA Instrument DHR3 with DMA Module), and we use a source meter (Keithley 2400) for real-time measurement of resistance.

4.3 Results and Discussion

We 3D printed and fabricated samples for different CNT percentages of 3%, 4%, and 5%, five samples for each percentage. The resistances are 211 kΩ, 46.7 kΩ, and 10.7 kΩ with standard deviation of 25 kΩ, 5.5 kΩ, and 1.2 kΩ for CNT percentages of 3%, 4%, and 5%, respectively. Figure 4-2(a-b) displays a fabricated sample. Figure 4-3 shows the resistances of the fabricated samples after 3D printing.

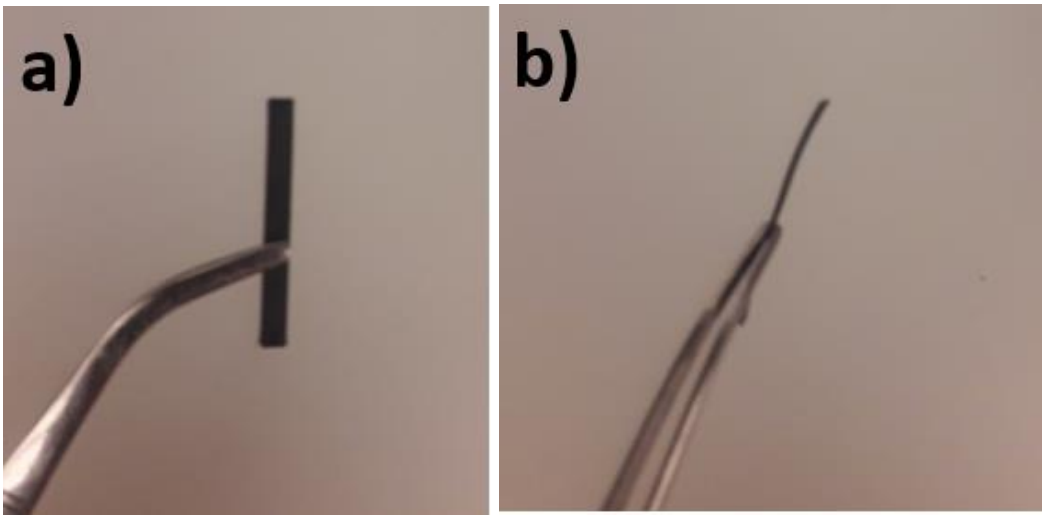

Figure 4-2: A 3D printed CNT/TPU composite. (a) Front view. (b) Side view.

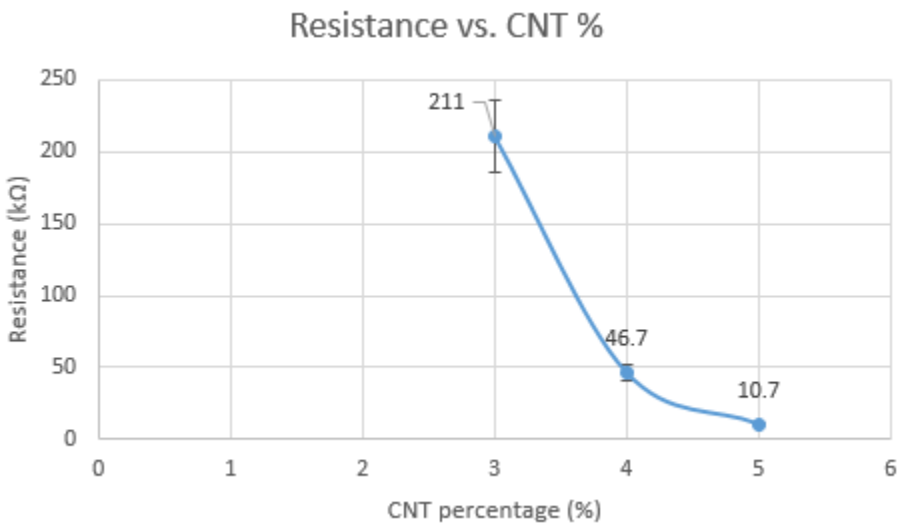

Figure 4-3: The resistance of 3D printed samples for different CNT percentages.

After the foaming process for the timing of 30, 60, and 120 minutes, the obtained results are provided in Table 4-2.

Table 4-2: Volume expansion ratio for different timing of foaming process.

Time of foaming process (minutes)	**Volume expansion ratio**
30	1.40
60	1.45
120	1.47

As it can be seen, there is not a considerable difference between volume expansion ratios of different timings. Thus, we select 30-minutes foaming in order to save time. We also analyzed the change of physical shape before and after the foaming process. The data for the physical dimensions before foaming, after 30 minutes, and after 120 minutes is provided in the Table 4-3.

Table 4-3: Physical change before and after foaming.

	Length	**Width**	**Thickness**
Before foaming	30 mm	3.00 mm	0.37 mm
After 30min foaming	30 mm	3.6 mm	0.68 mm
After 120min foaming	30 mm	3.66 mm	0.66 mm

After the foaming process, we pasted some silver glue on both ends of the sample to connect two wires. A fabricated and foamed sample with silver paste and connected wires is displayed in Figure 4-4.

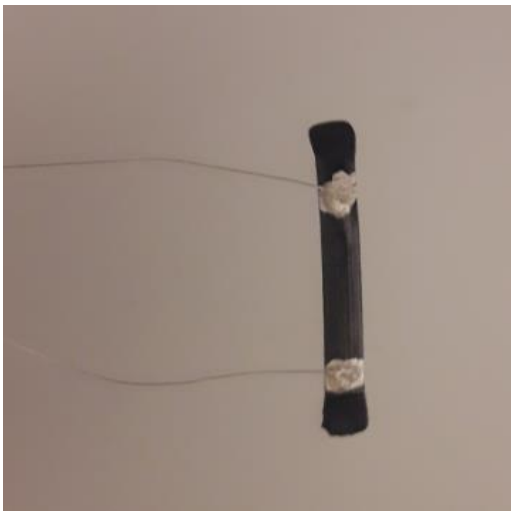

Figure 4-4: A 3D fabricated and foamed sample with silver paste and connected wires.

We performed the mechanical test for four different tensile strains including 2.5%, 5%, 7.5%, and 10%. The obtained results are provided in Figure 4-5.

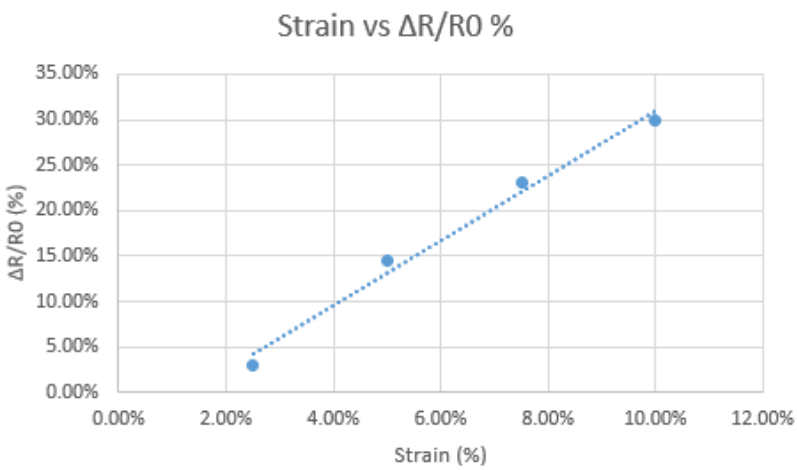

Figure 4-5: Effect of strain applied on the 3D printed piezoresistive strain sensor with 4% of CNTs.

Finally, the gauge factor of the fabricated sensor was found to be 3.58.

4.4 Conclusion

In this chapter, we fabricated strain sensors via another 3D printing technology for comparison purposes with our proposed method described in the previous chapters in order to see the advantages and disadvantages of the proposed method. The strain sensors were TPU-based polymer blends filled with CNTs. The mechanical characterization of the fabricated sensor showed that it could be used within the range of 0-10% strain, while providing $\Delta R/R0$ of between 0-30%. The obtained gauge factor was linear and equal to 3.58.

This methodology, however, has some limitations:

(1) This methodology requires extra and time consuming processes as the customized materials are not commercially available and needed to be fabricated which increases the number of steps and required equipment.

(2) Although we can 3D print any customized geometry using the FFF printer, we concluded that 3D FFF printing of customized nanocomposites is challenging, and it needs printing parameter optimization, which sometimes are limited.

(3) Besides, we can change the electrical resistance of the samples by varying the percentage of CNTs, which is limited due to printability issues; as we cannot go beyond the range of 3% and 5% of CNTs.

Chapter 5: Conclusion and Future Works

In this chapter, the overall summary of the conclusions of the previous chapters are provided. Besides, the future work are also suggested according to the results of this thesis.

5.1 Discussion and Conclusions

The first chapter of this thesis reviewed the motivations and some previous works performed similar to this work.

In Chapter 2, we inkjet printed silver nanoparticle lines onto a 3D FFF printed substrate and achieved a highly conductive single line. In order to overcome the problems of the AgNP ink attacking the PLA substrate and reduce the surface roughness of the PLA substrate, we applied an intermediate layer onto the 3D printed PLA substrate, which was UV curable acrylated urethane adhesive. We deposited this adhesive onto the 3D printed substrate using an extrusion printer, and subsequently, we UV cured the adhesive. We noticed that, in order to obtain the best result of silver lines, the optimal UV time is 135 seconds.

Thereafter, we started the inkjet printing of AgNP ink onto the substrate. We found that the suitable drop spacing for this substrate is 80 µm. For the drying process, the optimal conditions found was the temperature of 60℃ for 30 minutes.

For sintering the silver films, we used flash sintering method, IPL. In order to make the films highly sintered and avoid the length shrinkage, we used one single pulse of 1400 V with 2000 µs on-time. We also noticed that the color of 3D substrate is also effective and the white color provides the highest conductivity. Finally, we obtained silver lines onto 3D FFF printed substrate with a sheet resistance of 0.07 Ω/sq and a conductivity of $2.23 * 10^6$ (S/m).

In the third chapter, we fabricated a strain gauge sensor as an electronic device in order to validate our method. Thanks to digital inkjet printing technology, we were able to readily modify the device pattern, including the dimensions or patterns.

Once we fabricated the strain gauge onto a 3D PLA cube, we performed the mechanical experiment, which was a compression/tension test. The mechanical characterization of the fabricated sensor showed that it could be used within the range of 0-2.69% strain, while providing ΔR/R0 up to 23.5%. The obtained gauge factor was linear and equal to 9.16.

In the fourth chapter, we fabricated a strain sensor using another 3D printed electronics to compare with our novel method. We created a (semi-conducting) nanocomposite filament out of TPU/CNT nanocomposite. The fabricated samples were then foamed via batch foaming using $ScCO_2$ which decreases the cost of manufacturing and enhances some properties of polymers.

We used tensile strain test for the mechanical characterization of the fabricated strain sensor. The results showed that it could be used within the range of 0-10% strain, while providing $\Delta R/R0$ up to of 30%. The obtained gauge factor was 3.58.

However, this method had serious limitations and challenges:

- As the composite materials are not commercially available, we need to create the functional filament. This imposes extra equipment and time.
- Even for fabricating the customized filament, there are limitations. For instance, we cannot precisely determine the conductivity of the material. As we saw, we are only limited in the range of 3% to 5% of CNTs in order to make a 3D printable filament.
- Even once we fabricated the filament with limited functionality, still printing it is a challenge with a usual 3D printer as the mechanical properties and dimensions of the filament are different to what it is designed for.

5.2 Future Work

This thesis, generally, integrate inkjet printing with 3D FFF printing technology. Although we fabricated a strain gauge sensor with one single ink, it is only an example of electronic devices can be fabricated. This research provides the possibility of developing devices and circuits by low-cost direct writing techniques.

Future work that can be performed could be more advanced electronic devices with more inks and layers, such as chemical sensors, antennas, transistors, organic solar cells, etc.

While we only used one ink, AgNP, and one layer, the future work can use multiple and different inks and layers. As we used a highly aggressive ink and overcame the challenges, other types of inks can also be used likely without any serious problem, in particular water-based inks; various inks are required in electronics manufacturing for different electrical properties including conductors, semiconductors, and dielectrics. Besides, as the modified substrate has very low

surface roughness, multiple layers of materials can be used over each other to form more advanced electronic devices such as transistors and OPVs.

Besides, the different materials for the 3D printed part can be used according the application. For instance, flexile TPU filament can be easily 3D printed and be used as the flexible 3D substrate to make a flexible substrate; therefore, the electronic devices can be inkjet printed onto substrate with different materials and properties.

Finally, using this method, electronic circuits and systems are possible to be fabricated onto 3D FFF printed substrates.

References

[1] G. Cho, *Printed Electronics: Materials, Technologies and Applications*, vol. 53, no. 5 SPEC. ISSUE 3. 2014.

[2] K. Suganuma, *Introduction to Printed Electronics*. 2014.

[3] H. Marien, M. Steyaert, and P. Heremans, *Analog Organic Electronics*. .

[4] A. C. Arias, J. D. MacKenzie, I. McCulloch, J. Rivnay, and A. Salleo, "Materials and applications for large area electronics: Solution-based approaches," *Chem. Rev.*, vol. 110, no. 1, pp. 3–24, 2010, doi: 10.1021/cr900150b.

[5] E. Cantatore, *Applications of Organic and Printed Electronics*. 2013.

[6] V. Subramanian *et al.*, "Progress toward development of all-printed RFID tags: Materials, processes, and devices," *Proc. IEEE*, vol. 93, no. 7, pp. 1330–1338, 2005, doi: 10.1109/JPROC.2005.850305.

[7] G. McKerricher, J. G. Perez, and A. Shamim, "Fully inkjet printed RF inductors and capacitors using polymer dielectric and silver conductive ink with through vias," *IEEE Trans. Electron Devices*, vol. 62, no. 3, pp. 1002–1009, 2015, doi: 10.1109/TED.2015.2396004.

[8] Y. Y. Noh, N. Zhao, M. Caironi, and H. Sirringhaus, "Downscaling of self-aligned, all-printed polymer thin-film transistors," *Nat. Nanotechnol.*, vol. 2, no. 12, pp. 784–789, 2007, doi: 10.1038/nnano.2007.365.

[9] H. Y. Tseng and V. Subramanian, "All inkjet-printed, fully self-aligned transistors for low-cost circuit applications," *Org. Electron.*, vol. 12, no. 2, pp. 249–256, 2011, doi: 10.1016/j.orgel.2010.11.013.

[10] T. Schneider *et al.*, "P-171: A Flexible Touch-Sensitive Writing Tablet," *SID Symp. Dig. Tech. Pap.*, vol. 39, no. 1, p. 1840, 2008, doi: 10.1889/1.3069540.

[11] McKinsey & Company *et al.*, "Lighting the way: Perspectives on the global lighting market," *McKinsey Co.*, pp. 1–58, 2012.

[12] T. Tokuno *et al.*, "Fabrication of silver nanowire transparent electrodes at room temperature," *Nano Res.*, vol. 4, no. 12, pp. 1215–1222, 2011, doi: 10.1007/s12274-011-0172-3.

[13] D.-H. Kim, H. Keum, M. Mccormick, P. Liu, Y. Zhang, and F. G. Omenetto, "Epidermal Electronics," vol. 333, no. September, 2011.

[14] K. Crowley *et al.*, "Fabrication of an ammonia gas sensor using inkjet-printed polyaniline nanoparticles," *Talanta*, vol. 77, no. 2, pp. 710–717, 2008, doi: 10.1016/j.talanta.2008.07.022.

[15] S. Garner, S. Glaesemann, and X. Li, "Ultra-slim flexible glass for roll-to-roll electronic device fabrication," *Appl. Phys. A Mater. Sci. Process.*, vol. 116, no. 2, pp. 403–407, 2014, doi: 10.1007/s00339-014-8468-2.

[16] S. M. Garner, S. C. Lewis, and D. Q. Chowdhury, "Flexible glass and its application for electronic devices," *AM-FPD 2017 - 24th Int. Work. Act. Flatpanel Displays Devices TFT Technol. FPD Mater. Proc.*, pp. 28–33, 2017.

[17] M. Kaltenbrunner *et al.*, "An ultra-lightweight design for imperceptible plastic electronics,"

Nature, vol. 499, no. 7459, pp. 458–463, 2013, doi: 10.1038/nature12314.

[18] G. Grau, E. J. Frazier, and V. Subramanian, "Printed unmanned aerial vehicles using paper-based electroactive polymer actuators and organic ion gel transistors," *Microsystems Nanoeng.*, vol. 2, no. April, pp. 1–8, 2016, doi: 10.1038/micronano.2016.32.

[19] G. Grau, R. Kitsomboonloha, S. L. Swisher, H. Kang, and V. Subramanian, "Printed transistors on paper: Towards smart consumer product packaging," *Adv. Funct. Mater.*, vol. 24, no. 32, pp. 5067–5074, 2014, doi: 10.1002/adfm.201400129.

[20] D. Espalin, D. W. Muse, E. MacDonald, and R. B. Wicker, "3D Printing multifunctionality: Structures with electronics," *Int. J. Adv. Manuf. Technol.*, vol. 72, no. 5–8, pp. 963–978, 2014, doi: 10.1007/s00170-014-5717-7.

[21] N. Shahrubudin, T. C. Lee, and R. Ramlan, "An overview on 3D printing technology: Technological, materials, and applications," *Procedia Manuf.*, vol. 35, pp. 1286–1296, 2019, doi: 10.1016/j.promfg.2019.06.089.

[22] T. D. Ngo, A. Kashani, G. Imbalzano, K. T. Q. Nguyen, and D. Hui, "Additive manufacturing (3D printing): A review of materials, methods, applications and challenges," *Compos. Part B Eng.*, vol. 143, no. December 2017, pp. 172–196, 2018, doi: 10.1016/j.compositesb.2018.02.012.

[23] S. A. M. Tofail, E. P. Koumoulos, A. Bandyopadhyay, S. Bose, L. O'Donoghue, and C. Charitidis, "Additive manufacturing: scientific and technological challenges, market uptake and opportunities," *Mater. Today*, vol. 21, no. 1, pp. 22–37, 2018, doi: 10.1016/j.mattod.2017.07.001.

[24] C. Y. Yap *et al.*, "Review of selective laser melting: Materials and applications," *Appl. Phys. Rev.*, vol. 2, no. 4, 2015, doi: 10.1063/1.4935926.

[25] F. Fina, A. Goyanes, S. Gaisford, and A. W. Basit, "Selective laser sintering (SLS) 3D printing of medicines," *Int. J. Pharm.*, vol. 529, no. 1–2, pp. 285–293, 2017, doi: 10.1016/j.ijpharm.2017.06.082.

[26] J. Huang, Q. Qin, and J. Wang, "A review of stereolithography: Processes and systems," *Processes*, vol. 8, no. 9, 2020, doi: 10.3390/PR8091138.

[27] F. P. W. Melchels, J. Feijen, and D. W. Grijpma, "A review on stereolithography and its applications in biomedical engineering," *Biomaterials*, vol. 31, no. 24, pp. 6121–6130, 2010, doi: 10.1016/j.biomaterials.2010.04.050.

[28] Y. Zhuang *et al.*, "3D–printing of materials with anisotropic heat distribution using conductive polylactic acid composites," *Mater. Des.*, vol. 126, no. April, pp. 135–140, 2017, doi: 10.1016/j.matdes.2017.04.047.

[29] B. M. Tymrak, M. Kreiger, and J. M. Pearce, "Mechanical properties of components fabricated with open-source 3-D printers under realistic environmental conditions," *Mater. Des.*, vol. 58, pp. 242–246, 2014, doi: 10.1016/j.matdes.2014.02.038.

[30] P. Tran, T. D. Ngo, A. Ghazlan, and D. Hui, "Bimaterial 3D printing and numerical analysis of bio-inspired composite structures under in-plane and transverse loadings," *Compos. Part B Eng.*, vol. 108, pp. 210–223, 2017, doi: 10.1016/j.compositesb.2016.09.083.

[31] G. Postiglione, G. Natale, G. Griffini, M. Levi, and S. Turri, "Conductive 3D microstructures by

direct 3D printing of polymer/carbon nanotube nanocomposites via liquid deposition modeling," *Compos. Part A Appl. Sci. Manuf.*, vol. 76, pp. 110–114, 2015, doi: 10.1016/j.compositesa.2015.05.014.

[32] J. uk Yang, J. H. Cho, and M. J. Yoo, "Selective metallization on copper aluminate composite via laser direct structuring technology," *Compos. Part B Eng.*, vol. 110, pp. 361–367, 2017, doi: 10.1016/j.compositesb.2016.11.041.

[33] C. R. Garcia *et al.*, "3D printing of anisotropic metamaterials," *Prog. Electromagn. Res. Lett.*, vol. 34, no. August, pp. 75–82, 2012, doi: 10.2528/PIERL12070311.

[34] M. D. Monzón, I. Gibson, A. N. Benítez, L. Lorenzo, P. M. Hernández, and M. D. Marrero, "Process and material behavior modeling for a new design of micro-additive fused deposition," *Int. J. Adv. Manuf. Technol.*, vol. 67, no. 9–12, pp. 2717–2726, 2013, doi: 10.1007/s00170-012-4686-y.

[35] X. Wang, M. Jiang, Z. Zhou, J. Gou, and D. Hui, "3D printing of polymer matrix composites: A review and prospective," *Compos. Part B Eng.*, vol. 110, pp. 442–458, 2017, doi: 10.1016/j.compositesb.2016.11.034.

[36] F. C. Krebs, "Fabrication and processing of polymer solar cells: A review of printing and coating techniques," *Sol. Energy Mater. Sol. Cells*, vol. 93, no. 4, pp. 394–412, 2009, doi: 10.1016/j.solmat.2008.10.004.

[37] G. Grau, J. Cen, H. Kang, R. Kitsomboonloha, W. J. Scheideler, and V. Subramanian, "Gravure-printed electronics: Recent progress in tooling development, understanding of printing physics, and realization of printed devices," *Flex. Print. Electron.*, vol. 1, no. 2, 2016, doi: 10.1088/2058-8585/1/2/023002.

[38] J. M. Lee and W. Y. Yeong, "A preliminary model of time-pressure dispensing system for bioprinting based on printing and material parameters: This paper reports a method to predict and control the width of hydrogel filament for bioprinting applications," *Virtual Phys. Prototyp.*, vol. 10, no. 1, pp. 3–8, 2015, doi: 10.1080/17452759.2014.979557.

[39] Ainurrafiq, Risnah, and M. U. Azhar, "Review of digital printing technologies for electronic materials," *Fakt. Presdiposisi Ibu Usia Remaja Terhadap Pemberian ASI Eksklus. pada Bayi di Kec. Luahagundre Maniamolo Kabupaten Nias Selatan*, vol. 2, no. 2, pp. 192–199, 2019.

[40] M. Singh, H. M. Haverinen, P. Dhagat, and G. E. Jabbour, "Inkjet printing-process and its applications," *Adv. Mater.*, vol. 22, no. 6, pp. 673–685, 2010, doi: 10.1002/adma.200901141.

[41] Hue P. Le, "Progress and Trends in Ink-jet Printing Technology," *J. Imaging Sci. Technol.*, vol. 42, no. 1, pp. 49–62, 1998.

[42] J. Mei, M. R. Lovell, and M. H. Mickle, "Formulation and processing of novel conductive solution inks in continuous inkjet printing of 3-D electric circuits," *IEEE Trans. Electron. Packag. Manuf.*, vol. 28, no. 3, pp. 265–273, 2005, doi: 10.1109/TEPM.2005.852542.

[43] H. C. Nallan, J. A. Sadie, R. Kitsomboonloha, S. K. Volkman, and V. Subramanian, "Systematic design of jettable nanoparticle-based inkjet inks: Rheology, acoustics, and jettability," *Langmuir*, vol. 30, no. 44, pp. 13470–13477, 2014, doi: 10.1021/la502903y.

[44] H. Y. Tseng, B. Purushothaman, J. Anthony, and V. Subramanian, "High-speed organic transistors fabricated using a novel hybrid-printing technique," *Org. Electron.*, vol. 12, no. 7, pp. 1120–1125,

2011, doi: 10.1016/j.orgel.2011.04.004.

[45] H. Sirringhaus, “Device physics of solution-processed organic field-effect transistors,” *Adv. Mater.*, vol. 17, no. 20, pp. 2411–2425, 2005, doi: 10.1002/adma.200501152.

[46] K. Woo, C. Bae, Y. Jeong, D. Kim, and J. Moon, “Inkjet-printed Cu source/drain electrodes for solution-deposited thin film transistors,” *J. Mater. Chem.*, vol. 20, no. 19, pp. 3877–3882, 2010, doi: 10.1039/c000162g.

[47] D. H. Lee, S. Y. Han, G. S. Herman, and C. H. Chang, “Inkjet printed high-mobility indium zinc tin oxide thin film transistors,” *J. Mater. Chem.*, vol. 19, no. 20, pp. 3135–3137, 2009, doi: 10.1039/b822893k.

[48] S. H. Ko, H. Pan, C. P. Grigoropoulos, C. K. Luscombe, J. M. J. Fréchet, and D. Poulikakos, “All-inkjet-printed flexible electronics fabrication on a polymer substrate by low-temperature high-resolution selective laser sintering of metal nanoparticles,” *Nanotechnology*, vol. 18, no. 34, 2007, doi: 10.1088/0957-4484/18/34/345202.

[49] S. H. Lee, M. H. Choi, S. H. Han, D. J. Choo, J. Jang, and S. K. Kwon, “High-performance thin-film transistor with 6,13-bis(triisopropylsilylethynyl) pentacene by inkjet printing,” *Org. Electron.*, vol. 9, no. 5, pp. 721–726, 2008, doi: 10.1016/j.orgel.2008.05.002.

[50] B. Chen, T. Cui, Y. Liu, and K. Varahramyan, “All-polymer RC filter circuits fabricated with inkjet printing technology,” *Solid. State. Electron.*, vol. 47, no. 5, pp. 841–847, 2003, doi: 10.1016/S0038-1101(02)00443-4.

[51] Y. Liu, T. Cui, and K. Varahramyan, “All-polymer capacitor fabricated with inkjet printing technique,” *Solid. State. Electron.*, vol. 47, no. 9, pp. 1543–1548, 2003, doi: 10.1016/S0038-1101(03)00082-0.

[52] T. Kaydanova *et al.*, “Direct inkjet printing of composite thin barium strontium titanate films,” *J. Mater. Res.*, vol. 18, no. 12, pp. 2820–2825, 2003, doi: 10.1557/JMR.2003.0393.

[53] S. M. Bidoki, J. Nouri, and A. A. Heidari, “Inkjet deposited circuit components,” *J. Micromechanics Microengineering*, vol. 20, no. 5, 2010, doi: 10.1088/0960-1317/20/5/055023.

[54] A. Bietsch, J. Zhang, M. Hegner, H. P. Lang, and C. Gerber, “Rapid functionalization of cantilever array sensors by inkjet printing,” *Nanotechnology*, vol. 15, no. 8, pp. 873–880, 2004, doi: 10.1088/0957-4484/15/8/002.

[55] F. Loffredo, G. Burrasca, L. Quercia, and D. Della Sala, “Gas sensor devices obtained by ink-jet printing of polyaniline suspensions,” *Macromol. Symp.*, vol. 247, pp. 357–363, 2007, doi: 10.1002/masy.200750141.

[56] B. Li *et al.*, “Inkjet printed chemical sensor array based on polythiophene conductive polymers,” *Sensors Actuators, B Chem.*, vol. 123, no. 2, pp. 651–660, 2007, doi: 10.1016/j.snb.2006.09.064.

[57] C. T. Wang, K. Y. Huang, D. T. W. Lin, W. C. Liao, H. W. Lin, and Y. C. Hu, “A flexible proximity sensor fully fabricated by inkjet printing,” *Sensors*, vol. 10, no. 5, pp. 5054–5062, 2010, doi: 10.3390/s100505054.

[58] M. Mäntysalo and P. Mansikkamäki, “An inkjet-deposited antenna for 2.4 GHz applications,” *AEU - Int. J. Electron. Commun.*, vol. 63, no. 1, pp. 31–35, 2009, doi: 10.1016/j.aeue.2007.10.004.

[59] A. Rida, L. Yang, R. Vyas, and M. M. Tentzeris, “Conductive inkjet-printed antennas on flexible low-cost paper-based substrates for RFID and WSN applications,” *IEEE Antennas Propag. Mag.*, vol. 51, no. 3, pp. 13–23, 2009, doi: 10.1109/MAP.2009.5251188.

[60] A. Rida, L. Yang, and M. M. Tentzeris, “Design and characterization of novel paper-based inkjet-printed UHF antennas for RFID and sensing applications,” *IEEE Antennas Propag. Soc. AP-S Int. Symp.*, pp. 2749–2752, 2007, doi: 10.1109/APS.2007.4396104.

[61] Y. Amin *et al.*, “Low cost paper based bowtie tag antenna for high performance UHF RFID applications,” *Nanotechnol. 2009 Fabr. Part. Charact. MEMS, Electron. Photonics - Tech. Proc. 2009 NSTI Nanotechnol. Conf. Expo, NSTI-Nanotech 2009*, vol. 1, no. January, pp. 538–541, 2009.

[62] G. Shaker, M. Tentzeris, and S. Safavi-Naeini, “Low-cost antennas for mm-wave sensing applications using inkjet printing of silver nano-particles on liquid crystal polymers,” *2010 IEEE Int. Symp. Antennas Propag. CNC-USNC/URSI Radio Sci. Meet. - Lead. Wave, AP-S/URSI 2010*, no. 2, pp. 40–43, 2010, doi: 10.1109/APS.2010.5562281.

[63] A. Rida, L. Yang, T. Reynolds, E. Tan, S. Nikolaou, and M. M. Tentzeris, “Inkjet-printing UHF antenna for RFID and sensing applications on liquid crystal polymer,” *IEEE Antennas Propag. Soc. AP-S Int. Symp.*, no. tan 8, pp. 7–10, 2009, doi: 10.1109/APS.2009.5171791.

[64] C. N. Hoth, P. Schilinsky, S. A. Choulis, and C. J. Brabec, “Cells 2008,” *Nano Lett.*, vol. 8, no. 9, pp. 2806–2813, 2008, [Online]. Available: 10.1021/nl801365k.

[65] C. N. Hoth, S. A. Choulis, P. Schilinsky, and C. J. Brabec, “On the effect of poly(3-hexylthiophene) regioregularity on inkjet printed organic solar cells,” *J. Mater. Chem.*, vol. 19, no. 30, pp. 5398–5404, 2009, doi: 10.1039/b823495g.

[66] S. H. Eom *et al.*, “Polymer solar cells based on inkjet-printed PEDOT:PSS layer,” *Org. Electron.*, vol. 10, no. 3, pp. 536–542, 2009, doi: 10.1016/j.orgel.2009.01.015.

[67] S. H. Eom *et al.*, “High efficiency polymer solar cells via sequential inkjet-printing of PEDOT:PSS and P3HT:PCBM inks with additives,” *Org. Electron.*, vol. 11, no. 9, pp. 1516–1522, 2010, doi: 10.1016/j.orgel.2010.06.007.

[68] T. Sekitani *et al.*, “Printed nonvolatile memory for a sheet-type communication system,” *IEEE Trans. Electron Devices*, vol. 56, no. 5, pp. 1027–1035, 2009, doi: 10.1109/TED.2009.2015169.

[69] J. Leppäniemi, M. Aronniemi, T. Mattila, A. Alastalo, M. Allen, and H. Seppä, “Printed WORM memory on a flexible substrate based on rapid electrical sintering of nanoparticles,” *IEEE Trans. Electron Devices*, vol. 58, no. 1, pp. 151–159, 2011, doi: 10.1109/TED.2010.2088402.

[70] T. N. Ng, B. Russo, and A. C. Arias, “Degradation mechanisms of organic ferroelectric field-effect transistors used as nonvolatile memory,” *J. Appl. Phys.*, vol. 106, no. 9, 2009, doi: 10.1063/1.3253758.

[71] J. Bharathan and Y. Yang, “Polymer electroluminescent devices processed by inkjet printing: I. Polymer light-emitting logo,” *Appl. Phys. Lett.*, vol. 72, no. 21, pp. 2660–2662, 1998, doi: 10.1063/1.121090.

[72] J. Daniel, A. C. Arias, B. Russo, and B. Krusor, “44.3: Flexible Electrophoretic Displays with Jet-Printed Backplanes,” *SID Symp. Dig. Tech. Pap.*, vol. 40, no. 1, p. 660, 2009, doi: 10.1889/1.3256867.

[73] H. Kiguchi, “I nkjet Printing of,” *Direct*, no. November, pp. 821–827, 2003.

[74] C. Lin, C. Hung, P. Kuo, and M. Cheng, “Materials and Applications for Large Area Electronics: Solution-Based Approaches,” *J. Disp. Technol.*, vol. 8, no. 12, pp. 681–683, 2010, [Online]. Available: http://www.creol.ucf.edu/Research/Publications/3182.pdf.

[75] T. R. Hebner, C. C. Wu, D. Marcy, M. H. Lu, and J. C. Sturm, “Ink-jet printing of doped polymers for organic light emitting devices,” *Appl. Phys. Lett.*, vol. 72, no. 5, pp. 519–521, 1998, doi: 10.1063/1.120807.

[76] S. C. Chang *et al.*, “Dual-color polymer light-emitting pixels processed by hybrid inkjet printing,” *Appl. Phys. Lett.*, vol. 73, no. 18, pp. 2561–2563, 1998, doi: 10.1063/1.122533.

[77] D. Soltman and V. Subramanian, “Inkjet-printed line morphologies and temperature control of the coffee ring effect,” *Langmuir*, vol. 24, no. 5, pp. 2224–2231, 2008, doi: 10.1021/la7026847.

[78] D. Soltman, B. Smith, H. Kang, S. J. S. Morris, and V. Subramanian, “Methodology for inkjet printing of partially wetting films,” *Langmuir*, vol. 26, no. 19, pp. 15686–15693, 2010, doi: 10.1021/la102053j.

[79] D. Soltman, B. Smith, S. J. S. Morris, and V. Subramanian, “Inkjet printing of precisely defined features using contact-angle hysteresis,” *J. Colloid Interface Sci.*, vol. 400, pp. 135–139, 2013, doi: 10.1016/j.jcis.2013.03.006.

[80] M. Layani, M. Gruchko, O. Milo, I. Balberg, D. Azulay, and S. Magdassi, “Transparent conductive coatings by printing coffee ring arrays obtained at room temperature,” *ACS Nano*, vol. 3, no. 11, pp. 3537–3542, 2009, doi: 10.1021/nn901239z.

[81] Z. Zhang, X. Zhang, Z. Xin, M. Deng, Y. Wen, and Y. Song, “Controlled inkjetting of a conductive pattern of silver nanoparticles based on the coffee-ring effect,” *Adv. Mater.*, vol. 25, no. 46, pp. 6714–6718, 2013, doi: 10.1002/adma.201303278.

[82] D. Mampallil and H. B. Eral, “A review on suppression and utilization of the coffee-ring effect,” *Adv. Colloid Interface Sci.*, vol. 252, pp. 38–54, 2018, doi: 10.1016/j.cis.2017.12.008.

[83] B. Derby, “Inkjet printing of functional and structural materials: Fluid property requirements, feature stability, and resolution,” *Annu. Rev. Mater. Res.*, vol. 40, pp. 395–414, 2010, doi: 10.1146/annurev-matsci-070909-104502.

[84] U. Kalsoom, P. N. Nesterenko, and B. Paull, “Recent developments in 3D printable composite materials,” *RSC Adv.*, vol. 6, no. 65, pp. 60355–60371, 2016, doi: 10.1039/c6ra11334f.

[85] P. Parandoush and D. Lin, “A review on additive manufacturing of polymer-fiber composites,” *Compos. Struct.*, vol. 182, pp. 36–53, 2017, doi: 10.1016/j.compstruct.2017.08.088.

[86] Q. W. Lu and C. W. Macosko, “Comparing the compatibility of various functionalized polypropylenes with thermoplastic polyurethane (TPU),” *Polymer (Guildf).*, vol. 45, no. 6, pp. 1981–1991, 2004, doi: 10.1016/j.polymer.2003.12.077.

[87] P. Ghariniyat and S. N. Leung, “Development of thermally conductive thermoplastic polyurethane composite foams via CO2 foaming-assisted filler networking,” *Compos. Part B Eng.*, vol. 143, no. December 2017, pp. 9–18, 2018, doi: 10.1016/j.compositesb.2018.02.008.

[88] L. T. Hoang, S. N. Leung, and Z. H. Zhu, “Eliminating common biases in modelling the electrical

conductivity of carbon nanotube-polymer nanocomposites," *Phys. Chem. Chem. Phys.*, vol. 20, no. 19, pp. 13118–13121, 2018, doi: 10.1039/c8cp01715h.

[89] E. Bilotti, R. Zhang, H. Deng, M. Baxendale, and T. Peijs, "Fabrication and property prediction of conductive and strain sensing TPU/CNT nanocomposite fibres," *J. Mater. Chem.*, vol. 20, no. 42, pp. 9449–9455, 2010, doi: 10.1039/c0jm01827a.

[90] P. Ghariniyat and S. N. Leung, "Preparation and characterization of thermoplastic polyurethane (TPU) foams with a large variety of cell sizes," *Annu. Tech. Conf. - ANTEC, Conf. Proc.*, vol. 2017-May, pp. 2394–2398, 2017.

[91] J. Stringer *et al.*, "Integration of additive manufacturing and inkjet printed electronics: A potential route to parts with embedded multifunctionality," *Manuf. Rev.*, vol. 3, 2016, doi: 10.1051/mfreview/2016011.

[92] L. E. Murr *et al.*, "Next-generation biomedical implants using additive manufacturing of complex cellular and functional mesh arrays," *Philos. Trans. R. Soc. A Math. Phys. Eng. Sci.*, vol. 368, no. 1917, pp. 1999–2032, 2010, doi: 10.1098/rsta.2010.0010.

[93] J. H. P. Pallari, K. W. Dalgarno, and J. Woodburn, "Mass customization of foot orthoses for rheumatoid arthritis using selective laser sintering," *IEEE Trans. Biomed. Eng.*, vol. 57, no. 7, pp. 1750–1756, 2010, doi: 10.1109/TBME.2010.2044178.

[94] B.-H. Lu, H.-B. Lan, and H.-Z. Liu, "Additive manufacturing frontier: 3D printing electronics," *Opto-Electronic Adv.*, vol. 1, no. 1, pp. 17000401–17000410, 2018, doi: 10.29026/oea.2018.170004.

[95] A. H. Espera, J. R. C. Dizon, Q. Chen, and R. C. Advincula, "3D-printing and advanced manufacturing for electronics," *Prog. Addit. Manuf.*, vol. 4, no. 3, pp. 245–267, 2019, doi: 10.1007/s40964-019-00077-7.

[96] E. MacDonald and R. Wicker, "Multiprocess 3D printing for increasing component functionality," *Science (80-.).*, vol. 353, no. 6307, 2016, doi: 10.1126/science.aaf2093.

[97] M. Austin, "Systems health monitoring - From ground to air - The aerospace challenges," *AIP Conf. Proc.*, vol. 894, no. March, pp. 1477–1484, 2007, doi: 10.1063/1.2718140.

[98] L. Yang, R. Zhang, D. Staiculescu, C. P. Wong, and M. M. Tentzeris, "A novel conformal RFID-enabled module utilizing inkjet-printed antennas and carbon nanotubes for gas-detection applications," *IEEE Antennas Wirel. Propag. Lett.*, vol. 8, pp. 653–656, 2009, doi: 10.1109/LAWP.2009.2024104.

[99] J. M. Hoey *et al.*, "Rapid prototyping RFID antennas using direct-write," *IEEE Trans. Adv. Packag.*, vol. 32, no. 4, pp. 809–815, 2009, doi: 10.1109/TADVP.2009.2021768.

[100] J. T. Muth *et al.*, "Embedded 3D printing of strain sensors within highly stretchable elastomers," *Adv. Mater.*, vol. 26, no. 36, pp. 6307–6312, 2014, doi: 10.1002/adma.201400334.

[101] A. Islam and H. N. Hansen, "Micro-MID Manufacturing By Two-Shot injection Moulding," *OnBoard Technol.*, no. June, pp. 10–13, 2008.

[102] J. Hoerber, J. Glasschroeder, M. Pfeffer, J. Schilp, M. Zaeh, and J. Franke, "Approaches for additive manufacturing of 3D electronic applications," *Procedia CIRP*, vol. 17, pp. 806–811, 2014, doi: 10.1016/j.procir.2014.01.090.

[103] A. J. Lopes, E. MacDonald, and R. B. Wicker, “Integrating stereolithography and direct print technologies for 3D structural electronics fabrication,” *Rapid Prototyp. J.*, vol. 18, no. 2, pp. 129–143, 2012, doi: 10.1108/13552541211212113.

[104] J. A. Palmer *et al.*, “Mesoscale RF relay enabled by integrated rapid manufacturing,” *Rapid Prototyp. J.*, vol. 12, no. 3, pp. 148–155, 2006, doi: 10.1108/13552540610670726.

[105] R. Wicker, F. Medina, and C. Elkins, “Multiple material micro-fabrication: extending stereolithography to tissue engineering and other novel applications,” *Proc. 15th …*, no. January 2004, pp. 754–764, 2004, [Online]. Available: http://utwired.engr.utexas.edu/lff/symposium/proceedingsArchive/pubs/Manuscripts/2004/2004-73-Wicker.pdf.

[106] S. Y. Wu, C. Yang, W. Hsu, and L. Lin, “3D-printed microelectronics for integrated circuitry and passive wireless sensors,” *Microsystems Nanoeng.*, vol. 1, no. April, pp. 1–9, 2015, doi: 10.1038/micronano.2015.13.

[107] J. A. Paulsen, M. Renn, K. Christenson, and R. Plourde, “Printing conformal electronics on 3D structures with aerosol jet technology,” *FIIW 2012 - 2012 Futur. Instrum. Int. Work. Proc.*, pp. 47–50, 2012, doi: 10.1109/FIIW.2012.6378343.

[108] D. J. Roach *et al.*, “Surface modification of fused filament fabrication (FFF) 3D printed substrates by inkjet printing polyimide for printed electronics,” *Addit. Manuf.*, vol. 36, no. August, p. 101544, 2020, doi: 10.1016/j.addma.2020.101544.

[109] H. Jeong, Y. Cui, M. M. Tentzeris, and S. Lim, “Hybrid (3D and inkjet) printed electromagnetic pressure sensor using metamaterial absorber,” *Addit. Manuf.*, vol. 35, no. June, p. 101405, 2020, doi: 10.1016/j.addma.2020.101405.

[110] T. N. Mangoma, S. Yamamoto, G. G. Malliaras, and R. Daly, “Hybrid 3D/Inkjet-Printed Organic Neuromorphic Transistors,” *Adv. Mater. Technol.*, vol. 2000798, pp. 1–6, 2020, doi: 10.1002/admt.202000798.

[111] D. R. Aldrich, C. Ayranci, and D. S. Nobes, “OSM-Classic: An optical imaging technique for accurately determining strain,” *SoftwareX*, vol. 6, pp. 225–230, 2017, doi: 10.1016/j.softx.2017.08.007.

[112] K. Kim, J. Park, J. hoon Suh, M. Kim, Y. Jeong, and I. Park, “3D printing of multiaxial force sensors using carbon nanotube (CNT)/thermoplastic polyurethane (TPU) filaments,” *Sensors Actuators, A Phys.*, vol. 263, pp. 493–500, 2017, doi: 10.1016/j.sna.2017.07.020.

[113] J. E. Lee, Y. Guo, R. E. Lee, and S. N. Leung, “Fabrication of electroactive poly(vinylidene fluoride) through non-isothermal crystallization and supercritical CO2 processing,” *RSC Adv.*, vol. 7, no. 77, pp. 48712–48722, 2017, doi: 10.1039/c7ra09162a.